Relativistic Corrections to the Power Spectrum

by

Didam Gwazah Adams Duniya

Thesis submitted in fulfilment of the requirements for the Doctor of Philosophy degree in Physics at the University of the Western Cape

August 2015

Supervisor: Prof. Roy Maartens

Declaration:

I, DIDAM GWAZAH ADAMS DUNIYA, hereby declare that the work contained in this thesis is my original work, and that any work done by others or by myself, alone or with others previously, has been acknowledged and referenced accordingly.

Signed: _____

Date: 06 August, 2015

"I know that I am intelligent, because I know that I know nothing."

– Socrates

Acknowledgements

I would like to thank my supervisor, Roy Maartens, for the opportunity to work with him, and also for his careful guidance and support. I would also like to thank Daniele Bertacca, for his time and kind mentoring.

My indebtedness goes to the South African Square Kilometre Array Project and the South African National Research Foundation, for funding my research and studies. Thanks also to the Astrophysics Group, University of the Western Cape, for the vibrant academic environment they provide.

My appreciation and indebtedness goes to my family for all the love, support and encouragement. What a wonderful home they provide.

Contents

Publications

Two papers have been published on the basis of the work done in this thesis, and a third paper has been submitted for publication. The papers are given as follows:

1. Didam Duniya, Daniele Bertacca, and Roy Maartens. Clustering of quintessence on horizon scales and its imprint on HI intensity mapping. *JCAP*, 1310:015, 2013. doi: 10.1088/1475-7516/2013/10/015.

2. Didam Duniya, Daniele Bertacca, and Roy Maartens. Probing the imprint of interacting dark energy on very large scales. *Phys.Rev.*, D91:063530, 2015. doi: 10.1103/PhysRevD.91.063530.

3. Didam Duniya. Dark energy homogeneity in general relativity: are we applying it correctly?, arXiv:1505.03436, 2015. (Submitted to *Physical Review D.*)

Papers 1 and 2 are based on chapters 4 and 6, respectively, while chapter 5 constitutes paper 3.

List of Figures

Abbreviations

FRW[1]	**F**riedmann-**R**obertson-**W**alker
CMB	**C**osmic **M**icrowave **B**ackground
ISW	**I**ntegrated **S**achs-**W**olfe
BAO	**B**aryon **A**ccoustic **O**scillation
MeerKAT	**Meer**kat **K**aroo **A**rray **T**elescope
SKA	**S**quare **K**ilometer **A**rray
BOSS	**B**aryon **O**scillation **S**pectroscopic **S**urvey
DES	**D**ark **E**nergy **S**urvey

[1] Also known as Friedmann-Lemaître-Robertson-Walker (FLRW).

Notations

Notation	Description
a	Scale factor (which is universal in a FRW Universe).
t	Physical (cosmic) time.
η	Conformal time, where $dt = a\, d\eta$.
α, β, μ, ν, σ	All Greek indices denote four dimensional quantities, e.g. $\alpha = 0, 1, 2, 3$.
i, j, l	All Latin indices denote spatial quantities, e.g. $i = 1, 2, 3$.
$g_{\alpha\beta}$	Total space-time metric tensor.
γ_{ij}	Curved space background metric tensor.
δ_{ij}	Flat space background metric tensor.
∂_α	Partial differentiation with respect to x^α, i.e. $\frac{\partial}{\partial x^\alpha}$.
∂_i	Partial differentiation with respect to x^i, i.e. $\frac{\partial}{\partial x^i}$.
∇_α	Covariant differentiation with respect to $g_{\alpha\beta}$.
$\vert_i$	Covariant differentiation with respect to γ_{ij}, i.e. ∇_i.
$\vert_{ij}$	Double covariant differentiation with respect to γ_{ij}, i.e. $\nabla_i \nabla_j$.
$'$	Differentiation with respect to η (unless specified otherwise), i.e. $\frac{d}{d\eta}$.

Physical Constants

Name	**Symbol**	=	**Value** (units)
Speed of Light	c	=	$2.997\ 924\ 58 \times 10^{5}$ km $\cdot$ s^{-1}
Boltzmann's Constant	k_B	=	$1.380\ 648\ 8 \times 10^{-23}$ J $\cdot$ K^{-1}
Plank's Constant	$\hbar$	=	$6.626\ 069\ 57 \times 10^{-34}$ J $\cdot$ s
Light Year	ly	=	$9.460\ 730\ 472\ 580\ 8 \times 10^{12}$ km
Mega parsec	Mpc	=	$3.085\ 677\ 6 \times 10^{13}$ km
Hubble Constant	H_0	=	$100h$ Mpc^{-1}

To the Duniya family

Relativistic Corrections to the Power Spectrum

Didam Gwazah Adams Duniya
Department of Physics, University of the Western Cape, P/Bag 17,
Cape Town 7535, August 2015

Abstract

The matter power spectrum is key to understanding the growth of large-scale structure in the Universe. Upcoming surveys of galaxies in the optical and HI will probe increasingly large scales, approaching and even exceeding the Hubble scale at the survey redshifts. On these cosmological scales, surveys can in principle provide the best constraints on dark energy (DE) and modified gravity models and will be able to test general relativity itself. However, in order to realise the potential of these surveys, we need to ensure that we are using a correct analysis, i.e. a general relativistic analysis, on cosmological scales.

There are two fundamental issues underlying the general relativistic (GR) analysis. Firstly, we need to correctly identify the galaxy overdensity that is observed on the past light cone. Secondly, we need to account for all the distortions arising from observing on the past light cone, including redshift distortions (with all general relativistic effects included) and volume distortions. These general relativistic effects appear in the angular power spectra of matter in redshift space. We compute these quantities, taking into account all general relativistic large-scale effects, and including the important contributions from redshift space distortions and lensing convergence.

This is done for self-consistent models of DE, known as 'quintessence', which have only been very recently treated in the GR approach. Particularly, we focus mainly on computing the predictions (i.e. the power spectra) that need to be confronted with future data. Hence we compute the GR angular power spectra, correcting the 3D Newtonian calculation for several quintessence models. We also compute the observed 3D power spectra for interacting DE (which until now have not previously been studied in the GR approach) – in which dark matter and DE exchange energy and momentum. Interaction in the dark sector can lead to large-scale deviations in the power spectrum, similar to GR effects or modified gravity.

For the quintessence case, we found that the DE perturbations make only a small contribution on the largest scales, and a negligible contribution on smaller scales. Ironically, the DE perturbations remove the false boost of large-scale power that arises if we impose the (unphysical) assumption that the DE perturbations vanish. However, for the interacting DE (IDE) case, we found that if relativistic effects are ignored, i.e. if they are not subtracted in order to isolate the IDE effects, the imprint of IDE will be incorrectly identified – which could lead to a bias in constraints on IDE, on horizon scales.

Moreover, we found that on super-Hubble scales, GR corrections in the observed galaxy power spectrum are able to distinguish a homogeneous DE (being one whose density perturbation in *comoving* gauge vanishes) from the concordance model (and from a clustering DE) – at low redshifts and for high magnification bias. Whereas the matter power spectrum is incapable of distinguishing a homogeneous DE from the concordance model. We also found that GR effects become enhanced with decreasing magnification bias, and with increasing redshift.

Chapter 1

Introduction

1.1 General Overview

The matter power spectrum is a key diagnostic of the growth, the evolution and the nature of large-scale structure in the Universe. It describes the cosmic distribution of matter: hence it is crucial to understanding the cosmic history and even, fate of the Universe. However, in reality the matter distribution is unobservable directly, only objects such as galaxies whose distribution trace that of the underlying matter are observable [1, 2]. Galaxies trace the matter only up to a certain factor, called *bias* [3–5]. Moreover, galaxy surveys with large sky-coverage, covering scales nearly and beyond the Hubble horizon and at high redshifts require *general relativistic* (GR) corrections [1, 3–24] to the simple Newtonian calculation of the observed power spectrum. This is because on these scales the Newtonian prediction of the galaxy distribution is no longer able to adequately trace the matter distribution, by not accounting for GR effects.

These effects are mainly owing to the effects of: (i) the gravitational potential both local at the observed galaxy and along the line of sight, and (ii) the peculiar velocity of the galaxy, both local at the galaxy and also relative to the observer. Together, these effects are referred to as the 'GR effects'. Present optical surveys only cover low redshifts and sky areas spanning cosmic distance scales smaller than the Hubble radius – hence having negligible GR effects. However, upcoming galaxy surveys in the optical, infrared and the radio, will extend to high redshifts and large sky area, covering scales nearly and exceeding the Hubble radius. On these scales, the GR effects become significant.

As we enter the era of precision cosmology, surveys at high redshifts and large volumes will provide unprecedented information (sharper, richer and deeper) on the observable Universe, but most importantly, on cosmological scales at the survey redshifts. Within this reach, these surveys should provide the best cosmological constraints on theoretical models. However, to realise the full potential of these surveys, theoretical work needs to be done to establish the correct framework, which fully corrects for the GR effects, for adequate and optimal analysis. Firstly, the intrinsic galaxy overdensity that is observed on the past light cone needs to be correctly identified, accounting for all the associated distortions including redshift distortions (with all the associated GR effects) and volume distortions. These effects surface in the power spectrum of matter in the redshift space.

The corrections from the GR effects can provide a sensitive test for theoretical ideas, e.g. these corrections will be crucial for probing dark energy (DE) [25–27] and modified gravity [28] models. For example, the predictions from these corrections can be compared to the large-scale surveys of DES [29], EUCLID [30], BOSS [31] and the SKA [32, 33]

to probe the nature of DE and modified gravity, and to test general relativity itself. The GR corrections will also be crucial for extracting the primordial non-Gaussianity [4, 5, 16, 32, 34, 35] signal that seeded the large-scale structure.

Over the past couple of decades, the amount and quality of observational data collected for characterising the Universe have increased substantially. It is becoming clearly evident that matter structures in the Universe are ubiquitous [36]. These structures range from planets and stars ($\sim 1\mathrm{M}_\odot$) up to galaxy superclusters ($\sim 10^{16}\mathrm{M}_\odot$) [37]. Importantly, the past recent years have remarkably transformed our understanding of the cosmic features in the galaxy distribution. However, as upcoming surveys stretch out even more to larger regions of the Universe, our current conception of the matter structure may likely change – portraying how much we still do not know about most of the accessible Universe.

Moreover the assumption that, out at large distances the Universe looks homogeneous and isotropic, remains only a guiding but crucial principle: now well known as the *cosmological principle*. By 'homogeneous' it is meant that at a given cosmic epoch all positions in the Universe look geometrically identical, and by 'isotropy' it is meant that the Universe (and hence, the galaxy distribution) possesses the same global properties when viewed at any angle at any cosmic epoch. Current galaxy maps however reveal significant level of inhomogeneity in the distribution of galaxies (for scales covering less than 150 Mpc) – with the galaxy clustering properties depending on both the galaxy local environment and on the inherent properties of the galaxy [38]. On these scales any cosmological parameters tied to perturbations in the underlying matter distribution will possibly show spatial variations. Hence the cosmological principle may be valid but only at scales $\gtrsim$ 150 Mpc, i.e. the linear regime, where spatial gradients vanish or are negligible. Fortunately, the observed cosmic inhomogeneities, and hence the GR corrections, can be well studied within cosmological perturbation theory.

This thesis aims at computing the predictions (i.e. power spectra) of the large-scale structure that needs to be confronted with future data – taking GR corrections into account. All computations are done within linear perturbation theory [39–46]: via the Einstein's field equations, generically given by [47–49]

$$G_{\mu\nu} \;=\; \frac{8\pi G}{c^4}T_{\mu\nu}, \qquad G_{\mu\nu} \equiv R_{\mu\nu} - \frac{1}{2}g_{\mu\nu}R, \tag{1.1}$$

where $R_{\mu\nu}$, $g_{\mu\nu}$ and $T_{\mu\nu}$ are the Ricci, the metric and the energy-momentum tensors, respectively; with $R = R^{\alpha}{}_{\alpha}$ being the Ricci scalar. The associated density transport equations are obtained by the *energy-momentum conservation*: $\nabla_{\mu}T^{\mu}{}_{\nu} = 0$. Solving Eq. (1.1) is preceded by introducing perturbations in the well known FRW metric for a homogeneous and isotropic background Universe, given in polar coordinates by

$$ds^2 \;=\; -c^2dt^2 + a^2(t)\left[\frac{dr^2}{1-Kr^2} + r^2(d\theta^2 + \sin^2\theta d\vartheta^2)\right], \tag{1.2}$$

where $a(t)$ is the scale factor, t is the physical time and the spacetime curvature is normalized to $K = 0, \pm 1$. Henceforth, we shall assume only FRW Universe.

In what follows, we give an overview of linear cosmological perturbation theory in a FRW Universe (i.e. in section 1.2).

1.2 Perturbations of a FRW Universe

The FRW cosmology allows only a preferred class of observers, being the 'fundamental' observers, which see the Universe as isotropic. An appropriate metric for this model then, is one with the (proper) time coordinate being tangent to the world lines of the fundamental observers, and with the spatial coordinates being constant along the world lines of these observers. In this case the observers are 'co-moving' with the cosmic content. Hence these observers are also referred to as *comoving observers*, with the coordinates as *comoving coordinates*. By implication, a consistent energy-momentum tensor for the cosmic content is one that has the 4-velocity of the cosmic content as the same as the fundamental 4-velocity of the comoving observers – making the comoving observers to be at rest relative to the cosmic content. Moreover, this velocity is invariably time-like, running along the time coordinate. This way, the FRW Universe will only admit a preferred vector field, being along the world line of the comoving observer [50].

In this section we give an overview of linear (classical) cosmological perturbation theory in a FRW Universe. This section is not meant to substitute a thorough treatment of the theory, but only serves to layout the basics of the parts relevant in this thesis. We begin by reviewing the metric tensor which prescribes the gravitational field; we then proceed through to the gravitational field and the energy-momentum conservation equations in general and in specific gauges; to hydrodynamical and scalar field perturbations, respectively. Henceforth we adopt: conformal time η, where $dt = ad\eta$, t is physical (cosmic) time and $a = a(\eta)$ is the 'scale factor' measuring the magnitude of the cosmic expansion; natural units where $\hbar = k_B = c = 1$; and only scalar perturbations.

1.2.1 The metric tensor

The spacetime is prescribed by a line element called the *metric* [27, 39, 40, 42, 43, 45, 51, 52], which measures the interval or distance between any two neighbouring points separated only by an infinitesimal displacement. It is often given as a squared quantity expressed in the form of a quadratic differential in terms of the (geometric) metric tensor[1] $g_{\mu\nu}$, given in real coordinates x^μ generically by

$$ds^2 \;=\; g_{\mu\nu}dx^\mu dx^\nu, \tag{1.3}$$

where Eq. (1.3) shows that the squared infinitesimal distance between any adjacent points is given by the sum of the product of the various differentials of the coordinates.

The metric tensor is a symmetric tensor function $g_{\mu\nu}(x^\alpha)$ of the spacetime coordinates x^α. In general relativity, the metric tensor components govern the matter distribution and motion through spacetime, and in turn, the motion and distribution of matter determine the metric tensor, via the gravitational field equations (1.1) [51]. Moreover, the metric tensor generates the gravitational field: described by a system of equations of functions of the metric tensor components and their derivatives, with the metric tensor components as the gravitational field (generating) functions.

In a perturbed FRW Universe, the metric tensor may be decomposed by

$$g_{\mu\nu} \;=\; \bar{g}_{\mu\nu} + \delta g_{\mu\nu}, \tag{1.4}$$

[1]Note that, unless the associated metric is initially of a flat spacetime (i.e. Minkowskian), the metric tensor of a curved spacetime can not be reduced by any coordinate transformations or other methods into the Minkowskian metric tensor [51].

where $\bar{g}_{\mu\nu} = \bar{g}_{\mu\nu}(\eta)$ is the background term, $\delta g_{\mu\nu} = \delta g_{\mu\nu}(\eta, x^i)$ is the perturbation, and

$$\bar{g}_{00} \;=\; -a^2, \qquad \bar{g}_{i0} \;=\; \vec{0} \;=\; \bar{g}_{0j}, \qquad \bar{g}_{ij} \;=\; a^2\gamma_{ij}, \tag{1.5}$$

where we consider (henceforth) only linear perturbations. Moreover, for the rest of this thesis we consider only scalar perturbations: since tensor modes give rise to gravitational waves which do not interact with neither energy density nor pressure fluctuations, and any primordial vector modes would have decayed out kinematically by now (i.e. the late Universe) in an expanding Universe [37, 40]. Thus the perturbation $\delta g_{\mu\nu}$ may be parametrised by scalar fields, i.e. if x^i denotes the space 3-vector, then we can express the perturbation of the metric tensor by the scalar quantities $\phi = \phi(\eta, x^i)$, $B = B(\eta, x^i)$, $D = D(\eta, x^i)$ and $E = E(\eta, x^i)$, accordingly by

$$\delta g_{00} \;=\; -2a^2\phi, \qquad \delta g_{i0} \;=\; a^2 B_i, \qquad \delta g_{ij} \;=\; -2a^2\left(D\gamma_{ij} - E_{ij}\right), \tag{1.6}$$

where $B_i = B_{|i}$ and $E_{ij} \equiv E_{|ij} - \frac{1}{3}\gamma_{ij}\nabla^2 E$ is a traceless transverse tensor[2]. The scalar ϕ corresponds to the perturbation amplitude in a (time) lapse function, which measures the ratio of proper-time distance to coordinate-time distance between any adjacent constant-η hypersurfaces; B corresponds to the shift vector perturbation amplitude, which measures the displacement rate of a constant spatial line from the normal of a constant-η hypersurface; D corresponds to the perturbation amplitude of a unit spatial volume; and E corresponds to the amplitude of anisotropic deformation of each constant-η hypersurface [39]. The total covariant metric tensor (1.4) thus becomes

$$g_{\mu\nu} \;= a^2 \begin{pmatrix} -(1+2\phi) & B_{|j} \\ B_{|i} & (1-2\psi)\gamma_{ij} + 2E_{|ij} \end{pmatrix}, \tag{1.7}$$

where $\psi \equiv D + \frac{1}{3}\nabla^2 E$. Therefore, the metric (1.3) in a perturbed FRW Universe is given completely by

$$ds^2 \;=\; a^2\left\{-(1+2\phi)d\eta^2 + 2B_{|i}dx^i d\eta + \left[(1-2\psi)\gamma_{ij} + 2E_{|ij}\right]dx^i dx^j\right\}, \tag{1.8}$$

where the various given scalar-field parametrizations of the metric perturbations completely exhaust the (scalar) perturbative degrees of freedom of the metric. Note that all the given scalar amplitudes of the metric (1.8) perturbations are coordinate-dependent.

Moreover, the metric (1.8) has two displeasing features [53]: (i) even by using only scalar perturbations in the metric, the resulting cosmological equations remain complicated; (ii) such generic perturbations (1.6) do give rise to ghost scalar and vector modes in the solutions of these equations. The latter difficulty can be removed while the former is alleviated if one fixes the coordinate system – by choosing a gauge (see section 1.2.6).

1.2.2 The energy-momentum tensor

The energy momentum tensor [27, 39, 40, 42, 43, 45, 51, 52] of a fluid, which describes the dynamics in the gravitational field, is given here in the contracted form by

$$T^{\mu}{}_{\nu} \;=\; (\rho + p)u^{\mu}u_{\nu} + p\delta^{\mu}{}_{\nu} + \pi^{\mu}{}_{\nu}, \tag{1.9}$$

where ρ, p and u^{μ} are the total energy density, pressure and 4-velocity, respectively; $\pi^{\mu}{}_{\nu}$ is the anisotropic stress tensor.

[2] That is $E^i{}_i = 0$, such that it has no contribution to the term $D\delta^i{}_i$ in the diagonal plane.

In a perturbed FRW Universe, the perturbative degrees of freedom follow from the decomposition by

$$T^{\mu}{}_{\nu} \;=\; \bar{T}^{\mu}{}_{\nu} + \delta T^{\mu}{}_{\nu}, \tag{1.10}$$

where the background components are given as follows

$$\bar{T}^{0}{}_{0} \;=\; -\bar{\rho}, \qquad \bar{T}^{i}{}_{0} \;=\; \vec{0} \;=\; \bar{T}^{0}{}_{j}, \qquad \bar{T}^{i}{}_{j} \;=\; \bar{p}\delta^{i}{}_{j}, \tag{1.11}$$

with $\bar{T}^{\mu}{}_{\mu} = -\bar{\rho} + 3\bar{p}$, and the perturbative degrees of freedom are given by

$$\delta T^{\mu}{}_{\nu} \;=\; \begin{pmatrix} -\delta\rho & (\bar{\rho}+\bar{p})(v+B)_{|i} \\ -(\bar{\rho}+\bar{p})v^{|i} & \delta p\,\delta^{i}{}_{j} + \pi^{i}{}_{j} \end{pmatrix}, \tag{1.12}$$

where $v^{|i} = v^{i} \equiv \delta u^{i}/\bar{u}^{0}$ is the 'peculiar' velocity, and v is the velocity potential. The 4-velocity decomposes by $u^{\mu} = \bar{u}^{\mu} + \delta u^{\mu}$, where it conforms to the normalization given by $u^{\mu}u_{\mu} = g_{\mu\nu}u^{\mu}u^{\nu} = -1$. A consequence of this yields

$$u^{\mu} \;=\; a^{-1}\left(1-\phi, v^{|i}\right), \tag{1.13}$$

$$u_{\mu} \;=\; a\left(-1-\phi, (v+B)_{|i}\right). \tag{1.14}$$

The peculiar velocities are irrotational, i.e. the curl of the velocity is $\vec{\nabla}\wedge\vec{v} = 0$, whence the velocity is obtainable as the spatial gradient of the potential v. The contracted anisotropic stress tensor, with scalar potential Π, is given by

$$\pi^{\mu}{}_{\nu} \;=\; \Pi^{|i}{}_{|j} - \frac{1}{3}\delta^{i}{}_{j}\nabla^{2}\Pi, \tag{1.15}$$

where both vectorial and tensorial contributions are neglected. Note that $\pi^{\mu}{}_{\nu}$ is a gauge-independent symmetric spatial quantity, with no temporal component.

1.2.3 The gravitational field equations

In this section we give the gravitational field equations in conformal general gauge, in terms of the generic forms of the scalar perturbations. We shall use the Einstein's field equations, here given by [27, 40, 43, 47, 50]

$$G^{\mu}{}_{\nu} \;=\; 8\pi G T^{\mu}{}_{\nu}, \qquad G^{\mu}{}_{\nu} \;\equiv\; R^{\mu}{}_{\nu} - \frac{1}{2}\delta^{\mu}{}_{\nu}R, \tag{1.16}$$

where $\delta^{\mu}{}_{\nu} = g^{\mu}{}_{\alpha}g^{\alpha}{}_{\nu}$ and, the Ricci tensor $R_{\mu\nu}$ is given by

$$R_{\mu\nu} \;=\; R^{\alpha}{}_{\mu\alpha\nu} \;\equiv\; \partial_{\alpha}\Gamma^{\alpha}{}_{\mu\nu} - \partial_{\nu}\Gamma^{\alpha}{}_{\mu\alpha} + \Gamma^{\alpha}{}_{\beta\alpha}\Gamma^{\beta}{}_{\mu\nu} - \Gamma^{\alpha}{}_{\beta\nu}\Gamma^{\beta}{}_{\mu\alpha}, \tag{1.17}$$

with the contraction convention implying $R^{\mu}{}_{\nu} = g^{\mu\alpha}R_{\alpha\nu}$ and $R = g^{\mu\nu}R_{\mu\nu}$. The Christoffel symbols[3] $\Gamma^{\alpha}{}_{\mu\nu}$ are given by

$$\Gamma^{\alpha}{}_{\mu\nu} \;=\; \frac{1}{2}g^{\alpha\beta}\left(\partial_{\nu}g_{\mu\beta} + \partial_{\mu}g_{\beta\nu} - \partial_{\beta}g_{\mu\nu}\right), \tag{1.18}$$

where here we take all quantities to denote the totals, i.e. having both background and perturbed parts; and the various metric tensor components $g_{\mu\nu}$ take values from

[3]But $\Gamma^{\alpha}{}_{\mu\nu}$ is also called *connection coefficients, affine connections*, or *Levi-Civita connections*, see, e.g. [47, 48, 50].

Eq. (1.7). Hence the equations decompose into background and perturbed parts, where the background Einstein's tensor is given by

$$\bar{G}^0{}_0 \;=\; 3a^{-2}\left(\mathcal{H}^2+K\right), \quad \bar{G}^0{}_j \;=\; \vec{0} \;=\; \bar{G}^i{}_0, \quad \bar{G}^i{}_j \;=\; a^{-2}\delta^i{}_j\left(\mathcal{H}^2+2\mathcal{H}'+K\right), \tag{1.19}$$

whence by Eqs. (1.16) and (1.11), we obtain the background Friedmann equation

$$\mathcal{H}^2 \;=\; \frac{8\pi G a^2}{3}\bar{\rho}-K, \tag{1.20}$$

where the associated background acceleration equation is given by

$$\mathcal{H}' \;=\; -\frac{4\pi G a^2}{3}\left(\bar{\rho}+3\bar{p}\right). \tag{1.21}$$

Similarly, by Eqs. (1.16) the perturbed Einstein's tensor evaluates:

$$\delta G^i{}_j \;=\; 2a^{-2}\left[\psi''+2\mathcal{H}\psi'+\mathcal{H}\phi'+\left(\mathcal{H}^2+2\mathcal{H}'\right)\phi-K\psi-\frac{1}{2}\nabla^2\mathcal{D}\right]\delta^i{}_j+\frac{\mathcal{D}^{|i}{}_{|j}}{a^2}, \tag{1.22}$$

$$\delta G^0{}_j \;=\; 2a^{-2}\left(\psi'+\mathcal{H}\phi+K\sigma\right)_{|j}, \tag{1.23}$$

$$\delta G^0{}_0 \;=\; 2a^{-2}\left\{\nabla^2\left(\psi+\mathcal{H}\sigma\right)+3K\psi-3\mathcal{H}\left(\mathcal{H}\phi+\psi'\right)\right\}, \tag{1.24}$$

where

$$\mathcal{D} \;=\; -\phi+\psi+2\mathcal{H}\sigma+\sigma', \qquad \sigma\equiv -B+E'. \tag{1.25}$$

Given Eq. (1.22), then for $i\neq j$ and for $i=j$ we have, respectively, the perturbed Einstein's field equations

$$\sigma'+2\mathcal{H}\sigma+\psi-\phi \;=\; 8\pi G a^2\Pi, \tag{1.26}$$

$$\psi''+2\mathcal{H}\psi'+\mathcal{H}\phi'+\left(\mathcal{H}^2+2\mathcal{H}'\right)\phi-K\psi \;=\; 4\pi G a^2\left(\delta p+\frac{2}{3}\nabla^2\Pi\right). \tag{1.27}$$

By Eqs. (1.24) and (1.23) we obtain the energy and the momentum densities constraint equations, respectively, given by

$$\left(\nabla^2+3K\right)\psi+\mathcal{H}\nabla^2\sigma-3\mathcal{H}\left(\psi'+\mathcal{H}\phi\right) \;=\; 4\pi G a^2\delta\rho, \tag{1.28}$$

$$\psi'+\mathcal{H}\phi+K\sigma \;=\; -4\pi G a^2(\bar{\rho}+\bar{p})\left(v+B\right), \tag{1.29}$$

which essentially constitute the equations of motion. Therefore, Eqs. (1.20), (1.21) and Eqs. (1.26) – (1.29) make up the background and the generic perturbed cosmological field equations, accordingly.

1.2.4 The energy-momentum conservation equations

Given that the total energy and momentum in the Universe are conserved, this provides that the covariant derivative of the total energy-momentum tensor vanishes, given by

$$\nabla_\mu T^\mu{}_\nu \;=\; \partial_\mu T^\mu{}_\nu+\Gamma^\mu{}_{\alpha\mu}T^\alpha{}_\nu-\Gamma^\alpha{}_{\nu\mu}T^\mu{}_\alpha \;=\; 0, \tag{1.30}$$

where this equation decomposes into background and perturbed parts. The background evaluates into a single equation given by

$$\bar{\rho}' + 3\mathcal{H}(\bar{\rho} + \bar{p}) \;=\; 0, \tag{1.31}$$

which is the background energy density continuity equation; the perturbed part evaluates into the continuity equations for the perturbed energy density and for the momentum density, respectively, given by

$$\delta\rho' + 3\mathcal{H}\left(\delta\rho + \delta p\right) \;=\; (\bar{\rho} + \bar{p})\left[3\psi' - \nabla^2\left(v + E'\right)\right], \tag{1.32}$$

$$[(\bar{\rho} + \bar{p})(v + B)]' + \delta p + \frac{2}{3}\left(\nabla^2 + 3K\right)\Pi \;=\; -(\bar{\rho} + \bar{p})\left[\phi + 4\mathcal{H}(v + B)\right]. \tag{1.33}$$

Note that the momentum density has no background conservation equation, which is a consequence of the background isotropy [42]. Moreover, the energy-momentum conservation (1.30), which states the equations of motion of objects in the gravitational field, is a consequence of the Bianchi identities [27, 50]: $\nabla_\mu G^\mu{}_\nu = 0$. (Given the Bianchi identities, the energy-momentum conservation (1.30) follows directly from Eq. (1.16).)

1.2.5 Gauge transformations

In general relativity there are no preferred coordinates – all physical laws, if expressed in tensors, retain the same form in all coordinate systems. Hence we are always free to choose or change coordinates. This is often referred to as 'coordinate freedom'. However, by changing coordinates, the scalar perturbations also change. How then do we deal with this coordinate freedom?

Given a set of initial coordinates $x^\mu = (\eta, x^i)$, consider the generic coordinate change:

$$x^\mu \;\to\; \tilde{x}^\mu \;=\; (\tilde{\eta}, \tilde{x}^i), \tag{1.34}$$

with the temporal and the spatial transformations being given, respectively, by

$$\tilde{\eta} \;=\; \eta + \xi^0(\eta, x^i), \qquad \tilde{x}^i \;=\; x^i + \xi^i(\eta, x^i), \tag{1.35}$$

where $\xi^\mu = (\xi^0, \xi^i)$ is the transformation 4-vector, ξ^0 is the 'time shift' whose magnitude measures the separation of two successive constant-η hypersurfaces, ξ^i is the 'space shift' between spatial coordinates on the hypersurface; and $|\xi^\mu| \ll 1$. Here (henceforth), in order that the scalar perturbations (and hence the metric (1.8)) preserve their scalar nature after the coordinate transformation (1.34), i.e. to prevent any induced vector and/or tensor modes – we have restricted the spatial component of the transformation vector to being strictly a scalar-generated quantity $\xi^i = \xi^{|i} = \partial^i\xi$, with ξ being a 4-scalar living in the perturbed FRW spacetime.

Consequently, the metric tensor transforms via the tensor transformation law by

$$\tilde{g}_{\mu\nu}(\tilde{x}^\sigma) \;=\; g_{\mu\nu}(x^\sigma) - \bar{g}_{\alpha\nu}\partial_\mu\xi^\alpha - \bar{g}_{\mu\alpha}\partial_\nu\xi^\alpha. \tag{1.36}$$

However, rather than working with such transformations, which affect both the coordinates and the unperturbed fields (as well as the perturbations to the fields), it is more suitable to use *gauge transformations*: which affect only the field perturbations [53]. Gauge transformations modify the coordinate-dependent perturbations into forms that enables the physical laws (equations) to maintain their usual form. In fact, the gauge

transformations that leave the field equations unchanged, may be given by

$$\delta g_{\mu\nu}(x^\sigma) \;\rightarrow\; \delta g_{\mu\nu}(x^\sigma) + \Delta g_{\mu\nu}(x^\sigma), \tag{1.37}$$

by which the field equations should indeed stay invariant, with $\Delta g_{\mu\nu}$ given by

$$\Delta g_{\mu\nu}(x^\sigma) \;\equiv\; \tilde{g}_{\mu\nu}(x^\sigma) - g_{\mu\nu}(x^\sigma), \tag{1.38}$$

where the background metric tensor $\bar{g}_{\mu\nu}(x^\sigma)$ remains the same. By first order Taylor expanding the tensor $\tilde{g}_{\mu\nu}(\tilde{x}^\sigma) = \tilde{g}_{\mu\nu}(x^\sigma) + \xi^\alpha \partial_\alpha \bar{g}_{\mu\nu}(x^\sigma)$ and applying Eq. (1.36), then

$$\tilde{g}_{\mu\nu}(x^\sigma) \;=\; g_{\mu\nu}(x^\sigma) - \bar{g}_{\alpha\nu}\partial_\mu \xi^\alpha - \bar{g}_{\mu\alpha}\partial_\nu \xi^\alpha - \xi^\alpha \partial_\alpha \bar{g}_{\mu\nu}, \tag{1.39}$$

whence we obtain the 'gauge transformation law' for the perturbations of the covariant metric tensor from Eq (1.37), under a given arbitrary coordinate change, given by

$$\delta\tilde{g}_{\mu\nu} \;=\; \delta g_{\mu\nu} - \mathcal{L}_\xi\, \bar{g}_{\mu\nu}, \tag{1.40}$$

where Eqs. (1.38) and (1.39) give $\Delta g_{\mu\nu} = -\mathcal{L}_\xi \bar{g}_{\mu\nu}$, with $\mathcal{L}_\xi$ being the Lie derivative by

$$\mathcal{L}_\xi\, \bar{g}_{\mu\nu} \;\equiv\; \xi^\alpha \partial_\alpha \bar{g}_{\mu\nu} + \bar{g}_{\alpha\nu}\partial_\mu \xi^\alpha + \bar{g}_{\mu\alpha}\partial_\nu \xi^\alpha. \tag{1.41}$$

Similarly, for any given scalar field A the gauge transformation law follows by

$$\delta\tilde{A} \;=\; \delta A - \mathcal{L}_\xi\, \bar{A}, \qquad \mathcal{L}_\xi\, \bar{A} \;=\; \xi^\alpha \partial_\alpha \bar{A}. \tag{1.42}$$

It should be noted that the transformation (1.40) holds generally for covariant tensors of rank 2. Moreover, Eqs. (1.40) and (1.41) directly yield

$$\delta\tilde{g}_{\mu\nu} \;=\; \tilde{a}^2 \begin{pmatrix} -2\left(\phi - \mathcal{H}\xi^0 - \xi^{0\prime}\right) & B_{|j} + \xi^0{}_{|j} - \xi'_{|j} \\ B_{|i} + \xi^0{}_{|i} - \xi'_{|i} & -2\left(\psi + \mathcal{H}\xi^0\right)\gamma_{ij} + 2\left(E - \xi\right)_{|ij} \end{pmatrix}, \tag{1.43}$$

where $\mathcal{H} \equiv a'/a$, and we have used the definition of E_{ij} (see below Eq. (1.6)). Hence given an arbitrary coordinate change (1.34), the gauge transformations (1.40) leave the spacetime metric (hence, the field equations) in same form:

$$ds^2 \;=\; \tilde{a}^2 \left[-(1+2\tilde{\phi})d\tilde{\eta}^2 + 2\tilde{B}_{|i} d\tilde{x}^i d\tilde{\eta} + \left[(1-2\tilde{\psi})\gamma_{ij} + 2\tilde{E}_{|ij}\right] d\tilde{x}^i d\tilde{x}^j\right], \tag{1.44}$$

where the *gauge transform* of the various metric perturbations are given by

$$\tilde{\phi} \;=\; \phi - \mathcal{H}\xi^0 - \xi^{0\prime}, \tag{1.45}$$
$$\tilde{B} \;=\; B + \xi^0 - \xi', \tag{1.46}$$
$$\tilde{\psi} \;=\; \psi + \mathcal{H}\xi^0, \tag{1.47}$$
$$\tilde{E} \;=\; E - \xi. \tag{1.48}$$

Given the definition of ψ, Eqs. (1.47) and (1.48) imply that D transforms as

$$\tilde{D} \;=\; D + \frac{1}{3}\nabla^2 \xi + \mathcal{H}\xi^0. \tag{1.49}$$

Moreover, Eqs. (1.45)–(1.48) reveal that there are mainly two independent scalar degrees of freedom in the metric, since they can be combined into two basic equations.

Similarly, following Eqs. (1.36)–(1.40), we obtain the gauge transformation law for the contracted energy-momentum tensor, given by

$$\delta\tilde{T}^{\mu}{}_{\nu} \;=\; \delta T^{\mu}{}_{\nu} - \mathcal{L}_{\xi}\bar{T}^{\mu}{}_{\nu}, \tag{1.50}$$

where the Lie derivative of the background mixed energy-momentum tensor is given by

$$\mathcal{L}_{\xi}\,\bar{T}^{\mu}{}_{\nu} \;\equiv\; \xi^{\alpha}\partial_{\alpha}\bar{T}^{\mu}{}_{\nu} + \bar{T}^{\mu}{}_{\alpha}\partial_{\nu}\xi^{\alpha} - \bar{T}^{\alpha}{}_{\nu}\partial_{\alpha}\xi^{\mu}. \tag{1.51}$$

Whence we compute the gauge transform of the energy-momentum tensor, given by

$$\delta\tilde{T}^{\mu}{}_{\nu} \;=\; \begin{pmatrix} -\delta\rho + \xi^{0}\bar{\rho}' & (\bar{\rho}+\bar{p})\,(v+\xi'+\tilde{B})_{|j} \\ -(\bar{\rho}+\bar{p})\,(v+\xi')^{|i} & \left(\delta p - \xi^{0}\bar{p}'\right)\delta^{i}{}_{j} + \pi^{i}{}_{j} \end{pmatrix}, \tag{1.52}$$

where $\tilde{B}$ is as given by Eq. (1.46) and that the anisotropic 3-tensor $\pi^{i}{}_{j}$ is gauge-invariant. From Eq. (1.52) we read off the gauge transforms of the energy density, pressure and peculiar velocity potential, respectively, given by

$$\delta\tilde{\rho} \;=\; \delta\rho - \xi^{0}\bar{\rho}', \qquad \delta\tilde{p} \;=\; \delta p - \xi^{0}\bar{p}', \qquad \tilde{v} \;=\; v + \xi'. \tag{1.53}$$

Clearly we notice that the parameters in Eq. (1.53), being scalars, only obey Eq. (1.42). Moreover, we see that the gauge transformations also leave the energy-momentum tensor in its usual form, just as with the metric tensor – hence all equations retain their usual forms (i.e.remain invariant 'on the whole') under gauge transformations.

1.2.6 Choosing a gauge

It is often suitable to split the entire spcaetime into constant-η slices or hypersurfaces, in which the coordinates are defined. Choosing a specific gauge corresponds to selecting a set of certain constant-η hypersurfaces, restricting them to a particular geometric orientation, by applying a given condition or set of conditions on the spacetime metric. This way, the spacetime coordinates are fixed. We often use the name of the gauge in place of the hypersurface since the hypersurface is actually fixed by the gauge (or gauge condition). However, the coordinate freedom of general relativity can be removed [53]: either by adopting a gauge-invariant formalism [39, 41, 54, 55] or by choosing a gauge[4].

The perturbative gauge types include the uniform curvature ($\tilde{\psi} = \tilde{E} = 0$) gauge, the co-moving ($\tilde{v} = 0$) time-orthogonal ($\tilde{B} = 0$) gauge and the uniform density ($\delta\tilde{\rho} = 0$) gauge, all of which are not being discussed in this thesis, but see e.g. [39, 42]. However, of interest in this thesis are the conformal Newtonian or longitudinal gauge and the conformal synchronous gauge.

1.2.6.1 Conformal Newtonian gauge

The conformal Newtonian ("N") gauge [40, 42, 45, 53, 56] is reached if we choose a condition such that all the gauge transforms on the off-diagonal plane of the metric completely vanish, i.e. by requiring $\delta\tilde{g}_{0j} = 0$ and $\delta\tilde{g}_{ij} \propto \gamma_{ij}$, which implies $\tilde{B} = \tilde{E} = 0$. This immediately fixes the spacetime coordinates into longitudinal hypersurfaces by

[4]Hence, invariably fixing the spacetime coordinates.

setting the transformation 4-vector components ξ^μ to

$$\xi^0 \;=\; \sigma, \qquad \xi^i \;=\; E^{|i}, \tag{1.54}$$

where σ is given by Eq. (1.25). The choice $\tilde{B} = 0$ uniquely specifies ξ^0, and $\tilde{E} = 0$ specifies ξ^i. Thus Eq. (1.54) removes completely all the gauge freedom in the conformal Newtonian frame: eliminating entirely all possibilities of any obscuring gauge modes in (physical) solutions. This then allows for the definition of new quantities given by

$$\phi_{_{\rm N}} \;\equiv\; \phi - \mathcal{H}\sigma - \sigma', \tag{1.55}$$
$$\psi_{_{\rm N}} \;\equiv\; \psi + \mathcal{H}\sigma, \tag{1.56}$$
$$v_{_{\rm N}} \;\equiv\; v + E', \tag{1.57}$$

where ψ is given by Eq. (1.7). It is easy to show that all these quantities are gauge-independent. Indeed, this directly establishes the fact that the (scalar) metric perturbations in the conformal Newtonian gauge are automatically gauge-invariant. Other advantages of working in this gauge include [56]: (i) the metric tensor $\tilde{g}_{\mu\nu}$ is diagonal and calculations simplify easily, leading to simple geodesic equations; and (ii) $\phi_{_{\rm N}}$ has a simple interpretation of representing the gravitational potential – in the Newtonian limit. In fact, when the spatial energy-momentum tensor is diagonal, i.e. $\delta\tilde{T}^i{}_j \propto \delta^i{}_j$, it implies $\psi_{_{\rm N}} = \phi_{_{\rm N}}$. In that case, there is only one free metric perturbation left – generalized as the Newtonian gravitational potential Φ [40]. Hence the name choice, *conformal Newtonian*, for this coordinate system.

Here we give the cosmological equations in the conformal Newtonian frame. Hence, given Eqs. (1.55) and (1.56), the field equations are given by

$$\psi_{_N} - \phi_{_N} \;=\; 8\pi G a^2 \Pi, \tag{1.58}$$
$$\psi''_{_N} + 2\mathcal{H}\psi'_{_N} + \mathcal{H}\phi'_{_N} + \left(\mathcal{H}^2 + 2\mathcal{H}'\right)\phi_{_N} - K\psi_{_N} \;=\; 4\pi G a^2\left(\delta p_{_N} + \frac{2}{3}\nabla^2\Pi\right), \tag{1.59}$$

where Π is invariant. In the same manner we write the energy-momentum constraint equations, respectively, given by

$$\left(\nabla^2 + 3K\right)\psi_{_N} - 3\mathcal{H}\left(\mathcal{H}\phi_{_N} + \psi'_{_N}\right) \;=\; 4\pi G a^2 \delta\rho_{_N}, \tag{1.60}$$
$$\psi'_{_N} + \mathcal{H}\phi_{_N} \;=\; -4\pi G a^2(\bar{\rho} + \bar{p})v_{_N}. \tag{1.61}$$

However, by combining Eqs. (1.60) and (1.61), we rightly obtain the *relativistic Poisson equation* in an expanding curved space, given by

$$\left(\nabla^2 + 3K\right)\psi_{_N} \;=\; 4\pi G a^2 \bar{\rho}\Delta_{_N}, \tag{1.62}$$

where $\bar{\rho}\Delta_{_N} \equiv \delta\rho_{_N} - 3\mathcal{H}(\bar{\rho}+\bar{p})v_{_N}$, with $\Delta_{_N}$ being dimensionless. Moreover, the respective conservation equations in the conformal Newtonian gauge are given by

$$\delta\rho'_{_N} + 3\mathcal{H}\left(\delta\rho_{_N} + \delta p_{_N}\right) \;=\; (\bar{\rho} + \bar{p})\left[3\psi'_{_N} - \nabla^2 v_{_N}\right], \tag{1.63}$$
$$\left[(\bar{\rho} + \bar{p})v_{_N}\right]' + \delta p_{_N} + \frac{2}{3}\left(\nabla^2 + 3K\right)\Pi \;=\; -(\bar{\rho} + \bar{p})\left[\phi_{_N} + 4\mathcal{H}v_{_N}\right]. \tag{1.64}$$

1.2.6.2 Conformal synchronous gauge

Under a coordinate change, the choice of transformation vector to the conformal synchronous ("S") gauge [40, 45, 53, 56] must be such that: $\delta\tilde{g}_{00} = \delta\tilde{g}_{0j} = 0$, which implies $\tilde{\phi} = \tilde{B} = 0$. The η-coordinate therefore defines proper time for all comoving observers. Whence we define new variables in the transformed synchronous coordinates by

$$\psi_{_S} \equiv \psi + \mathcal{H}\xi^0, \tag{1.65}$$
$$E_{_S} \equiv E - \xi, \tag{1.66}$$
$$v_{\rm S} \equiv v + \xi', \tag{1.67}$$

where the synchronous gauge condition is satisfied by the ξ^μ components given by

$$(a\xi^0)' = a\phi, \qquad \xi^{i\prime} = B^{|i} + \xi^{0|i}, \tag{1.68}$$

with the explicit forms of ξ^0 and ξ^i thus obtained from the solutions of Eq. (1.68). Note that the integration constants resulting in the solutions will imply extra residual degrees of freedom. These constants would lead to unphysical (gauge) modes, however they can be eliminated by a further choice of transformation which leaves the new solutions still within the synchronous gauge [45]. However, in a given initial coordinates (without transformations), the synchronous gauge is then achieved by: $\delta g_{00} = \delta g_{0j} = 0$, implying $\phi = B = 0$. Hence all frames in this gauge are simultaneous, i.e. synchronised to the same time – thus the choice of the name *synchronous* coordinates or gauge.

The field equations in the conformal synchronous coordinates, are given by

$$\sigma_{_S}' + 2\mathcal{H}\sigma_{_S} + \psi_{_S} = 8\pi G a^2 \Pi, \tag{1.69}$$
$$\psi_{_S}'' + 2\mathcal{H}\psi_{_S}' - K\psi_{_S} = 4\pi G a^2 \left(\delta p_{_S} + \frac{2}{3}\nabla^2\Pi\right), \tag{1.70}$$

where $\sigma_{_S} = E_{_S}'$, and the energy-momentum constraint equations are given by

$$\left(\nabla^2 + 3K\right)\psi_{_S} - 3\mathcal{H}\psi_{_S}' + \mathcal{H}\nabla^2\sigma_{_S} = 4\pi G a^2 \delta\rho_{_S}, \tag{1.71}$$
$$\psi_{_S}' + K\sigma_{_S} = -4\pi G a^2(\bar{\rho} + \bar{p})v_{_S}, \tag{1.72}$$

with the energy-momentum conservation equations given by

$$\delta\rho_{_S}' + 3\mathcal{H}\left(\delta\rho_{_S} + \delta p_{_S}\right) + (\bar{\rho} + \bar{p})\nabla^2 v_{_S} = (\bar{\rho} + \bar{p})\left[3\psi_{_S}' - \nabla^2\sigma_{_S}\right], \tag{1.73}$$
$$\left[(\bar{\rho} + \bar{p})v_{_S}\right]' + \delta p_{_S} + \frac{2}{3}\left(\nabla^2 + 3K\right)\Pi = -4(\bar{\rho} + \bar{p})\mathcal{H}v_{_S}. \tag{1.74}$$

However, in a given initial coordinates without any transformations, we will have that $\phi = B = 0$ and $\psi_{_S} = \psi$, $E_{_S} = E$ and so on.

1.2.7 Hydrodynamical perturbations

We consider a Universe entirely filled with a fluid-like multicomponent content which is governed by Einstein's general theory of relativity. For any fluid, understanding its equation of state is essential in describing its properties. The equation of state at any given time gives the current relationship among the associated state variables such as pressure, temperature, internal energy and entropy, describing the thermodynamic behaviour of the fluid. Henceforth we shall assume flat space, i.e. $K = 0$.

1.2.7.1 The background equations

Generally, the equation of state of an arbitrary species A is given by

$$\bar{p}_A \;=\; w_A\,\bar{\rho}_A, \tag{1.75}$$

where w_A is called the *equation of state parameter*, relating the background pressure $\bar{p}_A$ and energy density $\bar{\rho}_A$. Given Eq. (1.75), the background acceleration equation (1.21), for multicomponent hydrodynamical Universe, becomes

$$\mathcal{H}' \;=\; -\frac{1}{2}\,(1+3w)\,\mathcal{H}^2, \qquad w \;=\; \sum_A \Omega_A w_A, \tag{1.76}$$

where $\Omega_A \equiv \bar{\rho}_A/\bar{\rho}$ is the energy density parameter. The background conservation equation for A, follows from Eq. (1.31), and is given by

$$\bar{\rho}'_A \;=\; -3\mathcal{H}(1+w_A)\bar{\rho}_A, \tag{1.77}$$

where here the various species A are considered to have separate energy-momentum tensors $T^{\mu}_{A\nu}$, so that the total is $T^{\mu}{}_{\nu} = \sum_A T^{\mu}_{A\nu}$. Similarly, given Eqs. (1.75) and (1.77), we obtain that

$$w'_A \;=\; -3\mathcal{H}\,(1+w_A)\,\left(c^2_{aA} - w_A\right), \tag{1.78}$$

where $c^2_{aA} \equiv \bar{p}'_A/\bar{\rho}'_A$ is the adiabatic sound speed of A. Then given Eqs. (1.76)–(1.77), we obtain that

$$\Omega'_A \;=\; -3\mathcal{H}\,(w_A - w)\,\Omega_A, \tag{1.79}$$

where the total equation of state parameter w is given by Eq. (1.76).

1.2.7.2 The pressure perturbations

In this subsection, we give the pressure perturbation [57]. The physical sound speed c^2_{sA}, is defined in the rest frame (rf) of A, given by

$$c^2_{sA} \;\equiv\; \left.\frac{\delta p_A}{\delta \rho_A}\right|_{\rm rf} \;\geq\; 0, \tag{1.80}$$

which is essentially the speed of propagation of the pressure perturbation δp_A relative to the density perturbation $\delta\rho_A$ – when A is at rest. Then by changing from an arbitrary frame x^μ into the rest frame $x^\mu|_{\rm rf}$, i.e. given by $x^\mu \to x^\mu|_{\rm rf} = x^\mu + \xi^\mu$, this leads to a gauge transformation (1.50) of the energy-momentum tensor:

$$\delta T^{\mu}_{A\nu} \;\to\; \delta T^{\mu}_{A\nu}\big|_{\rm rf} \;=\; \delta T^{\mu}_{A\nu} - \mathcal{L}_\xi \bar{T}^{\mu}_{A\nu}, \tag{1.81}$$

where by Eq. (1.51), we have for the individual species A that

$$\mathcal{L}_\xi \bar{T}^{\mu}_{A\nu} \;=\; \xi^\alpha \partial_\alpha \bar{T}^{\mu}_{A\nu} + \bar{T}^{\mu}_{A\alpha}\partial_\nu \xi^\alpha - \bar{T}^{\alpha}_{A\nu}\partial_\alpha \xi^\mu. \tag{1.82}$$

Thus by Eq. (1.81), the (0-0)th and the (i-j)th components of $\delta T^{\mu}_{A\nu}|_{\rm rf}$ yield, respectively

$$\delta\rho_A|_{\rm rf} \;=\; \delta\rho_A - \xi^0\bar{\rho}'_A, \qquad \delta p_A|_{\rm rf} \;=\; \delta p_A - \xi^0\bar{p}'_A, \tag{1.83}$$

and the (0-j)th or (i-0)th component yields

$$(v_A + B)\,|_{\rm rf} \;=\; v_A + B + \xi^0. \tag{1.84}$$

However, in the rest frame we have that

$$\delta T^0_{Aj}\big|_{\rm rf} \;=\; 0 \;=\; \delta T^i_{A0}\big|_{\rm rf}\,, \tag{1.85}$$

where it follows that $(v_A + B)|_{\rm rf} = 0$. Hence it implies that

$$\xi^0 \;=\; -\,(v_A + B)\,. \tag{1.86}$$

Thus given Eqs. (1.80), (1.83) and (1.86), we obtain the pressure perturbation given by

$$\delta p_A \;=\; c^2_{aA}\delta\rho_A + (c^2_{sA} - c^2_{aA})\bar\rho_A\Delta_A, \tag{1.87}$$

where c^2_{aA} is given by Eq. (1.78), and the *comoving* density perturbation Δ_A is given by

$$\bar\rho_A\,\Delta_A \;\equiv\; \delta\rho_A + \bar\rho'_A(v_A + B) \tag{1.88}$$

$$\;=\; \delta\rho_A - 3\mathcal{H}(1 + w_A)(v_A + B)\bar\rho_A, \tag{1.89}$$

which is gauge-invariant. In Eq. (1.89) we used Eq. (1.77). Moreover, given Eqs. (1.83), (1.86) and (1.88), we have that

$$\delta\rho_A|_{\rm rf} \;=\; \bar\rho_A\Delta_A. \tag{1.90}$$

Thus the comoving density perturbation of any species corresponds to the density perturbation of that species in its rest frame. This implies that the rest frame coincides with the comoving coordinates, i.e. a fluid at rest in the gravitational field is comoving with the background Universe.

1.2.7.3 The perturbed field and conservation equations

Here we give the governing perturbation equations in a general gauge, with respect to the various species A. Given Eq. (1.75), the perturbed hydrodynamical gravitational field equation, i.e. Eq. (1.27), thus becomes

$$\psi'' + \mathcal{H}(2 + 3c^2_a)\psi' + \mathcal{H}\phi' + \left[2\mathcal{H}' + (1 + 3c^2_a)\mathcal{H}^2\right]\phi \;=\; \frac{3}{2}\mathcal{H}^2\left(c^2_s\Delta + \frac{2}{3\bar\rho}\nabla^2\Pi\right), \tag{1.91}$$

where $\bar\rho\Pi = \sum_A \bar\rho_A\Pi_A$ is the total anisotropic stress potential, and σ is given by Eq. (1.54). The parameters Δ, c^2_a and c^2_s are the respective totals, and it is easy to show that

$$\Delta \;=\; \sum_A \Omega_A\,\Delta_A, \quad c^2_a \;=\; \frac{1}{1+w}\sum_A \Omega_A(1 + w_A)c^2_{aA}, \quad c^2_s \;=\; \frac{1}{\Delta}\sum_A \Omega_A\Delta_A c^2_{sA}. \tag{1.92}$$

The perturbed (energy-momentum) constraint equations, i.e. Eqs. (1.60) and (1.61), are thus given with respect to A as follows

$$\nabla^2\left(\psi+\mathcal{H}\sigma\right)-3\mathcal{H}\left(\mathcal{H}\phi+\psi'\right) = \frac{3}{2}\mathcal{H}^2\sum_A \Omega_A\,\delta_A, \tag{1.93}$$

$$\psi'+\mathcal{H}\phi = -\frac{3}{2}\mathcal{H}^2\sum_A \Omega_A(1+w_A)(v_A+B), \tag{1.94}$$

where $\delta_A \equiv \delta\rho_A/\bar{\rho}_A$. Given Eqs. (1.75)–(1.79) and (1.87), the perturbed density and Euler equations, i.e. Eqs. (1.32) and (1.33), thus become

$$\delta_A'+3\mathcal{H}\left(c_{sA}^2-w_A\right)\Delta_A-3\mathcal{H}w_A'(v_A+B)=(1+w_A)\left[3\psi'-\nabla^2(v_A+B+\sigma)\right], \tag{1.95}$$

$$v_A'+B'+\mathcal{H}(v_A+B)+\phi = \frac{-1}{1+w_A}\left[c_{sA}^2\Delta_A+\frac{2}{3\bar{\rho}_A}\nabla^2\Pi_A\right]. \tag{1.96}$$

Equivalently, instead of Eq. (1.95) we can use the Δ_A evolution equation given by

$$\Delta_A'-3\mathcal{H}w_A\Delta_A = \frac{9}{2}\mathcal{H}^2(1+w_A)\sum_B \Omega_B(1+w_B)[V_A-V_B] - (1+w_A)\left[\nabla^2 V_A-\frac{2\mathcal{H}}{(1+w_A)\bar{\rho}_A}\nabla^2\Pi_A\right], \tag{1.97}$$

where we used the gauge-invariant velocity potential (given $v_{_N}$ (1.57))

$$V_A \equiv v_A+E'. \tag{1.98}$$

Thus by using V_A we transform Eq. (1.96), given by

$$V_A'+\mathcal{H}V_A = -\Phi-\frac{1}{1+w_A}\left[c_{sA}^2\Delta_A+\frac{2}{3\bar{\rho}_A}\nabla^2\Pi_A\right], \tag{1.99}$$

where $\Phi \equiv \phi-\mathcal{H}\sigma-\sigma'$ is a gauge-independent potential, which corresponds to $\phi_{_N}$ (1.55). Moreover, by combining Eqs. (1.93) and (1.94), we get

$$\nabla^2\Psi = \frac{3}{2}\mathcal{H}^2\sum_A \Omega_A\Delta_A, \tag{1.100}$$

where $\Psi \equiv \psi+\mathcal{H}\sigma$ (corresponding to $\psi_{_N}$ (1.56)), and Δ_A is given by Eq. (1.89). Thus given Eq. (1.26), Φ and Ψ (also called the Bardeen potentials [54]) are related by

$$\Psi-\Phi = 8\pi G a^2\sum_A \Omega_A\Pi_A. \tag{1.101}$$

Similarly, given Eqs. (1.76), (1.98) and, Φ and Ψ, we transform Eq. (1.94) to

$$\Psi'+\mathcal{H}\Phi = -\frac{3}{2}\mathcal{H}^2\sum_A \Omega_A(1+w_A)V_A, \tag{1.102}$$

Clearly, we see that Eqs. (1.97)–(1.102) are gauge-invariant equations. Hence it is often more suitable to use the evolution equations (1.97), (1.99) and (1.102), instead of Eqs. (1.94)–(1.96): ψ, ϕ, δ_A and v_A are gauge-dependent on large scales – which

make analyses ambiguous. However Ψ, Φ, Δ_A and V_A are all gauge-independent, thus eliminating any large-scale 'unphysical artefacts' arising from gauge choices.

1.2.8 Scalar field perturbations

It is now well known that scalar fields [40, 42, 46] play an important role in studying physical phenomena in modern cosmology, from the early-time inflation to the late-time dark energy scenarios. In this section we consider a cosmic component described by a scalar field, and therefore compute the associated evolution equations. We first give the equations in a general frame and then in both the Newtonian and the synchronous frames, respectively.

1.2.8.1 The energy-momentum tensor

The scalar field φ considered here is one with minimal coupling, evolving along a potential $U(\varphi)$, which is prescribed by a Lagrangian density $\mathcal{L}_\varphi$ given by

$$\mathcal{L}_\varphi \;=\; -\frac{1}{2}\partial^\mu\varphi\partial_\mu\varphi - U(\varphi). \tag{1.103}$$

For a scalar field φ, the energy-momentum tensor $T_{\mu\nu}$ is defined in terms of the Lagrangian density as follows

$$T_{\mu\nu} \;=\; -\frac{2}{\sqrt{-g}}\frac{\partial}{\partial g^{\mu\nu}}\left(\mathcal{L}_\varphi\sqrt{-g}\right) \;=\; \partial_\mu\varphi\partial_\nu\varphi + g_{\mu\nu}\mathcal{L}_\varphi, \tag{1.104}$$

where $g \equiv \det(g_{\mu\nu})$ and we have used the following identities, (i) from matrix algebra $\partial g/g = g^{\mu\nu}\partial g_{\mu\nu}$ and (ii) from product rule $g^{\alpha\beta}\partial g_{\alpha\beta} = -\,g_{\alpha\beta}\partial g^{\alpha\beta}$. Hence the contracted energy-momentum tensor $T^\mu{}_\nu$ is given by[5]

$$T^\mu{}_\nu \;=\; \partial^\mu\varphi\partial_\nu\varphi - \delta^\mu{}_\nu\left[U(\varphi) + \frac{1}{2}\partial^\beta\varphi\partial_\beta\varphi\right]. \tag{1.105}$$

We now introduce a first order perturbation in the field about its homogeneous background such that the field transforms perturbatively as follows

$$\varphi(\eta, x^i) \;=\; \bar{\varphi}(\eta) + \delta\varphi(\eta, x^i), \tag{1.106}$$

where $|\delta\varphi| \ll 1$, and the field potential changes as follows

$$U \;\to\; \tilde{U}(\varphi) \;=\; U(\bar{\varphi}) + U_{|\varphi}\delta\varphi, \tag{1.107}$$

where $U_{|\varphi} \equiv \partial U(\bar{\varphi})/\partial\bar{\varphi}$. Hence, by evaluating Eq. (1.105), we obtain the various components of the energy momentum tensor given by

$$T^0{}_0 \;=\; -a^{-2}\left[\frac{\bar{\varphi}'^2}{2} + a^2U + \bar{\varphi}'\left(\delta\varphi' - \phi\bar{\varphi}'\right) + a^2U_{|\varphi}\delta\varphi\right], \tag{1.108}$$

$$T^i{}_0 \;=\; a^{-2}\bar{\varphi}'\left(\delta\varphi + \bar{\varphi}'B\right)^{|i}, \qquad T^0{}_j \;=\; -a^{-2}\bar{\varphi}'\delta\varphi_{|j}, \tag{1.109}$$

$$T^i{}_j \;=\; -a^{-2}\left[-\frac{\bar{\varphi}'^2}{2} + a^2U - \bar{\varphi}'\left(\delta\varphi' - \phi\bar{\varphi}'\right) + a^2U_{|\varphi}\delta\varphi\right]\delta^i{}_j, \tag{1.110}$$

[5]Notice the typo in the definition of $T^\mu{}_\nu$ in [42] – where it is defined with respect to $\partial/\partial g_{\mu\nu}$ instead of $\partial/\partial g^{\mu\nu}$, which follows from the definition of $T_{\mu\nu}$.

where $U = U(\bar{\varphi})$, and we can then identify the various background and perturbed components, respectively, by comparing Eqs. (1.108)–(1.110) with Eqs. (1.11) and (1.12). We obtain the scalar field background energy density $\bar{\rho}_\varphi$ and pressure $\bar{p}_\varphi$, given by

$$\bar{\rho}_\varphi = \frac{\bar{\varphi}'^2}{2a^2} + U, \tag{1.111}$$

$$\bar{p}_\varphi = \frac{\bar{\varphi}'^2}{2a^2} - U, \tag{1.112}$$

and the perturbed energy density and pressure are given, respectively, by

$$\delta\rho_\varphi = a^{-2}\bar{\varphi}'(\delta\varphi' - \phi\bar{\varphi}') + U_{|\varphi}\delta\varphi, \tag{1.113}$$

$$\delta p_\varphi = a^{-2}\bar{\varphi}'(\delta\varphi' - \phi\bar{\varphi}') - U_{|\varphi}\delta\varphi, \tag{1.114}$$

where the scalar field does not support any anisotropic stresses, i.e. $\Pi = 0$. The peculiar velocity potential of the scalar field is given by

$$v_\varphi + B = -\frac{\delta\varphi}{\bar{\varphi}'}. \tag{1.115}$$

Note that, $\delta\rho_\varphi$ and v_φ will also follow Eqs. (1.95) and (1.96) (and hence, Eqs. (1.97) and (1.99)) – i.e. for any of the species A described by φ.

1.2.8.2 The conservation equations in general gauge

The energy-momentum conservation equations are herewith given in generic coordinates as the *Klein-Gordon* equations. The Klein-Gordon equation of the scalar field describes the motion of the field in time. By substituting $\bar{\rho}_\varphi$ and $\bar{p}_\varphi$, i.e. Eqs. (1.111) and (1.112), in the energy conservation Eq. (1.31), we get the background Klein-Gordon equation:

$$\bar{\varphi}'' + 2\mathcal{H}\bar{\varphi}' + a^2 U_{|\varphi} = 0. \tag{1.116}$$

This equation gives the time evolution of the background field in an expanding universe. Similarly, substituting $\delta\rho_\varphi$ and δp_φ – i.e. Eqs. (1.113) and (1.114), in Eq. (1.32) we obtain the perturbed Klein-Gordon equation given by

$$\delta\varphi'' + 2\mathcal{H}\delta\varphi' - \nabla^2\delta\varphi + a^2 U_{|\varphi\varphi}\delta\varphi + 2a^2\phi U_{|\varphi} - \bar{\varphi}'\phi' = \bar{\varphi}'\left[3\psi' - \nabla^2\sigma\right], \tag{1.117}$$

where $U_{|\varphi\varphi} \equiv \partial^2 U/\partial\bar{\varphi}^2$ is the second derivative of the potential with respect to the background scalar field $\bar{\varphi}$. We note that the sum $v_\varphi + B$ is gotten from the solutions of Eqs. (1.116) and (1.117).

1.2.8.3 The conservation equations in specific gauges

Here we consider the perturbed conservation equations in the conformal Newtonian and the synchronous gauges, respectively.

Conformal Newtonian gauge.

In the Newtonian gauge, given $\Pi = 0$, Eq. (1.58) (and hence, Eq. (1.100)) implies $\psi_{_N} = \phi_{_N} = \Phi$ and the perturbed Klein-Gordon equation thus becomes

$$\delta\varphi''_{_N} + 2\mathcal{H}\delta\varphi'_{_N} - \nabla^2\delta\varphi_{_N} + a^2U_{|\varphi\varphi}\delta\varphi_{_N} + 2a^2\Phi U_{|\varphi} - 4\bar{\varphi}'\Phi' \;=\; 0. \tag{1.118}$$

where $\delta\varphi_{_N} \equiv \delta\varphi - \bar{\varphi}'\sigma$, with σ being given by Eq. (1.25).

Conformal synchronous gauge.

The Klein-Gordon equation in the synchronous frame is simply given as follows

$$\delta\varphi''_{_S} + 2\mathcal{H}\delta\varphi'_{_S} - \nabla^2\delta\varphi_{_S} + a^2U_{|\varphi\varphi}\delta\varphi_{_S} \;=\; \bar{\varphi}'\left[3\psi'_{_S} - \nabla^2\sigma_{_S}\right], \tag{1.119}$$

where $\delta\varphi_{_S} \equiv \delta\varphi - \xi^0\bar{\varphi}'$, and other variables are as defined in subsection 1.2.6.2. Thus far in this chapter, we have succeeded in establishing the necessary probative framework, by setting the relevant equations in cosmological perturbation theory. These equations will be studied in different scenarios in the following chapters.

The rest of this thesis is given as follows. In chapter 2, we discuss linear clustering and the large-scale structure; in chapter 3 we derive the relativistic density perturbation, i.e. the true observed overdensity of galaxy redshift surveys. We use the GR corrections to investigate the clustering effects of quintessence on the growth of structure, on horizon scales – in chapter 4. In chapter 5 we discuss homogeneous dark energy in general relativity, and probe the effects of the GR corrections in the observed galaxy power spectrum, on horizon scales. In chapter 6, we investigate the large-scale imprint of interacting dark energy on the power spectrum – taking GR corrections into account.

Chapter 2

The Large Scale Structure

The large-scale structure is taken to comprise of galaxies, clusters, filaments, sheets and voids – on scales $\gtrsim 150$ Mpc, where all fluctuation modes are in the linear regime. A key reason for mapping the distribution of galaxies is that it measures the distribution of matter in space, which is a crucial pointer to the details of the past, present, and future of the Universe. It provides a clear window back to the prevalent conditions in the early Universe: on small scales, it is difficult to extract information about the initial fluctuations [38]. Moreover, observations have revealed that the distribution of structures is far from uniform – manifesting in inhomogeneities: in overdensities and underdensities in the galaxy distribution. On small scales, the distribution is very clumpy, while on the largest scales (e.g. at the CMB) the distribution exhibits a global isotropy.

Investigations of the large-scale structure are based on observations that depend on the physical properties of cosmic objects and their populations. Hence we need to gain some (theoretical) understanding of how these objects form and evolve, and how they relate to one another – locally, and otherwise. For convenience, we shall adopt flat space (i.e. $K = 0$) and vanishing anisotropic stresses (i.e. $\Pi = 0$) – and Eq. (1.101) implies $\Psi = \Phi$. Thus we describe the linear clustering (its origin and evolution) of large-scale structure – in section 2.1. We discuss the large-scale fluctuation spectrum in section 2.2. In section 2.3, we discuss biasing in the large-scale structure; and in section 2.4 we discuss the Kaiser approximation of the galaxy contrast. Moreover, in section 2.5, we outline the standard model of cosmology (ΛCDM).

2.1 Linear Clustering in the Universe

In this section, we discuss the origin and evolution of linear perturbations into structure formation. The evolution of the fluctuations can be easily followed once a spectrum of initial fluctuations is specified. This initial spectrum describes the 'initial conditions' necessary for the subsequent formation of structure.

2.1.1 Initial conditions

Large-scale objects (e.g. galaxies and clusters) would not have formed by now, if the Universe had started out 'perfectly' smooth. Hence there must have been a certain mechanism in the early Universe that caused the density to (slightly) fluctuate [38]. It is thought that, shortly after the Big Bang, tiny quantum oscillations in the primeval cosmic content would generate primordial fluctuations (gravitational potential, density,

velocity, etc). These fluctuations would thus serve as the initial conditions which would evolve to form the current observed large-scale structure: in the presence of inflation [58–60] (i.e. a rapid acceleration in the early Universe), these fluctuations get amplified very quickly such that they exit the (causality) horizon. While outside the horizon, these fluctuations would remain frozen until they re-enter the horizon at a later time.

When the Universe evolves to sufficient size, the modes that exited the horizon during inflation will re-enter the horizon again. Eventually, when the modes in different regions have developed into sufficient critical masses, and gravitational forces are significant, they will then collapse to form structures – on various scales. In general, the initial fluctuations will undergo a power-law growth in an expanding Universe due to the partial counteraction of the increase in gravitational force by the expansion, while in a static Universe the increase in gravitational force will rather result in an exponential gravitational instability [40].

Although these fluctuations could have definite evolution in time, their spatial amplitude (and/or distribution) is purely statistical – i.e. at a given (fixed) time, they are completely *random fields* in space, e.g. the perturbation $\Phi(\mathbf{x})$ at spatial position $\mathbf{x}$. Each field is a superposition of various Fourier modes with different amplitudes – i.e. like a wave packet. By 'random', it means that the occurrence of each field value (or the magnitude of the field at a point) is characterized by a given probability. Thus each perturbation (or field) is characterized by a probability density function, at a fixed time. Hence a statistical description of the initial fluctuations is needed.

Therefore, a fluctuation Φ can be expressed as a sum of Fourier modes, given by

$$\Phi(\mathbf{x}, a) \;=\; \int \frac{d^3k}{(2\pi)^3} \Phi(\mathbf{k}, a)\, e^{-i(\mathbf{k}\cdot\mathbf{x})}, \tag{2.1}$$

where $\mathbf{x}$ is the real-space position vector, $\mathbf{k}$ is the Fourier-space position vector, called the "wavevector"; $k = |\mathbf{k}|$ is the wave number, and the integral is evaluated over the entire sample volume. Conversely, the Fourier mode is given by

$$\Phi(\mathbf{k}, a) \;=\; \int d^3x\, \Phi(\mathbf{x}, a)\, e^{i(\mathbf{k}\cdot\mathbf{x})}, \tag{2.2}$$

where $x = |\mathbf{x}|$ is the norm of the position vector. Thus given the spatial stochastic nature of the cosmological fluctuations, we need statistical measures to describe their distribution – at specified times, in space.

One of such statistical measures is the *ensemble average*, which is essentially the expectation value of the given ensemble, denoted by $\langle \cdots \rangle$. The expectation value of an ensemble gives the centre of the distribution of the given ensemble. Thus to get the primordial fluctuation spectrum, which essentially gives the initial conditions, we take the expectation value of the primordial potential field for pairs of points in Fourier space. Inflation predicts a spectrum of initial fluctuations with amplitudes entirely drawn from a statistically homogeneous and isotropic distribution, i.e. a smooth, (nearly) scale-invariant primordial spectrum.

Thus given Eq. (2.2), we obtain the primordial spectrum given by the expectation value of Fourier-space pairs of the primordial potential Φ_p as

$$\left\langle \Phi_p(\mathbf{k}) \Phi_p^*(\mathbf{k}') \right\rangle \;=\; (2\pi)^3 \delta_{\mathrm{D}}(\mathbf{k} - \mathbf{k}') P_{\Phi_p}(k), \tag{2.3}$$

where $\mathbf{k}'$ is a generic wavevector, different from $\mathbf{k}$; asterisk denotes complex conjugate.

The spectrum is given by $k^3 P_{\Phi_p}(k) \propto (k\eta_O)^{n-1}$, where η_O is the time at the present epoch ($a = 1$) [9, 43, 61]. Moreover, statistical isotropy yields: $P_{\Phi_p}(\mathbf{k}) = P_{\Phi_p}(k)$. The exponent n is the spectral index of scalar modes. Inflation predicts a scale-free spectrum (at horizon crossing), i.e. $n \simeq 1$, so that $k^3 P_{\Phi_p} \simeq$ constant. This kind of spectrum is also known as the "Harrison-Zel'dovich" spectrum. Thus the different fluctuation modes will have the same (constant) amplitude at horizon crossing [37, 43]. Note however, that all other fluctuations (e.g. density, velocity) inherit the statistical properties of Φ_p.

2.1.2 Evolution of linear fluctuations

The growth of the large-scale structure progresses via gravitational instability: gravity enables overdense regions to pull in more mass from their surroundings, thus eventually becoming more overdense; while mass is pulled out of underdense regions, hence eventually becoming more underdense [38]. We can describe this growth and progression of structure within general relativity, by time evolution of linear perturbations – given by the equations in subsection 1.2.7.3.

Thus we discuss the growth and evolution of the linear perturbations, in the late times. We consider the late Universe which is dominated by (pressureless) matter, i.e. an 'Einstein-de Sitter' Universe, with the matter density parameter being $\Omega_m \approx 1$ (since other species are negligible), with an equation of state parameter $w = w_m = 0$. Hence we solve Eq. (1.76) to obtain

$$\mathcal{H} \propto a^{-\frac{1}{2}} \propto \eta^{-1}, \qquad \mathcal{H} = \frac{a'}{a} = \frac{2}{\eta}. \tag{2.4}$$

Then given that matter is pressureless, we have that the sound speeds are $c_{sm}^2 = 0 = c_{am}^2$, and given Eqs. (1.97), (1.99) and (1.100), we obtain the density evolution equation

$$\Delta_m'' + \mathcal{H}\Delta_m' = 4\pi G a^2 \bar{\rho}_m \Delta_m \simeq \frac{3}{2}\mathcal{H}^2 \Delta_m, \tag{2.5}$$

where we used that during matter domination, $8\pi G a^2 \bar{\rho}_m = 3\mathcal{H}^2 \Omega_m \approx 3\mathcal{H}^2$. Note that here we used the correct (gauge-independent) general relativistic density perturbation Δ_m, instead of the intrinsic (gauge-dependent) density perturbation δ_m: Δ_m gives the correct Poisson equation (1.100), which is valid on all scales; while δ_m approximates the Poisson equation, i.e. $\nabla^2\Phi \simeq 4\pi G a^2 \bar{\rho}_m \delta_m$ (the 'Newtonian' limit), which holds only on scales much smaller than the Hubble horizon. Thus we solve Eq. (2.5) to obtain the solution given by

$$\Delta_m(k, \eta) \simeq \hat{B}(k)\, \eta^2 \propto \hat{B}(k)\, a(\eta), \tag{2.6}$$

where $\hat{B}$ is an integration constant, and the proportionality follows from Eq. (2.4). In Eq. (2.6), we only give the (physical) growing mode, with the approximation taken at the limit $\eta \to \infty$. Moreover, given that in the matter era, the gravitational potential remains constant in time, i.e. $\Phi'' = 0 = \Phi'$, hence

$$\Phi(k, \eta) = \Phi_+(k), \tag{2.7}$$

where Φ_+ is the non-decaying solution of the gravitational potential evolution equation. Thus given Eq. (1.99), the matter Euler equation is given by

$$V_m' + \mathcal{H} V_m = -\Phi. \tag{2.8}$$

Given Eqs. (2.4) and (2.7), we solve the Euler equation to obtain the matter velocity potential, given by

$$V_m(k,\eta) \simeq -\frac{1}{3}\eta\,\Phi_+(k) \propto -\frac{1}{3}a(\eta)^{\frac{1}{2}}\Phi_+(k), \tag{2.9}$$

where, similarly, the approximation is taken at the limit $\eta \to \infty$: to give the only growing mode with time. Thus Eqs. (2.6) and (2.9) describe the evolution of the large-scale matter density and velocity perturbations, respectively, in the late epochs. We see that while the velocity potential evolves linearly with time, the density perturbation is a quadratic function of time. Conversely, the density perturbation evolves linearly with the scale factor, and the velocity potential evolves as the square root of the scale factor. During this regime, the gravitational potential (2.7) remains constant with time.

2.1.3 Linear transfer function

The perturbations from the primordial Universe can be split into three main regimes: the 'long-mode' regime (inflationary epoch), in which case the modes possess wavelengths longer than the horizon; the 'medium-mode' regime (radiation epoch), where the modes had intermediate wavelengths within the horizon; and the 'short-mode' regime (late epochs), when the modes have evolved well into the horizon – with wavelengths much shorter than the horizon. It is these (relatively) short modes that evolve to form the current large-scale (matter) structures in the Universe.

After the matter-radiation equality ($a = a_{eq}$), matter domination sets in – i.e. the late times ($a \gg a_{eq}$). Moreover, at horizon re-entry the modes get affected significantly, in amplitude and evolution. The smaller modes enter the horizon earlier (i.e. $a \ll a_{eq}$), and are affected differently from the longer modes, which enter the horizon much later (i.e. $a \gg a_{eq}$). But driven by radiation pressure, the modes lose most of their primordial information during the radiation domination. Hence after equality, into the late times, the evolutionary behaviour of the modes from the primordial times needs to be corrected for. This can be done conveniently via the linear *transfer function* $T(k)$, given by [43]

$$T(k) \equiv \frac{10}{9}\frac{\Phi_d(k)}{\Phi_p(k)}, \qquad \Phi_d = \Phi(a_d), \tag{2.10}$$

where a_d is the scale factor at the radiation-matter decoupling epoch. The factor, 9/10, accounts for the slight decline in amplitude of the large-scale mode of Φ_p: i.e. after crossing the equality epoch. Thus the linear transfer function accounts for the evolution of the linear perturbations from horizon crossing, through radiation domination, until radiation-matter transition. (See e.g. [43], for some fitting formulas for $T(k)$.)

2.1.4 Linear growth functions

In order to probe the large-scale structure of the late-time Universe ($a \gg a_{eq}$), we need to relate the linear perturbations at late epochs to the primordial potential via linear *growth functions* and the linear transfer function (2.10). Given Eq. (2.7), we connect the

primordial inflationary perturbations to the decoupling epoch via the potential [1, 2]:

$$\Phi(k,a) = \frac{D_\Phi(k,a)}{a}\Phi_d(k), \quad a \geq a_d, \tag{2.11}$$

$$\Phi_d(k) = \frac{9}{10}\Phi_p(k)T(k), \quad a_d > a_{eq}, \tag{2.12}$$

$$\Phi_p(k) = A\frac{\Omega_{m0}}{D_{\Phi 0}(k)}\left(\frac{k}{H_0}\right)^{(n-4)/2}. \tag{2.13}$$

where D_Φ is the gravitational potential linear growth function, which is normalized by $D_\Phi(k,a_d) = a_d$. The subscribe "0" denotes (hereafter) values at the present epoch. The constant $A = 5\sqrt{2}\,\pi\,\delta_H/(3H_0^{3/2})$ is the primordial amplitude of curvature perturbations, and δ_H (a constant) is the amplitude of scalar modes at horizon crossing [43].

Next we connect the matter density perturbation to the inflationary perturbations at decoupling. From Eq. (2.6), we get that $\Delta_m(k,a)/a = \Delta_m(k,a_d)/a_d$, hence we define the linear growth function D_m of matter density perturbation by

$$D_m(k,a) \equiv \frac{\Delta_m(k,a)}{\Delta_m(k,a_d)}\,a_d, \tag{2.14}$$

which also normalizes to $D_m(k,a_d) = a_d$. Thus at decoupling the gravitational potential is entirely driven by matter, such that both the gravitational potential and the matter density perturbations grow at the same rate – equal to the scale factor. Then by evaluating the Poisson equation (1.100) (i.e. with $K = 0 = \Pi$) at decoupling to obtain $\Delta_m(k,a_d)$, and using the solution $\bar{\rho}_m \propto a^{-3}$ of the continuity equation (1.77), Eq. (2.14) is thus given by [1, 2]

$$\Delta_m(k,a) = -\frac{2k^2}{3\Omega_{m0}H_0^2}D_m(k,a)\Phi_d(k), \tag{2.15}$$

where we assumed $(1-\Omega_m(a_d)) \ll 1$, hence we neglected other species in the Poisson equation – i.e. at decoupling, with Φ_d being given by Eq. (2.12). Similarly, from Eqs. (2.4) and (2.9) we have $V_m \propto \Phi/\mathcal{H}$. Hence we defined the matter velocity potential linear growth function D_{V_m}, given by

$$D_{V_m}(k,a) \equiv \frac{V_m(k,a)}{V_m(k,a_d)}\,a_d\,\mathcal{H}(a_d), \tag{2.16}$$

which normalizes to $D_{V_m}(k,a_d)/\mathcal{H}(a_d) = a_d$. In a similar manner, by evaluating the gravitational potential evolution equation (1.102) at the Einstein-de Sitter epoch $a = a_d$, i.e. with $\Phi'(a_d) = 0$, and using that $\bar{\rho}_m \propto a^{-3}$, Eq. (2.16) is thus given by [1, 2]

$$V_m(k,a) = -\frac{2}{3\Omega_{m0}H_0^2}D_{V_m}(k,a)\Phi_d(k), \tag{2.17}$$

where also we have used that $(1-\Omega_m(a_d)) \ll 1$, and thus have neglected velocities of other species in the potential equation (1.102) at decoupling. We see that while D_Φ and D_m are dimensionless, D_{V_m} has the dimension of the Hubble parameter $\mathcal{H}$.

2.2 The Large Scale Fluctuation Spectrum

Understanding the current spatial distribution of matter is crucial to describing the past and predicting the future of the Universe. For example, the large-scale matter distribution indicates that matter was very smoothly distributed at early times; the smaller the initial fluctuations, the longer it takes for these fluctuations to grow enough to form galaxies and other structures. Moreover, if the mean mass density on large scales becomes greater than a certain critical value, then the expansion of the Universe will eventually cease and reverse – to collapse. Conversely, if the average density becomes lower than this critical value, the cosmic expansion will continue infinitely [38].

However, it is difficult for any model of the Universe to give a *true* description of the matter distribution in the large-scale structure. This is because the observed large-scale structure around us depends on the specific initial conditions in the early Universe, which are highly statistical. Consequently, the distribution of the cosmological fluctuations in space (but not in time) is stochastic. Thus these fluctuations behave as random fields – such that at a given time, their occurrence at some points in space is purely statistical, characterized by a probability. Nevertheless, we can predict or estimate the (macroscopic) statistical properties of the matter distribution as a function of time, using statistical measures such as: the probability of a galaxy forming or being found within the vicinity of another galaxy, the average number density of clusters of galaxies above a given mass, and so on.

Moreover, inflation predicts statistical homogeneity and isotropy of the initial fluctuations: a feature which is preserved on the largest scales. This property allows for the simple description of the large-scale fluctuations by Gaussian random functions (or fields). Consequently, the statistics involved is somewhat straightforward. In the rest of this section we discuss the statistics used in describing the spatial distribution of the large-scale matter fluctuations.

2.2.1 The correlation function

The clustering of objects (hence, of matter) in the Universe is quantified by using a variety of statistical quantities which measure the degree to which the distribution of the objects differ from a purely random configuration [38]. A most widely used statistic is the two-point *correlation function* [38, 62], defined in real space, given by

$$C_m(|\mathbf{x}-\mathbf{y}|,a) \;\equiv\; \langle \Delta_m(\mathbf{x},a)\Delta_m^*(\mathbf{y},a)\rangle\,, \tag{2.18}$$

where given statistical isotropy we used that $C_m(\mathbf{x},\mathbf{y}) = C_m(\mathbf{x}-\mathbf{y}) = C_m(|\mathbf{x}-\mathbf{y}|)$, at a given epoch; asterisk denotes complex conjugate. Note that Δ_m is also expressed as in Eq. (2.1). The two-point correlation function is the 'expectation value' of finding pairs of objects at positions $\mathbf{x}$ and $\mathbf{y}$, separated by a distance $|\mathbf{x}-\mathbf{y}|$ at a given time – i.e. given a matter perturbation at a position $\mathbf{x}$, then C_m measures the probability of finding another perturbation (in its neighbourhood) at position $\mathbf{y}$ and distance $|\mathbf{x}-\mathbf{y}|$ away. Thus it gives the tendency of matter peaks to group or stay close to each other. For an uncorrelated distribution, we have $C_m = 0$; while $C_m > 0$ indicates strong correlation or clustering, and $C_m < 0$ indicates anti-correlation.

2.2.2 The power spectrum

The power spectrum is the Fourier transform of the two-point correlation function. The two quantities are complementary: features that are enhanced in the power spectrum will be diminished in the correlation function, and vice versa.

Thus the Fourier transform $\hat{\Delta}_m(\mathbf{k})$ (of $\Delta_m(\mathbf{x})$) is similarly given as in Eq. (2.2). Then by taking the expectation of pairs in Fourier space, we have [62]

$$\left\langle \hat{\Delta}_m(\mathbf{k},a)\hat{\Delta}^*_m(\mathbf{k}',a)\right\rangle = \int d^3x\, e^{i(\mathbf{k}\cdot\mathbf{x})} \int d^3x'\, \left\langle \Delta_m(\mathbf{x},a)\Delta^*_m(\mathbf{x}',a)\right\rangle\, e^{-i(\mathbf{k}'\cdot\mathbf{x}')}, \quad (2.19)$$

$$= \int d^3x\, e^{i(\mathbf{k}\cdot\mathbf{x})} \int d^3y\, C_m(y,a)\, e^{-i\,\mathbf{k}'\cdot(\mathbf{x}+\mathbf{y})}, \quad (2.20)$$

where we used Eq. (2.18) and that $\mathbf{x}' = \mathbf{x}+\mathbf{y}$, with $y = |\mathbf{y}|$; and $\mathbf{k}'$ is a generic wavevector, different from $\mathbf{k}$. Then by using the definition of the Dirac delta function $\delta_{\rm D}$, we have Eq. (2.20) to be given as follows

$$\left\langle \hat{\Delta}_m(\mathbf{k},a)\hat{\Delta}^*_m(\mathbf{k}',a)\right\rangle = (2\pi)^3\delta_{\rm D}(\mathbf{k}-\mathbf{k}') \int d^3y\, C_m(y,a)\, e^{i(\mathbf{k}\cdot\mathbf{y})}, \quad (2.21)$$

$$\equiv (2\pi)^3\delta_{\rm D}(\mathbf{k}-\mathbf{k}')\, P_m(k,a), \quad (2.22)$$

where $k = |\mathbf{k}|$ is the wave number. The dependence on k is a result of the statistical homogeneity and isotropy (or Gaussianity) prediction by inflation. The quantity P_m is thus the matter *power spectrum*, which describes the large-scale distribution of matter perturbations. Thus we obtain the relationship between the power spectrum and the correlation function, given by

$$P_m(k,a) = \int d^3y\, C_m(y,a)\, e^{i(\mathbf{k}\cdot\mathbf{y})}, \quad (2.23)$$

$$C_m(y,a) = \int \frac{d^3k}{(2\pi)^3}\, P_m(k,a)\, e^{-i(\mathbf{k}\cdot\mathbf{y})}, \quad (2.24)$$

where we see that P_m is indeed the Fourier transform of C_m, i.e. they are Fourier inverses of each other. For a Gaussian primordial fluctuations spectrum (i.e. with phases of the different Fourier modes being mutually independent), P_m, or equivalently C_m, is sufficient to give a complete statistical description of the matter distribution [38].

Now given Eqs. (2.3), (2.13), and (2.15), we then obtain from Eq. (2.22) the expression of the matter power spectrum, given by [1, 2]

$$P_m(k,a) = \frac{9A^2}{50\pi^3 H_0^n}\, k^n\, T^2(k) \left[\frac{D_m(k,a)}{D_{\Phi 0}(k)}\right]^2. \quad (2.25)$$

We see that any information induced by the underlying physics, will be imprinted in the matter power spectrum via the ratio $D_m/D_{\Phi 0}$, and will show on the large scales. Evaluating P_m at various epochs, hence a, will allow us to follow how matter clumps as a function of time; and at a particular epoch, P_m describes how matter perturbations are distributed over various cosmic scales (see chapters 4 and 5).

2.3 Biasing in Large Scale Structure

Observations of the large-scale structure is based on measuring the electromagnetic emissions from luminous objects. This probes the matter distribution over the given scales. However, the relation between fluctuations in the distribution of objects and fluctuations in the distribution of mass is not one-to-one – the emissions from these objects do not accurately trace the underlying matter content. The inability of these objects to map the true underlying mass is corrected by a factor, called the *bias*: i.e. the uncertainty between the distributions of objects and the underlying mass [38].

Here we discuss some of the biasing (or discrimination) in tracers of the large-scale (matter) structure. For the main goal of this thesis, we focus only on two key discrimination types: galaxy biasing, and magnification biasing.

2.3.1 Galaxy bias

Cosmological perturbation theory allows us to describe the evolution and distribution of matter density perturbations in the Universe. However, in reality the distribution of the matter perturbations is not directly observable: only luminous objects such as galaxies, whose distribution traces that of the matter, are observable [1, 2]. But the ability of galaxies to trace the underlying matter is influenced by the clustering properties of the galaxies, e.g. whether or not density is uniformly distributed. In turn, the clustering properties of galaxies depend on both the local environment and on the intrinsic properties of the galaxies [38]. However, observations also depend on the physics along the line of sight, i.e. along the photon path. On linear scales, where the Universe is (fairly) homogeneous and isotropic, the bias is scale-independent.

Consider the mass distribution of cold dark matter (being the dominant matter component) in a given halo. If the mass density perturbation of the dark matter is given by $\delta\hat{\rho}_m$, then the number density perturbation $\delta\hat{n}_{\rm g}$ of the galaxies associated with the halos of a given dark matter mass distribution is given by [63]

$$\left(\frac{\delta\hat{n}}{\bar{n}}\right)_{\rm galaxies} \;=\; b\left(\frac{\delta\hat{\rho}}{\bar{\rho}}\right)_{\rm mass}, \tag{2.26}$$

where b is the linear (scale-independent) *galaxy bias* [3–5, 7, 8] (see the given references regarding the link between linear scales and the scale-independent bias). Thus given the galaxy contrast, i.e. the fractional galaxy number density perturbation $\hat{\delta}_{\rm g} \equiv \delta\hat{n}_{\rm g}/\bar{n}_{\rm g} = (\hat{n}_{\rm g} - \bar{n}_{\rm g})/\bar{n}_{\rm g}$, to first order we have

$$\hat{\delta}_{\rm g} \;=\; \frac{1}{\bar{n}_{\rm g}}\frac{\partial\bar{n}_{\rm g}}{\partial\bar{\rho}_m}\,\delta\hat{\rho}_m \;\equiv\; b\,\hat{\delta}_m, \tag{2.27}$$

where $\hat{\delta}_m = \delta\hat{\rho}_m/\bar{\rho}_m$, and $\bar{n}_{\rm g}$ and $\bar{\rho}_m$ are the background galaxy number density and dark matter mass density, respectively. Here we define the linear galaxy bias by

$$b \;\equiv\; \left.\frac{\partial\ln n_{\rm g}}{\partial\ln\rho_m}\right|_a. \tag{2.28}$$

Hence, on very large scales, the galaxy bias $b = b(a)$ is scale-independent. Moreover, $\hat{\delta}_{\rm g}$ is an observable, hence is automatically gauge-invariant. By implication, $\hat{\delta}_m$ is also gauge-invariant. In fact, b is only physical when it is defined in the dark matter and

galaxy rest frames (which coincide on large scales), respectively. Thus $\hat{\delta}_m$ corresponds to the perturbation in the dark matter rest frame – and given Eq. (1.90), we have

$$\hat{\delta}_m \equiv \frac{\delta\rho_m}{\bar{\rho}_m}\Big|_{\rm rf} = \Delta_m, \tag{2.29}$$

where Δ_m is the comoving matter (mass) density perturbation. Similarly, by gauge transformation (1.42) (also Eq. (1.83)), we have that

$$\hat{\delta}_{\rm g} \equiv \frac{\delta n_{\rm g}}{\bar{n}_{\rm g}}\Big|_{\rm rf} = \delta_{\rm g} + \frac{\bar{n}'_{\rm g}}{\bar{n}_{\rm g}}(v_{\rm g} + B) = \Delta_{\rm g}, \tag{2.30}$$

where $\Delta_{\rm g}$ is the comoving galaxy number density perturbation, and $\delta_{\rm g} = \delta n/\bar{n}_{\rm g}$ is the galaxy number density perturbation. We have used, by Eq. (1.86), that in the rest frame of the galaxies $\xi^0 = -(v_{\rm g}+B)$, with $v_{\rm g}$ being the galaxy peculiar velocity potential. Thus the galaxy bias is given in the gauge-invariant form, by [1, 2]

$$\Delta_{\rm g}(k,a) = b(a)\,\Delta_m(k,a), \tag{2.31}$$

which is valid on all linear scales (and assuming Gaussian primordial perturbations). By Eq. (2.31), the scale-independent bias is physically defined. In the literature, Eq. (2.31) is often approximated in the Newtonian limit by $\Delta_{\rm g} \simeq b\,\delta_m$. On sub-Hubble scales, different gauge choices for δ_m agree, i.e. they result to the same matter power spectrum. However, on scales near and beyond the Hubble horizon, they disagree [2] – δ_m becomes gauge-dependent on very large scales, leading to different power spectra: thus cannot be used to define the physical bias [1]. This behaviour is previously illustrated in [9].

In the rest of this thesis, we shall not consider the (physical) galaxy bias in any further details than we have discussed in this section. For further details, e.g. on the relativistic context of the galaxy bias, see [3–5].

2.3.2 Magnification bias

Besides galaxy biasing, gravitational weak lensing (lensing, henceforth) can generate bias in the observed objects. It causes signals from objects to be amplified or magnified: a phenomenon called cosmic 'magnification'. For example, in flux-limited surveys, i.e. with a given (instrument) flux threshold, magnification can cause faint objects – whose signal, without lensing, would be too weak for inclusion – to be counted [62]. This increases the number, $\tilde{\mathcal{N}}$, of objects counted per unit solid angle (in redshift space).

The magnification $\tilde{\mathcal{M}}$ (measured in redshift space), is defined by [62]

$$\tilde{\mathcal{M}}^{-1} \equiv \frac{\tilde{\mathcal{N}}}{\bar{\mathcal{N}}}, \tag{2.32}$$

where $\bar{\mathcal{N}}$ is the mean number per solid angle, i.e. the number that would be observed in a unit solid angle in the absence of lensing. This gives the number of objects with unlensed fluxes in an average, homogeneous Universe. Thus a signal bundle moving through an overdense region (e.g. galaxies and clusters) will be more focused, with $\tilde{\mathcal{M}} > 1$, than a bundle moving through the average, homogeneous Universe. On the other hand, a signal bundle moving through an underdense region (e.g. a void) will be less focused, having $\tilde{\mathcal{M}} < 1$. A random sample will have a mean magnification of $\bar{\mathcal{M}} = 1$.

Nevertheless, the perturbation in the magnification $\delta\tilde{\mathcal{M}} = \tilde{\mathcal{M}} - \bar{\mathcal{M}}$ induces an excess distortion in the observed number density, given by $\check{\delta}_n = \check{\delta}_n(\tilde{\mathcal{M}})$ – i.e. depending on magnification. Hence the contribution solely from magnified sources, i.e. the magnification distortion in the observed galaxy number density, is given by

$$\left(\frac{\delta\check{n}}{\bar{n}}\right)_{\text{magnified galaxies}} = \mathcal{Q}\left(\frac{\delta\tilde{\mathcal{M}}}{\bar{\mathcal{M}}}\right)_{\text{magnification}}, \tag{2.33}$$

where $\mathcal{Q}$ is the *magnification bias* [5, 62]. Then to first order we have that

$$\check{\delta}_n(\tilde{\mathcal{M}}) \equiv \frac{\delta\check{n}_{\rm g}}{\bar{n}_{\rm g}}(\tilde{\mathcal{M}}) = \frac{1}{\bar{n}_{\rm g}}\frac{\partial\bar{n}_{\rm g}}{\partial\bar{\mathcal{M}}}\,\delta\tilde{\mathcal{M}}, \tag{2.34}$$

where $\check{n}_{\rm g}$ denotes the (extra) galaxy number density sourced purely by magnification. Thus from Eq. (2.34) we have that the magnification contrast $\tilde{\delta}_{\mathcal{M}} \equiv \delta\tilde{\mathcal{M}}/\bar{\mathcal{M}}$ traces the induced galaxy contrast $\check{\delta}_n$ up to the magnification bias, given by

$$\check{\delta}_n(k,a) = \mathcal{Q}(a)\,\tilde{\delta}_{\mathcal{M}}(k,a). \tag{2.35}$$

Note that $\check{\delta}_n$ is an observable, hence is independent of gauge. Here the magnification bias is given by

$$\mathcal{Q} \equiv \left.\frac{\partial\ln n_{\rm g}}{\partial\ln\mathcal{M}}\right|_a. \tag{2.36}$$

Again we have that, for linear perturbations (of large-scale structure), $\mathcal{Q}$ is a physical, scale-independent quantity – i.e. by virtue of the gauge-independence of Eq. (2.35). The magnification bias thus corrects for the discrimination introduced in the observation sample, owing to cosmic magnification.

Thus magnification will transform the galaxy contrast so that the effective large-scale bias corresponds to the sum of the given biases, i.e.

$$\Delta_{\rm gal}(k,a) = b(a)\,\Delta_m(k,a) + \mathcal{Q}(a)\,\tilde{\delta}_{\mathcal{M}}(k,a). \tag{2.37}$$

As we shall see later (chapter 3), although Δ_m solves the large-scale gauge problem posed by δ_m, the density contrast $\Delta_{\rm g}$ is only an approximation to the (physical) observed galaxy number density perturbation: $\Delta_{\rm g}$ does not match the physical galaxy number density perturbation on very large scales – it requires corrections to account for relativistic effects. We compute these corrections in chapter 4, where we also compute the magnification contrast $\tilde{\delta}_{\mathcal{M}}$, in the correct relativistic approach.

2.4 The Kaiser Approximation

In observational cosmology, observers measure the redshift-space coordinates $\mathbf{s}$ of sources, and not their real-space coordinates $\mathbf{x}$. In a perfectly homogeneous Universe, e.g. a background FRW Universe, the transformation from real to redshift space would be one-to-one: with redshifts directly replacing real (radial) distances. In such case, the evolution of sources would follow the cosmic expansion (i.e. the Hubble flow). However, in an inhomogeneous Universe, density fluctuations in sources would generate local gravitational fields which in turn cause distortions (i.e. deviations) to the flow of sources. These distortions would surface in redshift space as small peculiar velocity fields. Thus

the transformation between real and redshift space would no longer be one-to-one. These distortions are simply known as *redshift space distortions* [64–67].

Two of the observational consequences of the redshift space distortions include: the 'finger-of-God' effect, in which the dense central regions of galaxies and clusters appear elongated along the line of sight – caused by incoherent high-magnitude velocities, on small non-linear scales. This reduces the correlation function, hence the power spectrum. The second effect (being a large-scale effect), which is caused by the relative velocity field of oppositely flowing overdensity fields along the line of sight, is that a cluster appears to be compressed (or flattened) when viewed along the line of sight – on large scales. This way the correlation strength, and hence the power spectrum, is enhanced [64, 65].

Thus the galaxy contrast $\Delta_{\rm g}$ (2.31) (hence, $\Delta_{\rm gal}$ (2.37)) needs to be corrected for these effects. For the main goal of this thesis, we shall consider only the large-scale effect. Now, the peculiar gravitational fields imply that apart from the Hubble-flow velocity, cosmic sources will have an additional peculiar velocity, i.e. the redshift-space distance (in a unit expansion time) to a source may generally be given by [64–67]

$$\tilde{s} \;=\; \mathcal{H}\,\bar{r} \;-\; \mathbf{n}\cdot[\mathbf{V}(\mathbf{x}) - \mathbf{V}(\mathbf{0})]\,. \tag{2.38}$$

The first term on the right hand side corresponds to the Hubble's law (see e.g. [27]), and the second term is a consequence of Doppler effect on the peculiar velocities: $\mathbf{V}(\mathbf{x})$ is the comoving peculiar velocity at position $\mathbf{x} = \bar{r}\,\mathbf{n}$ in the photon path, where $\mathbf{n}$ is a unit vector along the photon path towards the observer, with $\bar{r} = |\mathbf{x}|$ being the background comoving radial distance – i.e. $\mathbf{x}$ is taken to lie along the comoving radial coordinate, for convenience; and $\mathbf{V}(\mathbf{0})$ is the comoving peculiar velocity at the observer. The Hubble term $\mathcal{H}\bar{r}$ corresponds to the distance travelled in a unit expansion time by sources moving purely by the cosmic expansion in a Universe with no distortions.

Note that in Eq. (2.38), the first term is a background quantity and the second term is a perturbation. This implies that a distance (or set of coordinates) in real space does not correspond to the same distance (or set of coordinates) in redshift space: the latter is distorted by peculiar velocities, via Doppler effect. (The peculiar velocities are perturbations by virtue of their definition.) Thus the total number of galaxies $\hat{n}_{\rm g}(\mathbf{x})d^3r$ counted in a volume element d^3r around $\mathbf{x}$, is given by

$$\hat{n}_{\rm g}(\mathbf{x})d^3r \;=\; \tilde{n}_{\rm g}(\mathbf{s})d^3s, \tag{2.39}$$

where $s = |\mathbf{s}|$, and $\mathbf{s}$ is the redshift-space position vector; $\tilde{n}_{\rm g}$ is the galaxy number density in redshift space, and d^3s is the volume element in redshift space. In Eq. (2.39) we used the fact that the number of observed sources is a physical quantity, which implies that in any given sky volume the measured number of galaxies remains the same – in redshift space and in real space. Then by assuming isotropy in both redshift space and real space, which follows from the isotropy of a FRW space, we get that $d^3s = [(s/\bar{r})^2\,\partial_r s]\,d^3r$. Thus by setting $s \equiv \tilde{s}/\mathcal{H}$, and using Eq. (2.38), we obtain (see also [64])

$$d^3r \;=\; \left[1 - \frac{V_\parallel(\mathbf{x}) - V_\parallel(\mathbf{0})}{\mathcal{H}\,\bar{r}}\right]^{-2}\left[1 - \frac{\partial_r V_\parallel(\mathbf{x})}{\mathcal{H}}\right]^{-1} d^3s, \tag{2.40}$$

where $V_\parallel$ is the component of the peculiar velocity along the line of sight, given by

$$V_\parallel \;\equiv\; \mathbf{n}\cdot\mathbf{V} \;=\; -\partial_r V, \tag{2.41}$$

with $\partial_r \equiv \partial/\partial r$ (henceforth) being the partial derivative with respect to the comoving radial distance. Note that the negative sign in Eq. (2.41) – which corresponds to the negative sign in front of the second term (in square brackets) in Eq. (2.38) – specifies the direction of observation, i.e. here we choose the direction of observation to be opposite that of the radial coordinate, given by $-\mathbf{n}$. Then given Eq. (2.40), the redshift-space galaxy number density (2.39) given (to first order) in terms of real coordinates is

$$\tilde{n}_{\rm g}(\mathbf{x}) \;=\; \bar{n}_{\rm g}\left[1+\hat{\delta}_{\rm g}(\mathbf{x})+\frac{\partial_r V_{\parallel}(\mathbf{x})}{\mathcal{H}}+2\frac{V_{\parallel}(\mathbf{x})-V_{\parallel}(\mathbf{0})}{\mathcal{H}\,\bar{r}}\right], \tag{2.42}$$

where $\hat{\delta}_{\rm g}$ is given by Eq. (2.27): the galaxy contrast without magnification. By using the definition of the large-scale physical galaxy bias (2.31), and neglecting the peculiar velocity at $\mathbf{0}$, we can express the galaxy contrast of redshift space – given by

$$\tilde{\delta}_{\rm g}(\mathbf{x}) \;=\; \Delta_{\rm g}(\mathbf{x})+\frac{\partial_r V_{\parallel}(\mathbf{x})}{\mathcal{H}}+2\frac{V_{\parallel}(\mathbf{x})}{\mathcal{H}\,\bar{r}}, \tag{2.43}$$

where $\tilde{\delta}_{\rm g} \equiv \delta\tilde{n}_{\rm g}/\bar{n}_{\rm g} = (\tilde{n}_{\rm g}-\bar{n}_{\rm g})/\bar{n}_{\rm g}$, with the background number density $\bar{n}_{\rm g}$ remaining the same in redshift space and real space. The two peculiar velocity terms in Eq. (2.43) give the total contributions from the redshift space distortions in the galaxy number density perturbation. Moreover, the last term is the contribution particularly from the Doppler effect – hence 'Doppler term', hereafter.

Furthermore, if we take the 'plane-parallel' or 'flat-sky' limit (i.e. the far-field approximation, where the galaxy is far away) in Fourier space, we get that the Doppler term is negligible compared to $\Delta_{\rm g}$. On the other hand, the term with the gradient of the peculiar velocity remains of the same order with $\Delta_{\rm g}$, owing to the shear of the peculiar velocity field gradient [64]. Hence we obtain the flat-sky limit, given by

$$\tilde{\delta}_{\rm g}(\mathbf{k},a) \;=\; \Delta_{\rm g}(\mathbf{k},a)+\frac{\partial_r V_{\parallel}(\mathbf{k},a)}{\mathcal{H}(a)} \;\equiv\; \hat{\Delta}_{\rm g}(\mathbf{k},a). \tag{2.44}$$

Thus Eq. (2.44) gives the correction to the changes caused purely by the gradient of the peculiar velocities. This correction was first computed by Kaiser [64], hence is otherwise known as the 'Kaiser approximation' – given the fact that it only provides an approximation to the other relevant large-scale effects (see chapter 3). The Kaiser approximation is conventionally taken as the standard expression for the galaxy number density perturbation, where the term $\partial_r V_{\parallel}/\mathcal{H}$ is popularly called, the 'Kaiser' or 'redshift distortion' term.

On very large scales where the matter and galaxy rest frames coincide (given the homogeneity and isotropy of the large scales), we have the matter and the galaxy velocities to be equal: $V_m^{\parallel} = V_{\parallel} = V_{\rm g}^{\parallel}$, i.e. galaxies follow trajectories that are parallel to that of the underlying matter, hence there is no momentum change (or exchange) between the two frames to cause velocity bias. Then given Eq. (2.44), we may define a redshift-distortion parameter, given by

$$f \;\equiv\; \frac{k^2 V_m}{\mathcal{H}\Delta_m}, \tag{2.45}$$

which determines the excess fluctuation sourced by the redshift space distortions, in the galaxy density perturbation. Then in Fourier space, given Eq. (2.41), we have

$$\partial_r V_m^{\parallel} \;=\; -\partial_r^2 V_m \;=\; \mu^2 k^2 V_m, \tag{2.46}$$

where $\partial_r^2 \to -\mu^2 k^2$, with $\mu = -\mathbf{n}\cdot\mathbf{k}/k$ being the cosine between $\mathbf{n}$ and $\mathbf{k}$. Thus given Eqs. (2.31), (2.45) and (2.46), we rewrite the Kaiser approximation (2.44) given by

$$\hat{\Delta}_{\rm g} \;=\; (b + f\mu^2)\Delta_m. \tag{2.47}$$

We see that apart from the normal galaxy bias b, the redshift space distortions induce an extra biasing via f: thus further preventing galaxies from accurately tracing the underlying matter – along the line of sight. Moreover, we obtain the redshift-space galaxy power spectrum, given by

$$P_{\rm g}(k,\mu,a) \;=\; \left[b(a) + f(k,a)\mu^2\right]^2 P_m(k,a), \tag{2.48}$$

i.e. neglecting the effect of cosmic magnification (see Eq. (2.37)), where P_m is given by Eq. (2.25). Of course, the Kaiser approximation does not include magnification effects. For investigations along the line of sight, i.e. parallel to the radial coordinate, we will have $\mu = 1$ – hence we obtain only the radial galaxy power spectrum; and $\mu = 0$ corresponds to the transverse power spectrum – i.e. only the power spectrum of the galaxy distribution normal to the direction of observation.

In chapter 3, we compute the corrections to the Kaiser approximations (2.47) and (2.48) – in the correct general relativistic approach: thus obtaining the relativistic density perturbation which corresponds to the true measured density perturbation of large-scale galaxy redshift surveys.

2.5 The Concordance Model

In this section we discuss the simplest, but standard model of cosmology, where DE is given as the (static) vacuum energy – whose density is determined by a constant Λ, called 'the cosmological constant', living in the background gravitational field. Here the Universe is assumed to be dominated by Λ and cold dark matter (CDM), hence is otherwise called the ΛCDM. In the presence of the cosmological constant, the Einstein's gravitational field equations are given by

$$G_{\mu\nu} + \Lambda g_{\mu\nu} \;=\; 8\pi G\, T_{\mu\nu}, \tag{2.49}$$

where the various terms are given by Eq. (1.1). Here, Λ serves as the quantity responsible for the late-time cosmic acceleration – which starts to dominate only at very recent times.

For the rest of this thesis (except for chapter 3), we shall maintain the conformal Newtonian gauge with vanishing anisotropic stress. Thus the perturbed metric is

$$ds^2 \;=\; a^2\left[-(1+2\Phi)d\eta^2 + (1-2\Phi)d\mathbf{x}^2\right], \tag{2.50}$$

where Φ is the gravitational potential, here being gauge-invariant (see chapter 1).

2.5.1 The background equations

By following the calculations in chapter 1, we obtain the comoving Hubble parameter from Eq. (2.49), given by

$$\mathcal{H}^2 \;=\; \frac{8\pi G a^2}{3}\bar{\rho}_m + \frac{\Lambda a^2}{3}. \tag{2.51}$$

Here the total background energy density is $\bar{\rho} = \bar{\rho}_m + \Lambda/(8\pi G)$. Whence we obtain

$$\Omega_m \;+\; \Omega_\Lambda \;=\; 1, \tag{2.52}$$

where the matter and Λ density parameters are given, respectively, by

$$\Omega_m \;\equiv\; \frac{8\pi G a^2}{3\mathcal{H}^2}\bar{\rho}_m, \qquad \Omega_\Lambda \;\equiv\; \frac{\Lambda a^2}{3\mathcal{H}^2}, \tag{2.53}$$

with the respective equation of state parameters being given by $w_m = 0$ and $w_\Lambda = -1$. We then have the evolution equation for the Hubble parameter to be given by

$$\mathcal{H}' \;=\; -\frac{1}{2}\left(1 - 3\Omega_\Lambda\right)\mathcal{H}^2. \tag{2.54}$$

Equation (2.54) is also known as the background acceleration equation, which describes the accelerated expansion of the late Universe.

2.5.2 The perturbations equations

Here we give the equations of the linear perturbations. Thus the gravitational potential in this scenario evolves by

$$\Phi' + \mathcal{H}\Phi \;=\; -\frac{3\mathcal{H}^2}{2}\Omega_m V_m, \tag{2.55}$$

which is constraint by the Poisson equation, given by

$$\nabla^2\Phi \;=\; \frac{3}{2}\mathcal{H}^2\Omega_m\Delta_m. \tag{2.56}$$

By definition, there are no perturbations in Λ, thus its peculiar velocity potential and density perturbation vanish, i.e. $V_\Lambda = 0 = \Delta_\Lambda$. The perturbed matter equations are

$$\Delta_m' \;=\; -\nabla^2 V_m, \tag{2.57}$$

$$V_m' + \mathcal{H}V_m \;=\; -\Phi, \tag{2.58}$$

which hold on all scales and epochs. The matter physical and adiabatic sound speeds are $c_{sm} = 0 = c_{am}$, respectively.

2.5.3 The linear growth rate

In ΛCDM, the gravitational potential growth function (2.11) is purely dependent on the scale factor (or time), and is equal to the matter density growth function (2.15) – on all scales and at all epochs. Consequently, the velocity potential growth function (2.17) is

equal to the time derivative of the density growth function, i.e. we have [1, 2]

$$\Lambda\text{CDM:} \qquad D_\Phi(k,a) \;=\; D(a) \;=\; D_m(k,a), \qquad D_{V_m}(k,a) \;=\; \frac{\partial D(a)}{\partial \eta}. \tag{2.59}$$

Thus given Eqs. (2.15), (2.45), (2.46), (2.57) and (2.59), we obtain that

$$f \;=\; \frac{\partial \ln D(a)}{\partial \ln a}, \tag{2.60}$$

which is valid for all scales and all epochs – i.e. in ΛCDM, we have $f(k,a) = f(a)$ where $f = \Delta_m'/(\mathcal{H}\Delta_m)$. Then during matter domination in particular, f is constant, hence we have $\Delta_m \propto a^f$: thus f determines the rate at which the linear density perturbations of matter grow with time, in which case it is called the *linear growth rate*. Moreover, in the matter domination we have $D(a) = a$, and by Eq. (2.60): $f(a) = 1$, which is also confirmed by Eq. (2.6). However, when Λ begins to set in, f consequently deviates from being constant and starts to evolve with the scale factor, i.e. $f(a) \neq 1$.

Chapter 3

The Relativistic Density Perturbation

Until recently, galaxy surveys had been considered to map the distribution of matter density perturbations (up to a bias factor), characterised by the comoving galaxy density perturbation $\Delta_{\rm g}$ (see chapter 2). However, there is a problem with using only $\Delta_{\rm g}$ as a probe of matter density perturbations, which is that it does not correspond to the *observed* galaxy overdensity [3, 5–7, 9, 19] on horizon scales, because of general relativistic (GR) effects – lightcone and redshift effects – in the observational process [1]. (These effects become significant on very large scales.) By observing on the past lightcone, the observed redshift is perturbed: by Doppler effect, owing to the motions of the galaxies relative to the observer; and by the gravitational potential, both local at the galaxies and also integrated along the line of sight. The survey volume is also deformed given that the observation angles are distorted [9], owing to gravitational weak lensing. Hence during observations, observers measure the volume perturbations along with the galaxy number density perturbations, per redshift bin in a given direction, and a given angle.

Forthcoming galaxy surveys in the optical, the infrared and in the 21 cm emission of neutral hydrogen (HI), e.g. upcoming surveys like DES [29], EUCLID [30], BOSS [31] and the SKA [32, 33], will extend to higher redshifts $z \gtrsim 1$ and wider areas of the sky, covering greater volumes – spanning scales approaching and larger than the Hubble radius (i.e. $a\mathcal{H}^{-1}$): on these scales, the usual Newtonian approach is inadequate [1]. A fully GR analysis [1, 3–24], is therefore necessary in order to extract maximal and accurate information from these large-volume galaxy surveys. Firstly, we need to incorporate the well-known effects of redshift-space distortions (see chapter 2) and weak lensing. These are typically the dominant GR effects in the observed overdensity. Secondly, there are also other GR effects that arise when we correctly define the physical, observed galaxy overdensity [1]. The cosmic magnification perturbation also sources additional terms. Nevertheless, current galaxy surveys only cover low z and smaller sky areas, hence the GR effects are negligible.

In this chapter we aim to compute what large-scale galaxy surveys really measure, i.e. the (physical) observed galaxy overdensity. This chapter draws largely from [9], but also from [5]. The outline of this chapter is thus *viz.*: in section 3.1, we derive and discuss the GR geodesic equations; in section 3.2 we derive the physical, observed galaxy overdensity, i.e. the relativistic density perturbation, where we compute the density distortion (subsection 3.2.1), the volume distortion (subsection 3.2.2) and the magnification distortion (subsection 3.2.3).

3.1 The Geodesic Equation

Consider a given arbitrary path x^μ, then an infinitesimal deformation δx^μ about any given point along the path will induce an infinitesimal distance which is measured by the spacetime metric ds. If the path is deformed at every point, from the initial i up to the final f, then in general relativity x^μ is said to be a geodesic when the following condition holds: $\delta(\int_i^f ds) = \int_i^f \delta(ds) = 0$. This implies that the terminal points of x^μ become fixed [68].

Thus to determine the equations of a geodesic, we perturb the metric (1.3), whence:

$$\delta(ds) \;=\; \frac{1}{2}\left[\delta x^\alpha\, \partial_\alpha g_{\mu\nu}\, \frac{dx^\mu}{ds} dx^\nu + \left(g_{\alpha\nu}\frac{dx^\nu}{ds} + g_{\mu\alpha}\frac{dx^\mu}{ds}\right) d(\delta x^\alpha)\right], \tag{3.1}$$

where $\delta g_{\mu\nu} = \delta x^\alpha\, \partial_\alpha g_{\mu\nu}$, and we have set the dummy indices $\mu \to \alpha$ and $\nu \to \alpha$ on the last two terms, respectively. Then upon integrating Eq. (3.1) and applying the stationary condition, a straightforward calculation (see Appendix A) we obtain the geodesic equation, given by [41, 46, 50, 51, 68]

$$\frac{d^2x^\sigma}{d\lambda^2} + \Gamma^\sigma{}_{\mu\nu}\frac{dx^\mu}{d\lambda}\frac{dx^\nu}{d\lambda} \;=\; 0, \tag{3.2}$$

where $\Gamma^\sigma{}_{\mu\nu}$ is given as in Eq. (1.18). Alternatively, Eq. (3.2) can be given by

$$n^\mu \nabla_\mu n^\sigma \;=\; 0, \tag{3.3}$$

where $n^\sigma = dx^\sigma/d\lambda$ is the tangent 4-vector along $x^\sigma(\lambda)$.

Any parameter such as λ that makes a given path $x^\sigma(\lambda)$ to obey Eq. (3.3), is said to be an *affine parameter*. Certainly, one can always find a parameter (by an appropriate transformation) such that $n^\mu \nabla_\mu n^\sigma \neq 0$, in which case the given parameter is not an affine parameter. Hence by default, general relativity assumes an affine parameterization for geodesics. The norm $n^\mu n_\mu$ for an affinely parametrized geodesic x^σ is sometimes called the 'constant of the motion' of the geodesic, since it remains constant along the geodesic. If the geodesic is time-like[1] then by suitable parametrization this constant can be normalized to $n^\mu n_\mu = -1$ (for a metric with $g_{00} < 0$), and $n^\mu n_\mu = 1$ for a space-like geodesic [50]. In fact, these geodesics (with $n^\mu n_\mu = \pm 1$) describe the propagation of 'massive' (i.e. non-zero rest-mass) test particles in the gravitational field [51].

Moreover, the acceleration along a curve x^μ is given by $n^\mu \nabla_\mu n^\sigma$ [39, 41, 42, 46]. Then from the geodesic equation (3.3) it follows that there is no acceleration along a geodesic, i.e. the net external force acting on any object automatically vanishes along a geodesic, and the object moves with constant 4-velocity. This way, an object may only be conveyed through the geodesic by steady 4-momentum.

3.1.1 The null geodesic: propagation of photons

From discussions above, it follows that the infinitesimal distance between any two adjacent points along a given geodesic x^μ may be given in terms of the tangent vectors by $ds^2 = n^\mu n_\mu\, d\lambda^2$. Hence for a null geodesic, defined by $ds^2 = 0$, it implies that

$$n^\mu n_\mu \;=\; 0, \tag{3.4}$$

[1] In any frame, along a timelike geodesic, $ds^2 < 0$ everywhere (i.e. for a metric with $g_{00} < 0$).

in which case Eqs. (3.2) and (3.3) hold for any choice of parametrization. Moreover, for a Killing vector K_μ (i.e. $K^\nu \nabla_{(\nu} K_{\mu)} = 0$) which is tangent to the geodesic x^μ, if K_μ (or n^μ) is time-like, then the energy associated with n^μ is given by $n^\mu K_\mu$ – and the norm $n^\mu n_\mu$, gives the squared rest-mass [50] (i.e. for $\hbar = c = 1$). Thus the null geodesic describes the propagation of 'massless' (i.e. zero-rest-mass) photons in the gravitational field – hence the null geodesic is otherwise known as the *photon geodesic*. Henceforth, the treatment of particle trajectories will be only for photon geodesics.

3.1.2 Perturbing the geodesic equation

Firstly, we specify a metric for the spacetime. For convenience we adopt a conformal transformation, which leaves the associated geodesic equations unchanged, given by

$$ds^2 \to d\tilde{s}^2 = a^2 ds^2, \tag{3.5}$$

$$= a^2 \left\{ -(1+2\phi)\, d\eta^2 + 2B_{|i}\, d\eta dx^i + \left[(1-2\psi)\delta_{ij} + 2E_{|ij}\right] dx^i dx^j \right\}, \tag{3.6}$$

where $d\tilde{s}^2$ is now given by Eq. (1.8), and for simplicity we shall adopt (henceforth) flat space, $K = 0$. This transformation therefore implies that

$$\tilde{g}_{\mu\nu} = a^2 \left(\bar{g}_{\mu\nu} + \delta g_{\mu\nu}\right), \qquad \bar{g}_{00} = -1, \qquad \bar{g}_{i0} = \vec{0} = \bar{g}_{0j}, \qquad \bar{g}_{ij} = \delta_{ij}, \tag{3.7}$$

with the 4-velocities of a particle moving in $d\tilde{s}$ being given by

$$\tilde{u}^\mu = a^{-1} u^\mu = a^{-1}\left(1-\phi,\ v^{|i}\right), \quad \tilde{u}_\mu = a u_\mu = a\left(-1-\phi,\ v_{|i} + B_{|i}\right), \tag{3.8}$$

i.e. from Eqs. (1.13) and (1.14). Moreover, the transformation by Eq. (3.5) implies that one possible choice for the affine parameters may be such that $d\tilde{\lambda} = a^2 d\lambda$ [41, 46], which yields $\tilde{n}^\mu = a^{-2} n^\mu$ – for a geodesic $x^\mu(\lambda)$. Then from Eq. (3.3), the set of equations characterizing the geodesic in space and time become

$$\frac{dn^\mu}{d\lambda} = -\Gamma^\mu{}_{\alpha\beta}\, n^\alpha n^\beta. \tag{3.9}$$

In a perturbed FRW Universe, we will have that

$$n^\mu = \bar{n}^\mu + \delta n^\mu, \qquad \Gamma^\mu{}_{\alpha\beta} = \bar{\Gamma}^\mu{}_{\alpha\beta} + \delta\Gamma^\mu{}_{\alpha\beta}. \tag{3.10}$$

Then given that the background terms obey Eq. (3.9), we obtain the perturbed geodesic equation, given by

$$\frac{d\delta n^\mu}{d\lambda} = -\bar{g}^{\mu\nu}\frac{d}{d\lambda}\left(\bar{n}^\beta \delta g_{\nu\beta}\right) + \frac{1}{2}\bar{g}^{\mu\nu}\bar{n}^\alpha \bar{n}^\beta \partial_\nu \delta g_{\alpha\beta}, \tag{3.11}$$

where we used $d\bar{g}_{\mu\nu}/d\lambda = 0$, whence we get $\bar{\Gamma}^\mu{}_{\alpha\beta}\bar{n}^\alpha \delta n^\beta = 0$, and that

$$\delta\Gamma^\mu{}_{\alpha\beta}\bar{n}^\alpha\bar{n}^\beta = \frac{1}{2}\bar{g}^{\mu\nu}\bar{n}^\alpha\bar{n}^\beta\left(2\partial_\alpha \delta g_{\nu\beta} - \partial_\nu \delta g_{\alpha\beta}\right). \tag{3.12}$$

Therefore integrating the perturbed geodesic equation (3.11), from the initial point i until the final point f, we obtain the perturbed tangent vector given by [41]

$$\delta n^\mu|_i^f = -\left[\bar{g}^{\mu\nu}\delta g_{\nu\beta}\,\bar{n}^\beta\right]_i^f + \frac{1}{2}\bar{g}^{\mu\nu}\int_i^f d\lambda\, \bar{n}^\alpha\bar{n}^\beta\partial_\nu\delta g_{\alpha\beta}, \tag{3.13}$$

which gives the general perturbation in an arbitrary tangent 4-vector along any geodesic.

In fact, for a photon geodesic particularly, we have that

$$\tilde{n}^\mu \;=\; a^{-2}n^\mu \;=\; a^{-2}(1+\delta n^0,\, \bar{n}^i + \delta n^i), \tag{3.14}$$

where[2] $\bar{\tilde{n}}^\mu \bar{\tilde{n}}_\mu = \bar{n}^\mu \bar{n}_\mu = 0$, and $\bar{n}^0 \bar{n}_0 = -1$ with $\bar{n}^0 = 1$, $\bar{n}^i \bar{n}_i = 1$. The perturbations δn^0 and δn^i can therefore be computed directly from Eq. (3.13), as we shall see subsequently.

3.1.3 The deviation vector

In the background FRW Universe, a photon from a source S moving through the gravitational field in the direction $\mathbf{n}$ will have an instantaneous position vector $\mathbf{x}(\bar{\eta}) = \bar{r}(\bar{\eta})\mathbf{n}$. Here we define (as in section 2.4) $\bar{r} = |\mathbf{x}|$ as the comoving distance from the observer O to the source, such that at the observer $\bar{r}(\bar{\eta}_O) = 0$, and at the source $\bar{r}(\bar{\eta}_S) = \bar{r}_S$. Furthermore, we define the affine parameter by the norm of the photon position vector, i.e. given by $\lambda = -\mathbf{n}\cdot\mathbf{x}$. Thus we get $d\lambda = -d\bar{r}$, in the background.

However, in a perturbed Universe trajectories suffer some deviation – which is given by the 4-displacement or deviation 4-vector δx^μ. It describes infinitesimal deviations in motion of objects, away from their original background world lines. To compute δx^μ, we first compute the total 4-vector x^μ given by [9]

$$\frac{dx^\mu}{d\eta} \;=\; \frac{n^\mu}{n^0} \;=\; \bar{n}^\mu + \delta n^\mu - \bar{n}^\mu \delta n^0, \tag{3.15}$$

where here $\eta = \bar{\eta} + \delta\eta$ (similarly for x^μ), while n^μ retains its previous definition. Thus by integrating Eq. (3.15) from S up to O, we obtain that

$$x^\mu(\bar{\eta}_S) \;=\; -\left(\bar{\eta}_O - \bar{\eta}_S\right)\bar{n}^\mu - \int_0^{\bar{r}_S} d\bar{r}\,\left(\delta n^\mu - \bar{n}^\mu \delta n^0\right), \tag{3.16}$$

where we used that to lowest order along the photon geodesic,

$$d\bar{\eta} \;=\; -d\bar{r} \;=\; d\lambda. \tag{3.17}$$

Given Eqs. (3.13) and (3.17) we obtain the following (see Appendix A)

$$\delta n^0\big|_O^S \;=\; \delta g_{0\beta}\,\bar{n}^\beta\Big|_O^S - \frac{1}{2}\int_{\bar{r}_S}^0 d\bar{r}\,\delta g'_{\alpha\beta}\,\bar{n}^\alpha \bar{n}^\beta, \tag{3.18}$$

$$\delta n^i\big|_O^S \;=\; -\,\bar{g}^{ij}\delta g_{j\beta}\,\bar{n}^\beta\Big|_O^S + \frac{1}{2}\bar{g}^{ij}\int_{\bar{r}_S}^0 d\bar{r}\,\partial_j \delta g_{\alpha\beta}\,\bar{n}^\alpha \bar{n}^\beta. \tag{3.19}$$

From Eq. (3.16), we see that $x^\mu(\bar{\eta}_O) = 0 = \delta x^0(\bar{\eta}_S)$. Then we have the position deviation 4-vector to be a purely spatial perturbation at the source only – i.e. we have $\delta x^\mu = \delta x^i(\bar{\eta}_S)$, given by

$$\delta x^i(\bar{\eta}_S) \;=\; \int_0^{\bar{r}_S} d\bar{r}\,\left(\bar{g}^{ij}\delta g_{j\beta} + \delta g_{0\beta}\bar{n}^i\right)\bar{n}^\beta - \frac{1}{2}\int_0^{\bar{r}_S} d\bar{r}(\bar{r}-\bar{r}_S)\left(\bar{g}^{ij}\partial_j \delta g_{\alpha\beta} + \delta g'_{\alpha\beta}\bar{n}^i\right)\bar{n}^\alpha \bar{n}^\beta, \tag{3.20}$$

[2]For a time-like geodesic, $\bar{n}^\mu \bar{n}_\mu = \bar{n}^0 \bar{n}_0$; while for a space-like geodesic, $\bar{n}^\mu \bar{n}_\mu = \bar{n}^i \bar{n}_i$.

where by combining Eqs. (3.18) and (3.19) appropriately (as in Eq. (3.16)), we have integrated by parts once and applied the stationary condition – which gives surface terms that vanish (or do not contribute to physical solutions, hence are discarded).

3.2 The Observed Density Perturbation

The aim of galaxy redshift surveys is to map the three-dimensional (3D) distribution of galaxies, with the purpose of understanding the properties of this distribution and its implications for the contents and evolution of the Universe [38]. In these surveys, observers usually look at a certain volume $v(\mathbf{n}, z)$ of the sky in a given direction $-\mathbf{n}$, at a given redshift z away. This volume may be split into intervals $dv(\mathbf{n}, z)$ determined by redshift bins dz and solid angle interval $d\Omega_{\mathbf{n}}$. A volume interval of the observed patch of the sky will contain $dN(\mathbf{n}, z)$ number of galaxies. The physical galaxy number density $\tilde{n}_{\rm g}$, i.e. the number of galaxies counted per physical volume interval, is given by

$$dN \;=\; \tilde{n}_{\rm g} dv \;\equiv\; \tilde{\mathcal{N}}_{\rm g}(\mathbf{n}, z)\, dz\, d\Omega_{\mathbf{n}}, \tag{3.21}$$

where $\tilde{\mathcal{N}}_{\rm g} = \tilde{n}_{\rm g}\tilde{\mathcal{V}}$ is the number of galaxies counted in a given redshift bin dz in a given solid angle interval $d\Omega_{\mathbf{n}}$, with $\tilde{\mathcal{V}}$ being the corresponding volume per redshift bin per solid angle interval. Whence the redshift distribution of the galaxies is obtained by averaging over the solid angles, by $d\bar{N}(\bar{z}) \equiv \langle\tilde{\mathcal{N}}_{\rm g}\rangle(\bar{z})dz$.

Thus one obtains the observable number counts overdensity $\tilde{\delta}_n$, given by [9]

$$\tilde{\delta}_n(\mathbf{n}, z) \;\equiv \frac{\tilde{\mathcal{N}}_{\rm g}(\mathbf{n}, z) - \langle\tilde{\mathcal{N}}_{\rm g}\rangle(\bar{z})}{\langle\tilde{\mathcal{N}}_{\rm g}\rangle(\bar{z})} \;=\; \tilde{\delta}_{\rm g}(\mathbf{n}, z) + \tilde{\delta}_{\mathcal{V}}(\mathbf{n}, z), \tag{3.22}$$

i.e. by following correct definitions, the galaxy number density perturbation (2.43) transforms as $\tilde{\delta}_{\rm g} \to \tilde{\delta}_n = \tilde{\delta}_{\rm g} + \tilde{\delta}_{\mathcal{V}}$, where the volume contrast $\tilde{\delta}_{\mathcal{V}} = \delta\tilde{\mathcal{V}}/\bar{\mathcal{V}}$ is the fractional volume density perturbation, with

$$\tilde{n}_{\rm g}(\mathbf{n}, z) \;=\; \bar{n}_{\rm g}(\bar{z}) + \delta\tilde{n}_{\rm g}(\mathbf{n}, z), \qquad \tilde{\mathcal{V}}(\mathbf{n}, z) \;=\; \bar{\mathcal{V}}(\bar{z}) + \delta\tilde{\mathcal{V}}(\mathbf{n}, z). \tag{3.23}$$

The mean number of galaxies per redshift bin per solid angle is $\langle\tilde{\mathcal{N}}_{\rm g}\rangle(\bar{z}) = \bar{n}_{\rm g}(\bar{z})\bar{\mathcal{V}}(\bar{z})$, where $z = \bar{z} + \delta z$. The volume perturbation arises from the fact that both the redshift and the solid angle are perturbed. Moreover, $\tilde{\delta}_n$ being an observable, is therefore *gauge-invariant*. Hence its measurement is independent of the gauge choice of the observer.

3.2.1 The density distortion

Here we compute the distortion $\tilde{\delta}_{\rm g}$ arising in the galaxy number density $\tilde{n}_{\rm g}$ mainly owing to the fluctuation in the redshift at the source. In order to compute $\tilde{\delta}_{\rm g}(\mathbf{n}, z)$, which is in redshift space, we need to relate it to the distortion $\delta_{\rm g}(\mathbf{x}, \eta)$ in real space. By taking a gauge transformation (1.42), we get

$$\tilde{\delta}_{\rm g}(\mathbf{n}, z) \;=\; \delta_{\rm g}(\mathbf{n}, z) - \frac{d\ln\bar{n}_{\rm g}}{d\bar{z}}\,\delta z(\mathbf{n}, z), \tag{3.24}$$

where $\delta_{\rm g} \equiv \delta n_{\rm g}/\bar{n}_{\rm g}$, with the background part $\bar{n}_{\rm g}$ remaining the same. We have used that, to first order, $\delta\eta = (\partial\bar{\eta}/\partial\bar{z})\delta z$. Thus Eq. (3.24) becomes

$$\tilde{\delta}_{\rm g}(\mathbf{n}, z) \;=\; \delta_{\rm g}(\mathbf{n}, z) - (3 - b_e(\bar{z}))\;\frac{\delta z}{1+\bar{z}}, \tag{3.25}$$

where $a = (1+\bar{z})^{-1}$, and the galaxy *evolution bias* [5] is given by

$$b_e \;\equiv\; \left.\frac{\partial \ln(a^3 n_{\rm g})}{\partial \ln(a)}\right|_a, \tag{3.26}$$

with $a^3 n_{\rm g}$ being the comoving galaxy number density. Hereafter, we will work with the gauge-invariant potentials Φ, Ψ and V (see subsection 1.2.7.3), given by

$$\Phi \;=\; \phi - \mathcal{H}\sigma - \sigma', \tag{3.27}$$

$$\Psi \;=\; D + \frac{1}{3}\nabla^2 E + \mathcal{H}\sigma, \tag{3.28}$$

$$V \;=\; v + E', \tag{3.29}$$

which correspond to the gauge-invariant potentials $\phi_{_N}$, $\psi_{_N}$ and $v_{_N}$ computed in the conformal Newtonian gauge (see subsection 1.2.6.1).

Next we compute the observed redshift z. A photon which propagates along the direction $\mathbf{n}$ from a source S will be seen by an observer O, located elsewhere in the Universe with fundamental 4-velocity $\tilde{u}^\mu$ in the metric $d\tilde{s}^2$ (3.5), to be moving with an energy[3] $E = -\tilde{n}^\mu \tilde{u}_\mu$ under the direction $-\mathbf{n}$. The redshift z, which is the fractional change in energy of the photon in propagating through the gravitational field from S to O, is given by

$$1 + z \;=\; \frac{(\tilde{n}^\mu \tilde{u}_\mu)_{_S}}{(\tilde{n}^\mu \tilde{u}_\mu)_{_O}} \;=\; \frac{a_{_O}}{a_{_S}}\Big[1 + \delta\left(n^\mu u_\mu\right)\big|_{_S}^{^O}\Big], \tag{3.30}$$

where we used Eqs. (3.8) and (3.14). Given that $z = \bar{z} + \delta z$, then by perturbing Eq. (3.30) to first order we get

$$\frac{\delta z}{1+\bar{z}} \;=\; \delta\left(n^\mu u_\mu\right)\big|_{_S}^{^O} \;=\; \left[\bar{n}^i v_{|i} + \bar{n}^i B_{|i} - \delta n^0 - \phi\right]_{_S}^{^O}, \tag{3.31}$$

where $a_{_O}/a_{_S} = 1 + \bar{z}$. By using Eqs. (3.18), (3.27)–(3.29), then Eqs. (3.30) and (3.31) yield (see Appendix A) the total redshift of the propagating photon, given by

$$1 + z \;=\; (1+\bar{z})\left[1 + \left(\Phi + \Psi + V_{\parallel} - \psi\right)\big|_{z_S}^0 - \int_{\bar{r}_S}^0 d\bar{r}\left(\Phi' + \Psi'\right)\right], \tag{3.32}$$

where we have neglected the unobservable metric term $\partial_r E'$ in $\mathbf{n}\cdot\mathbf{v} = V_{\parallel} - \bar{n}^i\partial_i E'$. Note that the perturbations in the square bracket in Eq. (3.32) correspond to $\delta z/(1+\bar{z})$: from Eq. (3.31). Thus the redshift-space density distortion (3.25), becomes

$$\begin{aligned}\tilde{\delta}_{\rm g}(\mathbf{n}, z) \;=\;& \Delta_\psi(\mathbf{n}, z) + 3\left(\Phi + \Psi\right)(\mathbf{n}, z) + 3V_{\parallel}(\mathbf{n}, z) + 3\int_{\bar{r}_S}^0 d\bar{r}\left(\Phi' + \Psi'\right)(\mathbf{n}, z) \\ & - b_e(\bar{z})\left[\Phi(\mathbf{n}, z) + V_{\parallel}(\mathbf{n}, z) + \int_{\bar{r}_S}^0 d\bar{r}\left(\Phi' + \Psi'\right)(\mathbf{n}, z)\right],\end{aligned} \tag{3.33}$$

[3] See discussion under Eq. (3.4) – given that u_μ is a conformal Killing vector.

where $\Delta_\psi \equiv \delta_{\rm g} - 3\psi - b_e\mathcal{H}\sigma$ is the density perturbation in uniform curvature gauge [9]. Note that the second line in Eq. (3.33) is (wrongly) omitted in [9]. Thus,

$$\Delta_\psi \;=\; \Delta_{\rm g} + (3 - b_e)\,\mathcal{H}V - 3\Psi, \tag{3.34}$$

where $\Delta_{\rm g}$ is given by Eq. (2.30), and given Eq. (3.26), we used that

$$\bar{n}'_{\rm g} \;=\; -\mathcal{H}\,(3 - b_e)\,\bar{n}_{\rm g}. \tag{3.35}$$

As before, $\Delta_{\rm g}$ is related to the comoving matter overdensity by Eq. (2.31). Moreover, we can relate the galaxy bias (2.28) to the evolution bias (3.26), given by

$$b \;=\; -\mathcal{H}\,(3 - b_e)\,\frac{\bar{\rho}_m}{\bar{\rho}'_m} \;=\; 1 - \frac{1}{3}b_e, \tag{3.36}$$

where the second equality follows from the continuity equation $\bar{\rho}'_m = -3\mathcal{H}\bar{\rho}_m$.

3.2.2 The volume distortion

In a flat background FRW Universe, geodesics are essentially straight lines. This implies that the photon emission angles – i.e. the zenith and azimuthal angles, $\theta_{_S}$ and $\vartheta_{_S}$, respectively – are equal to the corresponding observed angles $\theta_{_O}$ and $\vartheta_{_O}$, i.e. $\theta_{_O} = \theta = \theta_{_S}$. However, in a perturbed Universe these angles become perturbed, and are given by

$$\tilde{\theta}_{_S} \;=\; \theta_{_O} + \delta\theta, \qquad \tilde{\vartheta}_{_S} \;=\; \vartheta_{_O} + \delta\vartheta, \tag{3.37}$$

where we take $\delta\theta_{_O} = 0 = \delta\vartheta_{_O}$. Given the perturbations in the angles and in the redshift, the observed volume thus becomes perturbed. This give rise to a distortion $\tilde{\delta}_{_\mathcal{V}}$ in the volume which surfaces in the observed galaxy overdensity, in redshift space. Hence, similar to Eq. (3.24), in order to compute the volume distortion $\tilde{\delta}_{_\mathcal{V}}(\mathbf{n}, z)$, we take a gauge transformation from real space to the redshift space, given by

$$\tilde{\delta}_{_\mathcal{V}}(\mathbf{n}, z) \;=\; \delta_{_\mathcal{V}}(\mathbf{n}, z) - \frac{d\ln\bar{\mathcal{V}}}{d\bar{z}}\,\delta z(\mathbf{n}, z), \tag{3.38}$$

where $\delta_{_\mathcal{V}} \equiv \delta\mathcal{V}/\bar{\mathcal{V}}$ is the volume distortion given in real space. In real space, an infinitesimal element of the survey volume, containing a source with 4-velocity $\tilde{u}^\mu$ in the metric $d\tilde{s}^2$ (3.5), is given by [9]

$$dv \;=\; \sqrt{-\tilde{g}}\;\epsilon_{\mu\nu\alpha\beta}\tilde{u}^\mu d\tilde{x}^\nu d\tilde{x}^\alpha d\tilde{x}^\beta, \tag{3.39}$$

$$\equiv\; \mathcal{V}\,(z, \theta_{_O}, \vartheta_{_O})\,dz\,d\theta_{_O}d\vartheta_{_O}, \tag{3.40}$$

where the total volume density $\mathcal{V}$ is given here by

$$\mathcal{V} \;=\; \sqrt{-\tilde{g}}\;\epsilon_{\mu\nu\alpha\beta}\,\tilde{u}^\mu\frac{\partial\tilde{x}^\nu}{\partial z}\frac{\partial\tilde{x}^\alpha}{\partial\tilde{\theta}_{_S}}\frac{\partial\tilde{x}^\beta}{\partial\tilde{\vartheta}_{_S}}\left|\frac{\partial(\tilde{\theta}_{_S}, \tilde{\vartheta}_{_S})}{\partial\,(\theta_{_O}, \vartheta_{_O})}\right|. \tag{3.41}$$

Then given Eq. (3.37), the determinant of $J \equiv \partial(\tilde{\theta}_{_S}, \tilde{\vartheta}_{_S})/\partial\,(\theta_{_O}, \vartheta_{_O})$ becomes

$$|J| \;=\; 1 + \partial_\theta\delta\theta + \partial_\vartheta\delta\vartheta. \tag{3.42}$$

Moreover $\tilde{g} = \det(\tilde{g}_{\mu\nu})$, being the determinant of $\tilde{g}_{\mu\nu}$ (3.7), yields

$$\sqrt{-\tilde{g}} \;=\; a^4\left(1+\frac{1}{2}\delta g^{\alpha}{}_{\alpha}\right) \;=\; a^4(1+\phi-3D), \tag{3.43}$$

where by definition $E^i{}_i = 0$. Then we have the only non-vanishing terms of $\mathcal{V}$ giving

$$\mathcal{V} \;=\; a^3(1+\phi-3D)\left[\frac{dr}{dz}r^2|J|\sin\tilde{\theta}_{S} - \left(\phi\frac{d\bar{r}}{d\bar{z}} + v_r\frac{d\bar{\eta}}{d\bar{z}}\right)\bar{r}^2\sin\theta_{O}\right], \tag{3.44}$$

$$\;=\; \bar{\mathcal{V}}\left[1-3D-\mathbf{n}\cdot\mathbf{v}-\frac{d\delta r}{d\lambda}+\frac{a}{\mathcal{H}}\frac{d\delta z}{d\lambda}+2\frac{\delta r}{\bar{r}}+(\cot\theta+\partial_\theta)\,\delta\theta+\partial_\vartheta\delta\vartheta\right], \tag{3.45}$$

where $\bar{\mathcal{V}}(\bar{z}) \equiv a^4\bar{r}(\bar{z})^2\mathcal{H}(\bar{z})^{-1}\sin\theta_{O}$. We have used Eq. (3.17), and that to lowest order along the photon geodesic, $d\bar{r}/d\bar{z} = -d\bar{\eta}/d\bar{z} = a/\mathcal{H}$. Moreover, by assuming $\delta\theta$ to be very small, we used that $\sin\tilde{\theta}_{S} = (1+\delta\theta\cot\theta_{O})\sin\theta_{O}$. The comoving distance along the radial coordinate is $r = \bar{r} + \delta r$. We have also used that $v_r = e^i_r v_i = -\bar{n}^i v_i$, with e^i_r being the radial unit vector in polar coordinates. Here we define $\delta_{\mathcal{V}}$ (3.38) by

$$\delta_{\mathcal{V}}(\mathbf{n},z) \;\equiv\; \frac{\mathcal{V}(z)-\bar{\mathcal{V}}(\bar{z})}{\bar{\mathcal{V}}(\bar{z})}. \tag{3.46}$$

The perturbation in $\mathcal{V}$ arises mainly as a result of the perturbation in z. Hence given Eqs. (3.38), (3.45) and (3.46) we obtain

$$\tilde{\delta}_{\mathcal{V}} = -3D-\mathbf{n}\cdot\mathbf{v}-\frac{d\delta r}{d\lambda}+\frac{a}{\mathcal{H}}\frac{d\delta z}{d\lambda}+2\frac{\delta r}{\bar{r}}+(\cot\theta+\partial_\theta)\,\delta\theta+\partial_\vartheta\delta\vartheta+a\left(4-\frac{2}{\bar{r}\mathcal{H}}-\frac{\mathcal{H}'}{\mathcal{H}^2}\right)\delta z, \tag{3.47}$$

where the derivative of the background volume density is

$$\frac{d\bar{\mathcal{V}}}{d\bar{z}} \;=\; -a\left(4-\frac{2}{\bar{r}\mathcal{H}}-\frac{\mathcal{H}'}{\mathcal{H}^2}\right)\bar{\mathcal{V}}. \tag{3.48}$$

To compute the various terms of the volume distortion $\tilde{\delta}_{\mathcal{V}}$ (3.47), we consider the observer and the source to be enclosed in a (hypothetical) sphere – with the observer at the centre and the source on the circumference. Thus we need to relate the polar coordinates $\check{x}^\mu$ to Cartesian coordinates x^μ. The displacement 4-vectors in these coordinates are related (to first order) by

$$\delta\check{x}^\mu \;=\; \frac{\partial\check{x}^\mu}{\partial x^\nu}\delta x^\nu \;=\; \delta^\mu{}_\nu\,\delta x^\nu. \tag{3.49}$$

The spatial displacement vector of a particle in the polar coordinates is given by

$$\boldsymbol{\delta\check{x}} \;=\; \delta r\,\boldsymbol{e}_r + \bar{r}\,\delta\theta\,\boldsymbol{e}_\theta + \bar{r}\sin\theta\,\delta\vartheta\,\boldsymbol{e}_\vartheta, \tag{3.50}$$

where $\boldsymbol{e}_r$, $\boldsymbol{e}_\theta$ and $\boldsymbol{e}_\vartheta$ are the orthonormal[4] unit vectors of the polar coordinates $\check{x}^\mu$, with $\boldsymbol{e}_\theta = \partial_\theta\boldsymbol{e}_r$, $\boldsymbol{e}_\vartheta\sin\theta = \partial_\vartheta\boldsymbol{e}_r$. For convenience we have chosen that $\boldsymbol{e}_r = -\mathbf{n}$, which thus implies that $\partial_r = -\bar{n}^i\partial_i$. Moreover, given Eq. (3.50), we have that

$$\delta r \;=\; \boldsymbol{e}_r\cdot\boldsymbol{\delta\check{x}}, \qquad \bar{r}\,\delta\theta \;=\; \boldsymbol{e}_\theta\cdot\boldsymbol{\delta\check{x}}, \qquad \bar{r}\sin\theta\,\delta\vartheta \;=\; \boldsymbol{e}_\vartheta\cdot\boldsymbol{\delta\check{x}}. \tag{3.51}$$

[4]That is, $\boldsymbol{e}_r\cdot\boldsymbol{e}_r = \boldsymbol{e}_\theta\cdot\boldsymbol{e}_\theta = \boldsymbol{e}_\vartheta\cdot\boldsymbol{e}_\vartheta = 1$ and $\boldsymbol{e}_r\cdot\boldsymbol{e}_\theta = \boldsymbol{e}_\theta\cdot\boldsymbol{e}_\vartheta = \boldsymbol{e}_r\cdot\boldsymbol{e}_\vartheta = 0$.

Thus given Eqs. (3.20) and (3.51), we get that

$$\delta r \;=\; -\bar{n}_i\,\delta x^i \;=\; -\frac{1}{2}\int_0^{\bar{r}_S} d\bar{r}\,\delta g_{\alpha\beta}\,\bar{n}^\alpha\bar{n}^\beta, \tag{3.52}$$

where we have integrated by parts once and applied the stationary conditions on boundary terms, which then vanish. Similarly, given Eq. (3.51), we obtain that

$$\bar{r}_S\,\delta\theta \;=\; \int_0^{\bar{r}_S} d\bar{r}\,\delta g_{j\beta}\,e^j_\theta\,\bar{n}^\beta - \frac{1}{2}\int_0^{\bar{r}_S} d\bar{r}\,(\bar{r}-\bar{r}_S)\,e^j_\theta\partial_j\,(\delta g_{\alpha\beta})\,\bar{n}^\alpha\bar{n}^\beta, \tag{3.53}$$

$$\bar{r}_S\,\sin\theta\,\delta\vartheta \;=\; \int_0^{\bar{r}_S} d\bar{r}\,\delta g_{j\beta}\,e^j_\vartheta\,\bar{n}^\beta - \frac{1}{2}\int_0^{\bar{r}_S} d\bar{r}\,(\bar{r}-\bar{r}_S)\,e^j_\vartheta\partial_j\,(\delta g_{\alpha\beta})\,\bar{n}^\alpha\bar{n}^\beta, \tag{3.54}$$

where δx^i, $\delta\theta$ and $\delta\vartheta$ are all evaluated at S. Given Eqs. (3.17) and (3.52), we have

$$\frac{d\delta r}{d\lambda} \;=\; \frac{1}{2}\delta g_{\alpha\beta}\,\bar{n}^\alpha\bar{n}^\beta \;=\; -\,(\Phi+\Psi) + \frac{dB}{d\lambda} + \left(\frac{d^2E}{d\lambda^2} - 2\frac{dE'}{d\lambda}\right), \tag{3.55}$$

where we used Eqs. (3.27) and (3.28) and that $dX/d\lambda = X' + \bar{n}^i\partial_i X$ (for any scalar X). After some lengthy, but straightforward calculations (see Appendix A), we obtain

$$(\cot\theta + \partial_\theta)\,\delta\theta + \partial_\vartheta\delta\vartheta \;=\; \int_0^{\bar{r}_S} d\bar{r}\,(\bar{r}-\bar{r}_S)\,\frac{\bar{r}}{\bar{r}_S}\nabla^2_\perp\,(\Phi+\Psi) - \nabla^2_\perp E\Big|_O^S, \tag{3.56}$$

where $\nabla^2_\perp \equiv \nabla^2 - \partial_r^2 - 2\bar{r}^{-1}\partial_r$ is the 'screen space' Laplacian – i.e. in the plane of the source, transverse to the line of sight. By using that $\partial_r = -\bar{n}^i\partial_i$, we obtain

$$\nabla^2_\perp E \;=\; \nabla^2 E - \left(\frac{d^2E}{d\lambda^2} - 2\frac{dE'}{d\lambda} + E''\right) + \frac{2}{\bar{r}}\left(\frac{dE}{d\lambda} - E'\right). \tag{3.57}$$

Thus given Eqs. (3.47), (3.52), (3.55), (3.56), and (3.57), we have

$$\begin{aligned}\tilde{\delta}_{\mathcal{V}}(\mathbf{n},z) \;=\;& -4V_\parallel - 2\,(\Phi+\Psi) + \int_0^{\bar{r}_S} d\bar{r}\,(\bar{r}-\bar{r}_S)\,\frac{\bar{r}}{\bar{r}_S}\nabla^2_\perp\,(\Phi+\Psi)\\ &+ 3\int_0^{\bar{r}_S} d\bar{r}\,\left(\Phi'+\Psi'\right) + \frac{2}{\bar{r}_S}\int_0^{\bar{r}_S} d\bar{r}\,(\Phi+\Psi) + \frac{1}{\mathcal{H}}\left[\Psi' + \partial_r\Phi - \frac{dV_\parallel}{d\lambda}\right]\\ &+ \left(\frac{\mathcal{H}'}{\mathcal{H}^2} + \frac{2}{\bar{r}_S\mathcal{H}}\right)\left[\Phi + V_\parallel - \int_0^{\bar{r}_S} d\bar{r}\,\left(\Phi'+\Psi'\right)\right],\end{aligned} \tag{3.58}$$

where similarly, we have neglected the unmeasurable (metric) term in $\mathbf{n}\cdot\mathbf{v}$ – i.e. as given in Eq. (3.32). Moreover, given Eqs. (3.17) and (3.28), we have used that

$$\frac{1}{\mathcal{H}}\frac{d\Psi}{d\lambda} \;=\; \frac{1}{\mathcal{H}}\frac{d}{d\lambda}\left(D + \frac{1}{3}\nabla^2 E\right) + \left(\frac{dE'}{d\lambda} + \frac{\mathcal{H}'}{\mathcal{H}}E'\right) - \left(\frac{dB}{d\lambda} + \frac{\mathcal{H}'}{\mathcal{H}}B\right). \tag{3.59}$$

Equation (3.58) gives the distortion that arises in the observed volume of galaxy redshift surveys. Then by assuming that galaxies (hence, pressureless matter) move along geodesics, we have the Euler equation to be given by

$$V_\parallel{}' + \mathcal{H}V_\parallel - \partial_r\Phi \;=\; 0. \tag{3.60}$$

Finally, by combining Eqs. (3.33), (3.34), (3.58) and (3.60), we obtain the observed galaxy overdensity (3.22), given by

$$\begin{aligned}\tilde{\delta}_n(\mathbf{n},z) \;=\;& \Delta_{\rm g}(\mathbf{n},z)+\frac{1}{\mathcal{H}}\partial_r V_{\parallel}(\mathbf{n},z)\\ &+\int_0^{\bar{r}_S} d\bar{r}\,(\bar{r}-\bar{r}_S)\,\frac{\bar{r}}{\bar{r}_S}\nabla_\perp^2\,(\Phi+\Psi)\,(\mathbf{n},z)\\ &+\,(3-b_e)\,\mathcal{H}V(\mathbf{n},z)-\left(b_e-1-\frac{\mathcal{H}'}{\mathcal{H}^2}-\frac{2}{\bar{r}_S\mathcal{H}}\right)\Phi(\mathbf{n},z)\\ &+\frac{1}{\mathcal{H}}\Psi'(\mathbf{n},z)-2\Psi(\mathbf{n},z)+\frac{2}{\bar{r}_S}\int_0^{\bar{r}_S} d\bar{r}\,(\Phi+\Psi)\,(\mathbf{n},z)\\ &-\left(b_e-\frac{\mathcal{H}'}{\mathcal{H}^2}-\frac{2}{\bar{r}_S\mathcal{H}}\right)\left[V_{\parallel}-\int_0^{\bar{r}_S} d\bar{r}\,\left(\Phi'+\Psi'\right)\right](\mathbf{n},z). \end{aligned}\tag{3.61}$$

The first line in Eq. (3.61) contains the (comoving) density perturbation and the Kaiser redshift space distortion term, respectively. The second line gives the gravitational lensing term. These first two lines together constitute the most dominant terms in the observed overdensity. The third and fourth lines contain the potential terms, with the integral term corresponding to the time delay of signals along the geodesic. In the fifth line, the first and the second terms in the square bracket correspond to the Doppler and the ISW effects, respectively.

3.2.3 The magnification distortion

Apart from the redshift, the observation angle and the intrinsic properties of the observed galaxies, surveys may (generically) depend on the cosmic magnification (2.32) of the galaxies in the sky [5] – e.g. by depending on angular size and flux of the galaxies. When this happens, the magnification contrast (2.35) causes the number density perturbation (3.22) in redshift space to transform as

$$\tilde{\delta}_n \;\to\; \Delta_{\rm g}^{\rm obs}(\mathbf{n},z) \;=\; \tilde{\delta}_n(\mathbf{n},z)+\mathcal{Q}(z)\,\tilde{\delta}_{\mathcal{M}}(\mathbf{n},z), \tag{3.62}$$

which is unique and physically defined, hence is automatically gauge-invariant. Thus in general, $\Delta_{\rm g}^{\rm obs}$ is the truly *observed* density perturbation [1, 3, 5–7, 9].

Moreover, cosmic magnification causes the surface (transverse to the line of sight) containing the sources to be amplified – eventually increasing the number of sources in the observed sky area. Thus the sources get amplified by a factor (2.32), given by

$$\tilde{\mathcal{M}}^{-1} \;\equiv\; \frac{\tilde{\mathcal{N}}}{\bar{\mathcal{N}}} \;=\; \frac{\tilde{\mathcal{A}}}{\bar{\mathcal{A}}}, \tag{3.63}$$

where $\tilde{\mathcal{A}}$ is the area (in redshift space) per unit solid angle, i.e. in the surface transverse to the line of sight, corresponding to $\tilde{\mathcal{N}}$; $\bar{\mathcal{A}}$ is the mean area density at $\bar{z}$. Here the mean magnification $\bar{\mathcal{M}}=1$. The magnification contrast $\tilde{\delta}_{\mathcal{M}}$ (2.35), corresponds to the perturbation in the flux (or solid angle) of a galaxy, relative to another galaxy at the same $\bar{z}$. The area element transverse to the line of sight is given by [5, 24, 62]

$$dA \;=\; \tilde{\mathcal{A}}(\mathbf{n},z)d\Omega_{\mathbf{n}} \;=\; D_A^2(\mathbf{n},z)d\Omega_{\mathbf{n}}, \tag{3.64}$$

where D_A is the angular diameter distance. The area contrast, i.e. the fractional area density perturbation, is given by $\tilde{\delta}_{\mathcal{A}} \equiv \delta\tilde{\mathcal{A}}/\bar{\mathcal{A}} = (\tilde{\mathcal{A}} - \bar{\mathcal{A}})/\bar{\mathcal{A}}$.

Nevertheless, in real-space coordinates, the area element is given by

$$dA = \sqrt{-\tilde{g}}\,\epsilon_{\mu\nu\alpha\beta}\,\tilde{u}^{\mu}\tilde{\ell}^{\nu}d\tilde{x}^{\alpha}d\tilde{x}^{\beta}, \tag{3.65}$$

$$\equiv \mathcal{A}(\theta_{_O},\vartheta_{_O})\,d\theta_{_O}d\vartheta_{_O}, \tag{3.66}$$

which is evaluated at a fixed z, and the real-space area density is given by

$$\mathcal{A} = \sqrt{-\tilde{g}}\,\epsilon_{\mu\nu\alpha\beta}\,\tilde{u}^{\mu}\tilde{\ell}^{\nu}\frac{\partial\tilde{x}^{\alpha}}{\partial\tilde{\theta}_{_S}}\frac{\partial\tilde{x}^{\beta}}{\partial\tilde{\vartheta}_{_S}}\left|\frac{\partial(\tilde{\theta}_{_S},\tilde{\vartheta}_{_S})}{\partial(\theta_{_O},\vartheta_{_O})}\right|. \tag{3.67}$$

Note that Eq. (3.65) has only two differentials ($d\tilde{x}^{\alpha}$, $d\tilde{x}^{\beta}$), as oppose to Eq. (3.39) which has three ($d\tilde{x}^{\nu}$, $d\tilde{x}^{\alpha}$, $d\tilde{x}^{\beta}$). These give the dimensions of the area and the volume (elements), respectively. The vector $\tilde{\ell}^{\nu}$ is orthogonal to the line of sight, $\tilde{u}_{\nu}\tilde{\ell}^{\nu} = 0$, with its background part being purely spatial. It is given (see [5]) by

$$\tilde{\ell}^{\nu} = \tilde{u}^{\nu} + \frac{\tilde{n}^{\nu}}{\tilde{n}^{\alpha}\tilde{u}_{\alpha}}. \tag{3.68}$$

Thus, after some calculations (see Appendix A), we obtain the area density to be

$$\mathcal{A} = \bar{\mathcal{A}}\left[1 - 3D - \phi + \bar{n}^{i}B_{|i} - \frac{1}{2}\delta g_{\alpha\beta}\bar{n}^{\alpha}\bar{n}^{\beta} + 2\frac{\delta r}{\bar{r}} + (\cot\theta + \partial_{\theta})\,\delta\theta + \partial_{\vartheta}\delta\vartheta\right], \tag{3.69}$$

where $\bar{\mathcal{A}}(\bar{z}) = a(\bar{z})^2\bar{r}(\bar{z})^2\sin\theta$. By Eqs. (3.63) and (3.64), we have $\tilde{\mathcal{M}}^{-1} = \tilde{\mathcal{A}}/\bar{\mathcal{A}} = 1 + \tilde{\delta}_{\mathcal{A}}$. Thus by following Eqs. (3.24) and (3.38), a gauge transformation (1.42) yields

$$\tilde{\delta}_{\mathcal{A}}(\mathbf{n},z) = \delta_{\mathcal{A}}(\mathbf{n},z) - \frac{d\ln\bar{\mathcal{A}}}{d\bar{z}}\delta z(\mathbf{n},z), \tag{3.70}$$

where $\delta_{\mathcal{A}} \equiv \delta\mathcal{A}/\bar{\mathcal{A}} = (\mathcal{A} - \bar{\mathcal{A}})/\bar{\mathcal{A}}$, with mean area density $\bar{\mathcal{A}}$ remaining the same. Then given Eqs. (3.63), (3.69) and (3.70), we have that

$$\tilde{\mathcal{M}}^{-1} = 1 - 3D - \phi + \bar{n}^{i}B_{|i} - \frac{1}{2}\delta g_{\alpha\beta}\bar{n}^{\alpha}\bar{n}^{\beta} + 2\frac{\delta r}{\bar{r}} + (\cot\theta + \partial_{\theta})\,\delta\theta + \partial_{\vartheta}\delta\vartheta + 2a\left(1 - \frac{1}{\bar{r}\mathcal{H}}\right)\delta z, \tag{3.71}$$

where we have used the fact that

$$\frac{d\bar{\mathcal{A}}}{d\bar{z}} = -2a\left(1 - \frac{1}{\bar{r}\mathcal{H}}\right)\bar{\mathcal{A}}. \tag{3.72}$$

Then given Eqs. (3.27)–(3.29), (3.32), (3.52), (3.56) and (3.71), a straightforward calculation yields the relativistic expression for the magnification contrast (2.35), as

$$\begin{aligned}\tilde{\delta}_{\mathcal{M}}(\mathbf{n},z) = &-\int_0^{\bar{r}_S} d\bar{r}\,(\bar{r} - \bar{r}_{_S})\,\frac{\bar{r}}{\bar{r}_{_S}}\nabla_{\perp}^2\,(\Phi + \Psi)\,(\mathbf{n},z)\\ &+ 2\Psi(\mathbf{n},z) - \frac{2}{\bar{r}_{_S}}\int_0^{\bar{r}_S} d\bar{r}\,(\Phi + \Psi)\,(\mathbf{n},z)\\ &+ 2\left(1 - \frac{1}{\bar{r}_{_S}\mathcal{H}}\right)\left[\Phi + V_{\parallel} - \int_0^{\bar{r}_S} d\bar{r}\,\left(\Phi' + \Psi'\right)\right](\mathbf{n},z),\end{aligned} \tag{3.73}$$

where $\bar{\mathcal{M}} = 1$. From Eq. (3.73) we see that the lensing term, in the first line, is the standard term of the cosmic magnification. This is the term that appears in the Newtonian limit, where the magnification of sources arises mainly owing to gravitational lensing. However, in reality there are other contributions to the magnification owing to the Doppler effect, the ISW effect and the gravitational potential effect – both local at the source, and integrated along the line of sight: together these effects constitute the GR corrections to the magnification distortion.

Now by combing Eqs. (3.61), (3.62) and (3.73), the observed overdensity becomes

$$\begin{aligned}\Delta_{\rm g}^{\rm obs}(\mathbf{n},z) \;=\;& \Delta_{\rm g}(\mathbf{n},z) + \frac{1}{\mathcal{H}}\partial_r V_{\parallel}(\mathbf{n},z) \\ &+ (1-\mathcal{Q})\int_0^{\bar{r}_S} d\bar{r}\,(\bar{r}-\bar{r}_S)\,\frac{\bar{r}}{\bar{r}_S}\nabla_\perp^2\,(\Phi+\Psi)\,(\mathbf{n},z) \\ &+ \;(3-b_e)\,\mathcal{H}V(\mathbf{n},z) - \left(b_e - 1 - 2\mathcal{Q} - \frac{\mathcal{H}'}{\mathcal{H}^2} - \frac{2(1-\mathcal{Q})}{\bar{r}_S\mathcal{H}}\right)\Phi(\mathbf{n},z) \\ &+ \frac{1}{\mathcal{H}}\Psi'(\mathbf{n},z) - 2(1-\mathcal{Q})\Psi(\mathbf{n},z) + \frac{2(1-\mathcal{Q})}{\bar{r}_S}\int_0^{\bar{r}_S} d\bar{r}\,(\Phi+\Psi)\,(\mathbf{n},z) \\ &- \left(b_e - 2\mathcal{Q} - \frac{\mathcal{H}'}{\mathcal{H}^2} - \frac{2(1-\mathcal{Q})}{\bar{r}_S\mathcal{H}}\right)\left[V_{\parallel} - \int_0^{\bar{r}_S} d\bar{r}\,\left(\Phi'+\Psi'\right)\right](\mathbf{n},z),\end{aligned} \tag{3.74}$$

which is the correct (observed) 'relativistic density perturbation' of galaxy redshift surveys. This generalizes the observed overdensity for both: surveys that depend on magnification (i.e. $\mathcal{Q} \neq 0$), e.g. those that depend on the apparent flux and/or angular size of the sources (such as the HI surveys of the SKA, and BAO surveys of BOSS); and for surveys that are independent of magnification (i.e. $\mathcal{Q} = 0$), e.g. those whose selection probability depends only on the intrinsic (physical) properties, the redshifts and the observed sky positions of the sources (such as the galaxy surveys of DES and EUCLID).

The comoving galaxy density fluctuation, the Kaiser redshift-space distortion term and the magnification bias, give galaxy surveys the potential to probe the content and the geometry of the universe [23].

Chapter 4

Clustering Effects of Quintessence on Large Scales

In this chapter we discuss some self-consistent models of DE, known as 'quintessence' [1, 25, 26, 69–74], as suitable alternatives to Λ. Quintessence is given by a canonical scalar field φ (see subsection 1.2.8) evolving along a potential $U(\varphi)$, with a time-varying equation of state parameter: $-1 \leq w_q \leq 0$. Moreover, quintessence is known to exhibit the so-called 'tracker behaviour' [69–72] – i.e. where various evolutions from a broad set of initial conditions eventually come together into a single evolution. This property alleviates the problem associated with the choice of initial conditions. Other merits and challenges of the quintessence models (QCDM, hereafter) are discussed in e.g. [70, 73, 74]. In QCDM, the late cosmic acceleration is driven by φ, where the different models are given by various choices of $U(\varphi)$.

4.1 Quintessence Dynamics

Quintessence can cluster only on horizon scales, i.e. on distance scales of sizes near and greater than the Hubble radius. An important question then to ask is: what is the effect of this clustering on the observed matter distribution? To answer this, we need a relativistic approach (discussed in chapter 3) that goes beyond the standard Newtonian calculation and deals properly with large scales. In particular, we need to account for GR effects on super-Hubble scales. The GR effects become substantial on these scales, and are crucial for: testing of DE and modified gravity models; and measuring primordial non-Gaussianity – e.g. the Planck data has constrained the amplitude of local non-Gaussianity to be small, given by [1, 75]

$$f_{\rm NL} \;=\; 2.7 \pm 5.8. \tag{4.1}$$

Hence an accurate measurement of $f_{\rm NL}$ in large-scale structure will require careful accounting of the relativistic effects in the observed overdensity [4, 5, 10, 11, 16]. The key problem with quantifying large-scale clustering is cosmic variance, but this can be overcome if we have multiple tracers of the underlying matter distribution [11, 76].

Note that this chapter is based on the work by [1]. Until the work by [1], relativistic effects in the observed fractional HI brightness temperature fluctuations have been computed for flat ΛCDM models (except for [17, 18]). If DE is dynamical, e.g. a quintessence, then it can cluster on super-Hubble scales, unlike Λ which does not cluster

at all. The clustering of DE on horizon scales should have some effect on the matter power, and to accurately identify this effect, a fully relativistic analysis is needed. We illustrate this via three different QCDM potentials (see Appendix B) whose DE equation of state cannot be approximated by a constant or a simple parametrization.

We compute the large-scale linear matter power spectrum, and the angular power spectrum for an HI intensity mapping survey – comparing them to a ΛCDM model. The aim here is not to fit the QCDM models to the data, but simply to show how these models differ from ΛCDM. Therefore we choose parameters and initial conditions so that the QCDM models have the same Ω_{m0} and H_0 as the ΛCDM model. In particular, this normalizes the matter power spectra to be the same on small scales at $z = 0$, i.e. where $a = (1+z)^{-1}$: thus this isolates any changes by clustering or GR effects, on large scales. (Hereafter, we remove overbars on the background redshift.)

In the rest of this chapter we investigate the clustering effect of quintessence on HI intensity mapping – on horizon scales, taking GR corrections into account. We begin by outlining the background and the perturbations equations of the QCDM models: focusing on three well known quintessence potentials namely, the Ratra-Peebles (RP), the supergravity (SUGRA) and the double exponential (DExp) potentials, respectively (see Appendix B for details of these models). We follow the standard cosmologies, i.e. by considering that quintessence and matter interact only gravitationally.

4.1.1 The background equations

The Friedmann equation for a quintessence φ, driven by a general potential $U(\varphi)$, is

$$\mathcal{H}^2 = \frac{8\pi G a^2}{3}\left[\bar{\rho}_m + \frac{\bar{\varphi}'^2}{2a^2} + U\right] = \mathcal{H}^2(\Omega_m + \Omega_q), \tag{4.2}$$

where we used Eq. (1.111). The associated acceleration equation is given by

$$\mathcal{H}' = -\frac{1}{2}\left(1 + 3w_q\Omega_q\right)\mathcal{H}^2. \tag{4.3}$$

By using Eqs. (1.111), (1.112) and (1.75), we obtain the quintessence equation of state parameter $w_q \equiv \bar{p}_\varphi/\bar{\rho}_\varphi$, given by

$$w_q = \frac{\varphi'^2 - 2a^2U}{\varphi'^2 + 2a^2U}, \tag{4.4}$$

which is governed by

$$w_q' = -3\mathcal{H}(1 - w_q^2) - \bar{\varphi}'(1 - w_q)\frac{U_{|\varphi}}{U}. \tag{4.5}$$

Quintessence evolves under the Klein-Gordon equation, given by Eq. (1.116).

4.1.2 The perturbations equations

Given the perturbed metric (2.50), the gravitational potential Φ is determined by the relativistic Poisson equation, given by [1]

$$\nabla^2\Phi \;=\; \frac{3}{2}\mathcal{H}^2(\Omega_m\Delta_m + \Omega_q\Delta_q), \tag{4.6}$$

where the comoving density contrasts are defined by Eq. (1.88), and the velocity potentials V_m, V_q and V (1.98) are related to the 4-velocities by

$$u^\mu_A \;=\; a^{-1}(1-\Phi,\; \partial^i V_A), \qquad u^\mu \;=\; a^{-1}(1-\Phi,\; \partial^i V), \tag{4.7}$$

where $A = m,\, q$: denoting matter and quintessence, respectively. Here u^μ is the total 4-velocity of the system, and V is the total peculiar velocity potential, given by

$$V \;=\; \frac{1}{1+w}\sum_A \Omega_A(1+w_A)V_A, \qquad w \;=\; \sum_A \Omega_A w_A. \tag{4.8}$$

On sub-Hubble scales, we have $\Delta_q \ll \Delta_m$, hence we can neglect Δ_q – and $\Delta_m \approx \delta_m$, leading to the Newtonian Poisson equation: $\nabla^2\Phi = (3/2)\mathcal{H}^2\Omega_m\delta_m$. This is quite often used in the analysis of large-scale structure. However, on large scales, δ_m is no longer an accurate tracer of the potential and the relativistic Poisson equation (4.6) must be used. The relativistic Poisson equation shows that DE clustering (on large scales) enhances the potential for a given matter overdensity. In other words, to attain a given magnitude of potential, one requires less matter clustering when the dark energy clusters.

The evolution of the gravitational potential is driven by the total momentum density:

$$\Phi' + \mathcal{H}\Phi \;=\; -\frac{3}{2}\mathcal{H}^2\left[\Omega_m V_m + (1+w_q)\Omega_q V_q\right], \tag{4.9}$$

where the matter fluctuations obey the energy-momentum conservation, given by

$$\Delta'_m - \frac{9}{2}\mathcal{H}^2\Omega_q(1+w_q)\,(V_m - V_q) \;=\; -\nabla^2 V_m, \tag{4.10}$$

$$V'_m + \mathcal{H}V_m \;=\; -\Phi. \tag{4.11}$$

The corresponding perturbations equations for quintessence are given by

$$\Delta'_q - 3w_q\mathcal{H}\Delta_q \;=\; \frac{9}{2}\mathcal{H}^2\Omega_m(1+w_q)\,(V_q - V_m) - (1+w_q)\nabla^2 V_q, \tag{4.12}$$

$$V'_q + \mathcal{H}V_q \;=\; -\Phi - \frac{c^2_{sq}}{(1+w_q)}\Delta_q, \tag{4.13}$$

where c_{sq} is the quintessence physical sound speed, given by Eq. (1.80), which describes how DE pressure perturbations propagate in the gravitational field.

It should be noted that, Eqs. (4.6)–(4.13) hold for any form of DE: one simply needs to specify $w_q(a)$ and $c_{sq}(a)$. For example, fluid models of dark energy specify these parameters ad hoc. In the case of quintessence, these parameters are self-consistently determined: w_q is determined by the potential $U(\varphi)$ via (1.116), (4.4) and (4.5), and for any $U(\varphi)$, the physical sound speed of quintessence is $c_{sq} = 1$: which follows from Eq. (1.80), by using the fact that $\delta\varphi|_{\rm rf} = 0$ in Eqs. (1.113) and (1.114).

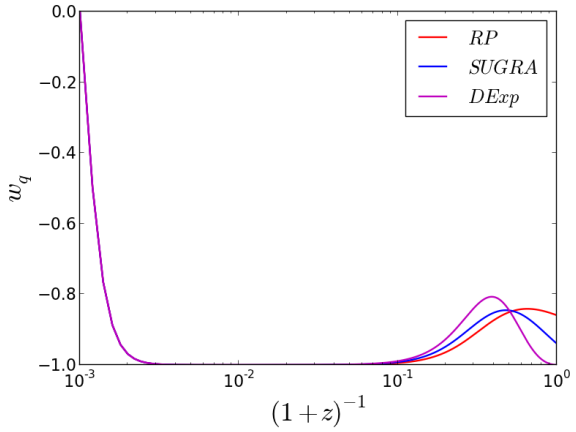

FIGURE 4.1: The cosmic evolution of the QCDM equation of state parameter w_q. The plots are given for the RP (B.1), SUGRA (B.2) and DExp (B.3) potentials, respectively.

4.2 Background Evolution of the Models

We initialize the integrations at decoupling $a_d = (1 + z_d)^{-1} = 10^{-3}$, neglecting photons and neutrinos. The initial background densities of matter and quintessence are determined by the requirement that Ω_{m0} and H_0 match the ΛCDM values (we take $\Omega_{m0} = 0.27$, $H_0 = 70.8$ Kms^{-1}Mpc). Here we assume quintessence is initially in a tracking regime, i.e. $w_q(z_d) = 0$. The effect of the radiation era on perturbations is modelled via a transfer function $T(k)$ (2.10), which is the same in QCDM and ΛCDM, since DE plays a negligible role in the radiation era.

In Fig. 4.1, we show the evolution of the equation of state parameters for the three QCDM models. Note that QCDM models are known to exhibit deviations in the equation of state: i.e. w_q departs from -1, for $z \lesssim 10$. Here, given our choice of initial conditions, we observe this deviation at $z \lesssim 9$ – while we see the tracker behaviour at $z \leq 10^3$. We show the evolution of the Hubble rate and the matter density parameter of QCDM, in comparison to those of ΛCDM, in Fig. 4.2. This evolution of the background parameters is driven by our normalization of the power spectra, i.e. the observed late-time deviations in Figs. 4.1 and 4.2 are govern by our fixing of the values of Ω_{m0} and H_0: to be equal for both QCDM and ΛCDM. Moreover, the late-time changes in Fig. 4.2 are a direct consequence of the deviations in w_q (Fig. 4.1).

4.3 The Large-scale Matter Power Spectrum

We connect the primordial inflationary perturbations to the decoupling epoch via the potential: Eqs. (2.11)–(2.13), where the potential suppression function $(1 + z)D_\Phi$, is normalized at decoupling by $(1 + z_d)D_\Phi(k, z_d) = 1$. We use the value $n = 0.96$, for the scalar spectral index. We adopt Eq. (2.15) for the matter overdensity.

Since at decoupling we have $\Omega_q(z_d) \ll 1$, we therefore use the Einstein-de Sitter initial condition $\Phi'(z_d) = 0$. The adiabatic initial conditions are specified by

$$S_{qm}(z_d) \;=\; 0 \;=\; S'_{qm}(z_d), \qquad S_{qm} \;=\; \frac{\delta_q}{(1 + w_q)} - \delta_m, \tag{4.14}$$

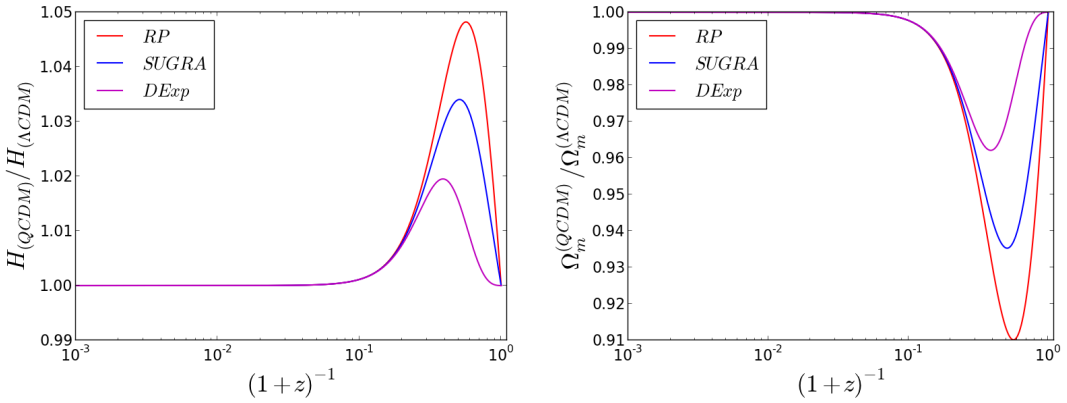

FIGURE 4.2: The cosmic evolution of the QCDM Hubble rate (*left*) and matter density parameter (*right*): relative to the ΛCDM – for the RP (B.1), SUGRA (B.2) and DExp (B.3) potentials, respectively.

where $\delta_q \equiv \delta\rho_\varphi/\bar{\rho}_\varphi$, and S_{qm} is the matter-quintessence relative entropy perturbation. Thus Eq. (4.14) together with the Poisson and other perturbation equations, determine the full initial matter and quintessence fluctuations: see Appendix C (section C.1).

For QCDM, Eq. (2.59) is no longer true. However, the normalization we have chosen means that Eq. (2.59) does hold at $z = 0$ on small scales, where the quintessence perturbations are negligible – i.e. we have $D_\Phi(k,z)$ and $D_m(k,z)$ to be

$$\text{QCDM:} \qquad D_\Phi(k,0) \;=\; D_m(k,0) \quad \text{for } k \gg H_0. \tag{4.15}$$

This property is shown in Fig. 4.3 (top panels) – where we show the gravitational potential growth function $D_\Phi(k,0)$, and the linear matter power factor $D_m(k,0)/D_\Phi(k,0)$. We see that indeed the given growth functions coincide on small scales at the present epoch, revealing the consequence of our normalization. They however begin to deviate on approaching horizon scales and beyond.

In order to incorporate the largest scales, we avoid the gauge-dependent density contrast δ_m, and use the comoving density contrast Δ_m, for the matter power spectrum: $P_m = P_{\Delta_m}$, given by Eq. (2.25). From (4.15), we see that the power spectrum for QCDM today will match that of ΛCDM on small scales. The changes induced by quintessence will be imprinted in P_m via $D_m/D_{\Phi 0}$ and will show up on the largest scales. These features are illustrated in Fig. 4.3, which shows the growth functions and power spectra for the QCDM models. Quintessence clusters on large scales, leading to a scale-dependent D_Φ on large scales. On small scales, D_Φ becomes scale-independent, since quintessence does not cluster on these scales. The offset between this constant value and that of ΛCDM follows from the different expansion history of quintessence that is necessary to achieve the same Ω_{m0}. This behaviour in Eq. (4.15) eventually propagates into the linear matter power spectrum $P_m(k,0)$ – bottom panels: Fig. 4.3.

We also show, in Fig. 4.3, the unphysical case of smooth quintessence – i.e. forcing quintessence perturbations to zero, given by $\Delta_q = \delta_q = V_q = 0$ with the evolution equations (4.12) and (4.13) being ignored. This approximation is often made, but it clearly breaks down badly on large scales. The smooth quintessence leads to an inconsistency in the perturbations equations, so that the results are gauge-dependent. In Newtonian gauge, smooth quintessence predicts a strong boost of matter power on the largest scales. Whereas in fact, the quintessence perturbations act to slightly *suppress* the matter power

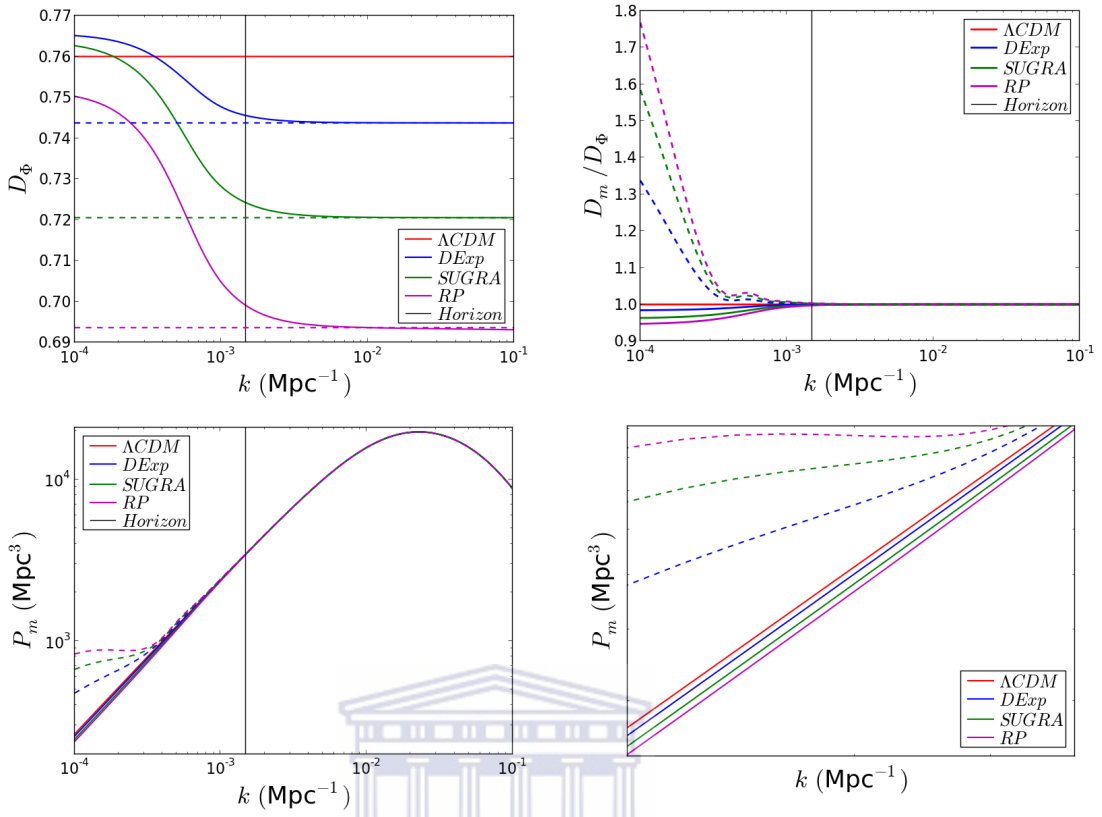

FIGURE 4.3: For the QCDM models, from top to bottom: the gravitational potential growth function $D_\Phi(k,0)$ (*top left*), and the linear matter power factor $D_m(k,0)/D_\Phi(k,0)$ (*top right*); the linear matter power spectrum $P_m(k,0)$ (*bottom left*), with zoom-in at large scales (*bottom right*). The dashed lines give the (unphysical) case of smooth quintessence – i.e. where quintessence perturbations are forced to zero.

on these scales, when the small-scale power is normalized to the ΛCDM power at $z = 0$. These results are consistent with previous works [77–83].

Owing to our normalization at $z = 0$, the QCDM power spectrum today matches that of ΛCDM on small scales. This is not true for $z > 0$, as illustrated in Fig. 4.4. In QCDM, the matter power is enhanced on sub-Hubble scales with increasing z. This is necessary in order to achieve the same power as ΛCDM today – given that in QCDM, $\Omega_m(z)$ is smaller and $H(z) = a^{-1}(z)\mathcal{H}(z)$ is bigger, for $0 < z \lesssim 10$. On super-Hubble scales, power is suppressed, more strongly at low redshifts, at the level of $\sim 5 - 10\%$ for the Ratra-Peebles potential. In the next subsection we extend previous results to consider the observable angular power spectrum $C_\ell(z)$, including all relativistic effects.

4.4 Relativistic Effects in the Observed Overdensity

Up to this point, we have worked with the matter density contrast Δ_m and its power spectrum P_m, i.e. with the perturbations in the total matter (dark and baryonic). However, we cannot observe the total matter fluctuations, only tracers of them, such

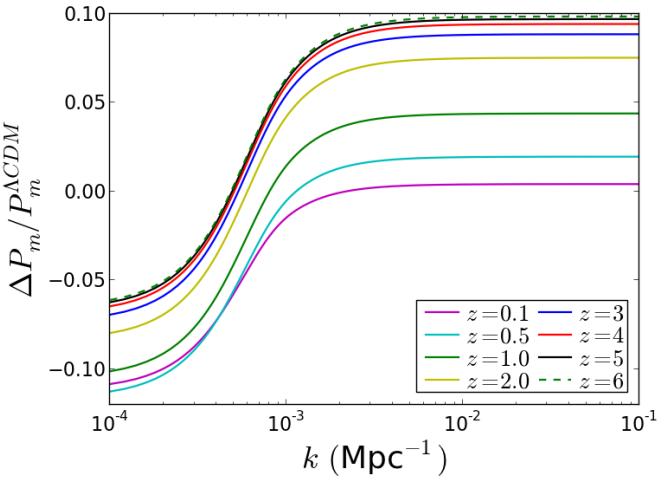

FIGURE 4.4: Plots of the fractional change in the linear matter power spectrum for inhomogeneous QCDM (using RP potential (B.1)), relative to ΛCDM at various redshifts z: where here we have $\Delta P_m \equiv P_m^{\rm QCDM} - P_m^{\Lambda\rm CDM}$.

as galaxies. Hence the galaxy density contrast that corresponds to Δ_m is the gauge-invariant overdensity $\Delta_{\rm g}$ (2.31). As often used in the literature, the relation

$$\delta_{\rm g}(k,z) \;=\; b(z)\delta_m(k,z), \tag{4.16}$$

is gauge-dependent on very large scales, and thus cannot be used to define the physical bias [3, 4]. Since the bias is physically defined in the matter rest frame, we must use the comoving density perturbation in the bias definition (2.31).

However, as pointed out in [1], owing to lightcone and redshift effects in the observational process, $\Delta_{\rm g}$ does not correspond to the observed overdensity on large scales, because of relativistic effects. The problem is that: (1) Firstly, we need to incorporate the well-known effects of redshift space distortions and weak lensing. These are typically the dominant relativistic effects in the observed overdensity. (2) Secondly, there are also other relativistic effects that arise when we correctly define the physical, observed galaxy overdensity $\Delta_{\rm g}^{\rm obs}$ [1, 3, 5–7, 9] (see chapter 4).

The observed overdensity (3.74) is unique and physically defined. It does not correspond to any of the standard gauge-invariant definitions of overdensity – but it is automatically gauge-invariant. We can write it in the form [1]

$$\Delta_{\rm g}^{\rm obs}(\mathbf{n},z) \;=\; \Delta_{\rm g}(\mathbf{n},z) + \Delta_{\rm loc}(\mathbf{n},z) + \Delta_{\rm int}(\mathbf{n},z). \tag{4.17}$$

The comoving position of the source is $\mathbf{x} = r(z)\mathbf{n}$, as given in section 2.4, where the comoving radial distance is thus given by

$$r(z) \;=\; \int_0^z \frac{d\tilde{z}}{(1+\tilde{z})\mathcal{H}(\tilde{z})}, \tag{4.18}$$

where (hereafter) we remove overbars on the background comoving radial distance. In the gauge we have chosen, the local and integrated terms are

$$\Delta_{\rm loc} = -\frac{1}{\mathcal{H}}(\bar{n}^i\partial_i)^2 V_m + \Delta^{\rm rel}_{\rm loc}, \tag{4.19}$$

$$\Delta_{\rm int} = -2\,(1-\mathcal{Q})\int_0^r d\tilde{r}\,(r-\tilde{r})\,\frac{\tilde{r}}{r}\nabla^2_\perp\Phi + \Delta^{\rm rel}_{\rm int}, \tag{4.20}$$

where $\nabla^2_\perp = \nabla^2 - (\bar{n}^i\partial_i)^2 - 2r^{-1}\bar{n}^i\partial_i$ is the screen-space Laplacian. Here, $r = r(z)$ is the comoving distance at the source, and z is the unperturbed observed redshift. The first term in Eq. (4.19) is the standard Kaiser term (2.44) and the first term in Eq. (4.20) is the standard weak lensing term. Both of these standard terms are relativistic corrections to a Newtonian approach; and $\mathcal{Q}(z)$ is the magnification bias (2.36).

The additional local relativistic correction term (see chapter 4) is [1, 5]

$$\begin{aligned}\Delta^{\rm rel}_{\rm loc} &= (3-b_e)\,\mathcal{H}V_m - \left[b_e - 2\mathcal{Q} - \frac{\mathcal{H}'}{\mathcal{H}^2} - 2\frac{(1-\mathcal{Q})}{r\mathcal{H}}\right]\bar{n}^i\partial_i V_m \\ &\quad + \left[4\mathcal{Q} - b_e - 1 + \frac{\mathcal{H}'}{\mathcal{H}^2} + 2\frac{(1-\mathcal{Q})}{r\mathcal{H}}\right]\Phi + \frac{1}{\mathcal{H}}\Phi',\end{aligned} \tag{4.21}$$

and the integrated relativistic term is given by

$$\Delta^{\rm rel}_{\rm int} = 4\frac{(1-\mathcal{Q})}{r}\int_0^r d\tilde{r}\,\Phi + 2\left[b_e - 2\mathcal{Q} - \frac{\mathcal{H}'}{\mathcal{H}^2} - 2\frac{(1-\mathcal{Q})}{r\mathcal{H}}\right]\int_0^r d\tilde{r}\,\Phi'. \tag{4.22}$$

Here the galaxy evolution bias b_e is given by Eq. (3.26).

4.5 The Observed Angular Power Spectrum

We could use the 3D power spectrum $P^{\rm obs}_{\rm g} \equiv P_{\Delta^{\rm obs}_{\rm g}}$ as a measure of the observed galaxy overdensity (see [18]). However, it describes fluctuations on a constant time slice, rather than on the observed past lightcone – on which observations are actually made. Hence it is useful to use instead the observed angular power spectrum $C_\ell(z)$, at different redshifts, which measures directly the matter distribution on surfaces on the past lightcone. (See [15] for an alternative approach based on the observed correlation function.) Note also that we avoid the flat-sky approximation by using $C_\ell(z)$. This is also important for consistently dealing with large scales.

The observed overdensity can be expanded in spherical harmonics, given by

$$\Delta^{\rm obs}_{\rm g}(\mathbf{n}, z) = \sum_{\ell m} a_{\ell m}(z) Y_{\ell m}(\mathbf{n}), \tag{4.23}$$

whence we get the angular power spectrum at a given redshift:

$$C_\ell(z) = \left\langle |a_{\ell m}(z)|^2 \right\rangle, \tag{4.24}$$

$$a_{\ell m}(z) = \int d^2\mathbf{n}\, Y^*_{\ell m}(\mathbf{n})\Delta^{\rm obs}_g(\mathbf{n}, z). \tag{4.25}$$

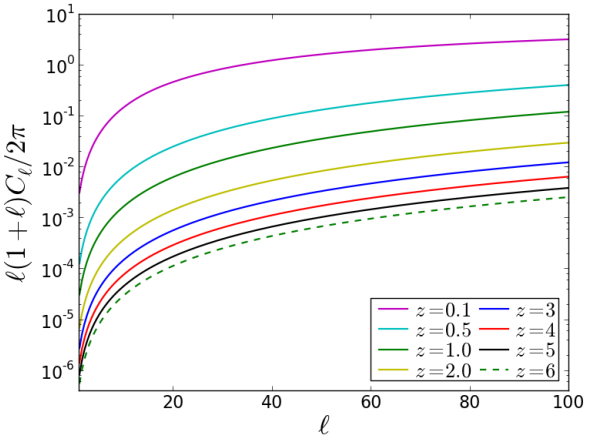

FIGURE 4.5: The angular power spectrum of the fractional HI brightness temperature fluctuations for QCDM (using RP potential (B.1)) at various redshifts z.

Thus $C_\ell(z)$ involves the auto- and cross-correlations of all the terms on the right of (4.17), using (4.19)–(4.22). For example,

$$\left\langle \left|\Delta_{\rm g}(\mathbf{n},z)\right|^2 \right\rangle_\ell \propto \frac{b^2(z)}{(\Omega_{m0}H_0^2)^2}\int dk\, k^6 P_{\Phi_p}(k) D_m^2(k,z)[j_\ell(k\bar{r}_z)]^2.$$

4.5.1 HI intensity map survey

For an intensity map in HI, the observed brightness temperature fractional perturbations are given by [1, 17]

$$\Delta_{T_b}^{\rm obs} = \Delta_{\rm g}^{\rm obs} - 2\frac{\delta D_L}{\bar{D}_L}, \tag{4.26}$$

where D_L is the luminosity distance. The relativistic expression for the perturbation δD_L contains the weak lensing and other relativistic terms above – and we obtain

$$\Delta_{T_b}^{\rm obs} = \Delta_{\rm g}^{\rm obs}\Big|_{\mathcal{Q}=1}. \tag{4.27}$$

In other words, the brightness temperature fractional perturbations in an HI intensity map are given by the galaxy overdensity in the case when the magnification bias is $\mathcal{Q}=1$. The most important consequence is that the weak lensing term cancels out in this case, and we get [1]

$$\begin{aligned}\Delta_{T_b}^{\rm obs} &= \Delta_{\rm g}(\mathbf{n},z) - \frac{1}{\mathcal{H}}(\bar{n}^i\partial_i)^2 V_m + 3\mathcal{H}V_m + \left(2+\frac{\mathcal{H}'}{\mathcal{H}^2}\right)\bar{n}^i\partial_i V_m \\ &\quad + \left(3+\frac{\mathcal{H}'}{\mathcal{H}^2}\right)\Phi + \frac{1}{\mathcal{H}}\Phi' - 2\left(2+\frac{\mathcal{H}'}{\mathcal{H}^2}\right)\int_0^{\bar{r}_z} d\bar{r}\,\Phi',\end{aligned} \tag{4.28}$$

where for simplicity, we used N_g = constant, so that $b_e = 0$. We notice the Kaiser distortion term as the second term in the first line, and the subsequent term are: the relativistic velocity and gravitational potential corrections, and the local and integrated relativistic terms. Thus the angular power spectrum of the *fractional* (i.e. dimensionless)

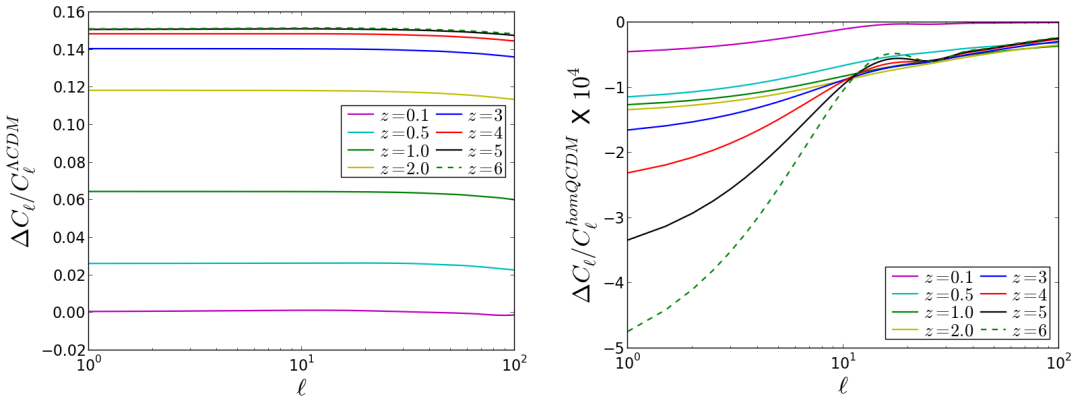

FIGURE 4.6: Plots of the fractional change in angular power spectrum: between QCDM and ΛCDM, where $\Delta C_\ell \equiv C_\ell^{\rm QCDM} - C_\ell^{\Lambda\rm CDM}$ (*left*); and between inhomogeneous and homogeneous QCDM, where $\Delta C_\ell \equiv C_\ell^{\rm QCDM} - C_\ell^{\rm homQCDM}$ (*right*).

HI brightness temperature fluctuations, is given by

$$C_\ell^{T_b}(z) = \left\langle |a_{\ell m}(z)|^2 \right\rangle, \tag{4.29}$$

$$a_{\ell m}(z) = \int d^2\mathbf{n}\, Y^*_{\ell m}(\mathbf{n}) \Delta^{\rm obs}_{T_b}(\mathbf{n}, z). \tag{4.30}$$

Figure 4.5 shows $C_\ell^{T_b}(z)$ for QCDM at various redshifts. As pointed out in [17], the integrated term in Eq. (4.28) makes a negligible contribution, and the dominant term is the Kaiser term.

In Fig. 4.6, the fractional difference between QCDM and ΛCDM (left panel) reflects the effect of the equation of state parameter w_q on the matter power spectrum of Fig. 4.4. This fractional difference increases with redshift and asymptotes to a maximum that is determined by our normalization. Note that the strongest growth in the fractional difference occurs for $1 \lesssim z \lesssim 2$, where the deviation of w_q from -1 is largest (Fig. 4.1). However, we do not observe any significant scale-dependence in the changes of the C_ℓ, compared with the matter power spectrum case in Fig. 4.4. This is due to the fact that the large-scale changes in $P_m(k, z)$ are suppressed by the integration over k to get $C_\ell(z)$ (see e.g., Eq. (4.26)). In other words, the $\sim 5 - 15\%$ suppression of power in P_m is reduced to sub-percent in the C_ℓ.

Furthermore, Fig. 4.6 (right panel) shows the small changes in the angular power spectrum of the (dimensionless) HI brightness temperature fluctuations between the physical model of clustering quintessence and the unphysical smooth quintessence. On large scales, smooth quintessence provides a false boost in angular power $C_\ell(z)$, which grows as z increases. This is consistent with the behaviour of $P_m(k, z)$ in Fig. 4.3.

Essentially, we show that the quintessence clustering reduces the super-Hubble scale power in the 3D (comoving-gauge) matter power spectrum, when the small-scale power is normalised to the ΛCDM power (at $z = 0$). Moreover, the large angular scales of the HI angular power spectrum are known to be relatively insensitive to the largest scale modes of the 3D power spectrum. However, it is shown that the redshift dependence of the HI angular power spectrum is sensitive to the quintessence model through changes in the background expansion history.

4.6 Conclusion

We have provided a fully relativistic investigation of dark energy and matter perturbations in the post-recombination large-scale power spectrum, by using standard (non-interacting) quintessence models. We carefully accounted for large-scale modes (and thus of gauge issues). We have also taken care to use the relativistic Poisson equation, and defined the bias in terms of the comoving matter overdensity. This is important for deriving the correct matter power spectrum in the presence of inhomogeneous dark energy. Our equations were a simple generalization of previous works – on relativistic effects in the observed overdensity – from ΛCDM to dynamical dark energy models (see also [18]).

We illustrated the implications of the generalized equations for three quintessence models, each of which has nontrivial evolution in the equation of state parameter at low z. In order to isolate the effect of quintessence on large-scale galaxy overdensity, we normalized the quintessence power spectrum at today ($z = 0$) so that it agrees on sub-Hubble scales with the ΛCDM power spectrum. We found that super-Hubble clustering had a very small effect on the large-scale power spectrum at $z = 0$. Nevertheless, it is essential to incorporate the large-scale quintessence perturbations: the unphysical assumption of smoothness of quintessence (i.e. forcing the perturbations to vanish) violates the Einstein equations, and leads to a false boost of large-scale power.

On the other hand, the self-consistent treatment of quintessence, i.e. by allowing perturbations in quintessence, showed a small suppression of large-scale power at $z = 0$. For higher z, we observed a boost of matter power on small scales. However this was mainly due to background evolution effects since a stronger growth of matter perturbations would be needed (given a lower matter density parameter $\Omega_m(z)$ and higher Hubble parameter $H(z) = a^{-1}(z)\mathcal{H}(z)$) in order to arrive at the ΛCDM value of Ω_{m0}.

Moreover we considered the case of an HI intensity map survey, where the observed fractional brightness temperature fluctuation is given by the observed galaxy (number) overdensity in the case of magnification bias $\mathcal{Q} = 1$, which removes the weak lensing convergence contribution. We computed the angular power spectrum for the case of an HI intensity map survey – using three quintessence potentials as examples.

By comparing to the concordance model with the same small-scale power at $z = 0$, quintessence showed a relative boost in the angular power by up to ∼15% at high z. The power spectra in quintessence and in ΛCDM appeared to converged at low z. The difference is mainly due to the background evolution, driven mostly by the normalization of the power spectrum at $z = 0$. The dark energy perturbations made only a small contribution on the largest scales, and a negligible contribution on smaller scales. Ironically, the dark energy perturbations removed the false boost of large-scale power that arises if we impose the (unphysical) assumption that the dark energy is smooth.

Chapter 5

Dark Energy Homogeneity in General Relativity

Dark energy is 'dark', but its underlying physics is even 'darker'. Understanding the nature of DE remains a puzzle in general relativity. A long standing question is that: is DE actually static vacuum energy Λ, i.e. like in the standard concordance model (ΛCDM); or a dynamic field, e.g. like in the quintessence models (QCDM)? If DE is described by Λ then it can not have perturbations (or evolve) at all. Moreover, although ΛCDM is the best-fit model to the current data, other alternatives have been considered in the literature, e.g. a homogeneous dynamical DE. However, if DE is dynamical then it can have perturbations. How then do we define a valid homogeneous (dynamical) DE?

Thusfar, there does not appear to be an agreed (or adequate) definition of homogeneous DE (except for [57]). For example, if the DE physical sound speed is $c_{sx} = 1$, then DE cannot cluster on sub-Hubble scales. Thus it is sometimes concluded that DE is approximately homogeneous (see e.g. [84–102]). The caveat to this assumption is that it only ensures a 'scale-dependent' homogeneity, in the sense that it makes DE homogeneous only on sub-Hubble scales, but on super-Hubble scales DE becomes significantly inhomogeneous. This is because, $c_{sx} = 1$ implies that the DE density perturbations propagate with the speed of light; hence DE fails to cluster, and is perturbatively insignificant. However, on horizon scales the perturbation behaviour is different and the homogeneity assumption breaks down – i.e. the implicit assumption of no clustering in DE on super-Hubble scales, given that $c_{sx} = 1$, is inconsistent.

Moreover, an assumption often used for DE homogeneity is the requirement that all its perturbations vanish [1, 77, 80, 83, 103–105], i.e. by setting the DE density perturbation and velocity potential to zero, given by [1, 57] (see also chapter 4)

$$\Delta_x \;=\; \delta_x \;=\; V_x \;=\; 0, \tag{5.1}$$

where the associated evolution equations are therefore discarded. However, it has been pointed out that a fluctuating, inhomogeneous component is the only valid way of introducing an additional energy component (i.e. DE): a smooth (non-fluctuating), time-varying component is unphysical – it violates the equivalence principle [106]. Moreover, it is known that Eq. (5.1) leads to a violation of the self-consistency of the equations of general relativity, by causing a contradiction in the equations. For example, it has been shown that Eq. (5.1) leads to a false boost in the matter power spectrum [1, 80], and in the ISW effect [83, 106] (of the CMB) – on horizon scales. (Also, recently it has been shown in [107] that neglecting the DE perturbations can lead to misleading estimation

of the matter growth index, giving up to $\sim 3\%$ deviation: which is a significant amount, as we enter an era of precision cosmology.) Nevertheless, none of the previous works (except for [57]) has shown explicitly what the inconsistency resulting from Eq. (5.1) is, nor has given any suggestions on how to solve or circumvent this problem.

In this chapter (which is based on the work by [57]) we try to address these issues, i.e. as outlined above. Firstly we show analytically the inconsistency resulting from Eq. (5.1). Then we propose an alternative way, via the intrinsic entropy perturbation, to define a valid, adequate condition for DE homogeneity – which corrects Eq. (5.1) to avoid the violation of the consistency of the equations of general relativity, and also eliminates c_{sx} from the equations (like in ΛCDM). It should be noted that the aim is not to fit the given homogeneous DE to the data (which might have been one other avenue to show the observational significance of the homogeneous DE), but to provide a suitable way to define a valid, adequate DE homogeneity condition – which currently seems to be non-existent. Furthermore, for illustration purpose, the effects of general relativistic corrections (and magnification bias) in the power spectrum is demonstrated.

Note that the evolution equations here are the same as those in chapter 4, except that (henceforth) we denote the DE parameters by a subscript "x". For convenience, we shall rewrite the necessary equations again. We begin by outlining the basic background equations in section 5.1; we give the perturbations equations in section 5.2. In section 5.3 we discuss the intrinsic entropy perturbation; and in section 5.4 we look at DE homogeneity in general relativity: discussing the 'unphysical' smooth DE and a 'true' homogeneous DE – illustrating their effects in the galaxy and matter power spectra. We conclude in section 5.5.

5.1 The Background Equations

The background gravitational field equations are given by

$$\mathcal{H}^2 \;=\; \frac{8\pi G a^2}{3}(\bar{\rho}_m + \bar{\rho}_x), \qquad \mathcal{H}' \;=\; -\frac{1}{2}(1 + 3\Omega_x w_x)\mathcal{H}^2, \tag{5.2}$$

where the matter equation of state parameter is $w_m = \bar{p}_m/\bar{\rho}_m = 0$, and $\Omega_A = \bar{\rho}_A/\bar{\rho}$ (with $A = m,\ x$) are the energy density parameters, which evolve according to Eq. (1.79). Similarly, the DE equation of state parameter $w_x = \bar{p}_x/\bar{\rho}_x$ evolves by

$$w_x' \;=\; -3\mathcal{H}(1 + w_x)(c_{ax}^2 - w_x), \tag{5.3}$$

where the matter (squared) sound speeds are $c_{am}^2 = 0 = c_{sm}^2$.

5.2 The General Perturbations Equations

Here we adopt the Newtonian metric (2.50). From subsection 1.2.7, the relativistic Poisson equation is given by

$$\nabla^2\Phi \;=\; \frac{3}{2}\mathcal{H}^2 \sum_A \Omega_A \Delta_A, \tag{5.4}$$

where the comoving density perturbations Δ_A are given by Eq. (1.88). The gravitational potential is driven by the total momentum density, given by

$$\Phi' + \mathcal{H}\Phi \;=\; -\frac{3}{2}\mathcal{H}^2 \sum_A \Omega_A(1+w_A)V_A, \tag{5.5}$$

where the velocity potentials V_A are given by Eq. (4.7).

We consider all species as perfect fluids. Thus for the species A, the perturbed energy-momentum tensor is

$$\delta T^{\mu\nu}_A \;=\; (\delta\rho_A + \delta p_A)\,\bar{u}^\mu_A \bar{u}^\nu_A + \delta p_A \bar{g}^{\mu\nu} + \bar{p}_A \delta g^{\mu\nu} + (\bar{\rho}_A + \bar{p}_A)\left[\delta u^\mu_A \bar{u}^\nu_A + \bar{u}^\mu_A \delta u^\nu_A\right], \tag{5.6}$$

where δp_A, δu^μ_A and $\delta g^{\mu\nu}$ are the perturbations in the pressure, 4-velocity and the metric tensor, respectively. The conservation of energy and momentum implies that

$$\nabla_\mu \sum_A \delta T^{\mu\nu}_A \;=\; 0 \;=\; \nabla_\mu \delta T^{\mu\nu}_A. \tag{5.7}$$

Thus given Eq. (5.7) the velocity potential V_A and the comoving overdensity Δ_A (see subsection 1.2.7) evolve by

$$V'_A + \mathcal{H}V_A \;=\; -\Phi - \frac{c^2_{sA}}{1+w_A}\Delta_A, \tag{5.8}$$

$$\Delta'_A - 3\mathcal{H}w_A\Delta_A \;=\; \mathcal{H}\hat{\Delta}_A - (1+w_A)\nabla^2 V_A, \tag{5.9}$$

where we have defined the parameter $\hat{\Delta}_A$, given by

$$\mathcal{H}\hat{\Delta}_A \;\equiv\; \frac{9}{2}\mathcal{H}^2(1+w_A)\sum_{B\neq A}\Omega_B(1+w_B)(V_A - V_B). \tag{5.10}$$

The index B runs through the entire species, for a given (fixed) value of A.

5.3 The Intrinsic Entropy Perturbation

The entropy of a given (thermodynamic) system or fluid, measures the degree of 'disorderliness' of that fluid; hence is a perturbed quantity. The intrinsic (or inherent) entropy perturbation δs_A of A, may be given by [57, 108–112]

$$\bar{p}_A\,\delta s_A \;\equiv\; \bar{p}'_A\left(\frac{\delta p_A}{\bar{p}'_A} - \frac{\delta\rho_A}{\bar{\rho}'_A}\right). \tag{5.11}$$

Then from subsection 1.2.7, we have the pressure perturbations (1.87) given by

$$\delta p_A \;=\; c^2_{aA}\delta\rho_A + (c^2_{sA} - c^2_{aA})\bar{\rho}_A\Delta_A. \tag{5.12}$$

Whence we obtain the intrinsic entropy perturbation (5.11), given by

$$\bar{p}_A\,\delta s_A \;=\; (c^2_{sA} - c^2_{aA})\bar{\rho}_A\Delta_A \;=\; (c^2_{sA} - c^2_{aA})\,\delta\rho_A|_{\mathrm{rf}}, \tag{5.13}$$

where the second equality follows from Eq. (1.90). Thus the intrinsic entropy perturbation of any specie corresponds to the density perturbation of that specie in its rest

frame. Moreover, we notice that δs_A is automatically gauge-invariant.

5.4 General Relativity and Dark Energy Homogeneity

In this section, we analytically discuss the inconsistency in the equations of general relativity – resulting from Eq. (5.1), i.e. we illuminate what the inconsistency really is: (analytically) describing its source/origin. We also propose a suitable way to define a valid, adequate condition for DE homogeneity in general relativity.

The equations of general relativity form a self-consistent system. An implication of this is that the gravitational potential evolution equation (5.5) should always reduce to the Poisson equation (5.4). To confirm this, it is only sufficient to show that the Poisson equation at any time solves the associated gravitational potential evolution equation.

By taking the time derivative of Eq. (5.4), and using the appropriate equations (see section 5.2, and also subsection 1.2.7), we get

$$\nabla^2\Phi' \;=\; -\mathcal{H}\nabla^2\Phi - \frac{3}{2}\mathcal{H}^2\sum_A \Omega_A(1+w_A)\nabla^2 V_A, \tag{5.14}$$

where by dividing through by the Laplacian ∇^2, we get Eq. (5.5) – as required. This way, the system of equations remain complete and consistent. Nevertheless, note that Eq. (5.14) is obtained mainly as a result of the fact that [57]

$$\sum_A \Omega_A\hat{\Delta}_A \;=\; 0, \tag{5.15}$$

where given Eq. (5.10), it is easy to establish Eq. (5.15). Obviously, Eq. (5.15) is essentially the statement of a 'consistency condition' for the system of equations of general relativity. This condition should always hold given any correct set up (within general relativity).

However, if in any adopted framework we have that this condition does not hold, i.e. $\sum_A \Omega_A\hat{\Delta}_A \neq 0$, then this will result in a contradiction: where we are unable to recover the standard gravitational potential evolution equation (5.5); effectively we will rather have a transformation, given by

$$\Phi' \;\rightarrow\; \Phi' + \mathcal{H}\hat{\Phi}, \tag{5.16}$$

where Φ' is given by Eq. (5.5), and

$$\mathcal{H}\hat{\Phi} \;\equiv\; \frac{3}{2}\mathcal{H}^3\nabla^{-2}\sum_A \Omega_A\hat{\Delta}_A. \tag{5.17}$$

Thus Eqs. (5.16) and (5.17) analytically express the 'unwanted' inconsistency (or contradiction) that will arise in the physical equations of general relativity, when Eq. (5.15) fails to hold. It should be noted that the parameter $\mathcal{H}\hat{\Delta}_A$ is physical, and will contribute to the comoving density perturbation via Eq. (5.9).

5.4.1 The particular perturbations equations

We assume (henceforth) the late Universe – dominated by DE and matter ("m"), i.e. baryons and cold dark matter. Thus the relativistic Poisson equation is

$$\nabla^2\Phi \;=\; \frac{3}{2}\mathcal{H}^2\left[\Omega_m\Delta_m + \Omega_x\Delta_x\right], \tag{5.18}$$

where we take care to use the correct overdensities $\Delta_{m,x}$, in order to avoid 'unphysical artefacts' (see e.g. [113]) in the results.

The gravitational potential evolution, driven by the matter and DE momentum densities, is given by

$$\Phi' + \mathcal{H}\Phi \;=\; -\frac{3}{2}\mathcal{H}^2\left[\Omega_m V_m + \Omega_x(1+w_x)V_x\right], \tag{5.19}$$

and the matter perturbations evolve according to

$$V_m' + \mathcal{H}V_m \;=\; -\Phi, \tag{5.20}$$

$$\Delta_m' - \frac{9}{2}\mathcal{H}^2\Omega_x(1+w_x)(V_m - V_x) \;=\; -\nabla^2 V_m. \tag{5.21}$$

Similarly, the DE velocity potential and density perturbation evolve by

$$V_x' + \mathcal{H}V_x \;=\; -\Phi - \frac{c_{sx}^2}{1+w_x}\Delta_x, \tag{5.22}$$

$$\Delta_x' - 3\mathcal{H}w_x\Delta_x \;=\; \frac{9}{2}\mathcal{H}^2\Omega_m(1+w_x)(V_x - V_m) - (1+w_x)\nabla^2 V_x, \tag{5.23}$$

where Eqs. (5.18)–(5.23) follow from Eqs. (5.4)–(5.10). Next we consider scenarios where the consistency condition (5.15) may or may not be violated.

5.4.2 Unphysical smooth dark energy

Given Eq. (1.88), the homogeneity condition (5.1) implies that $\Delta_x = 0 = \Delta_x'$. Thus by applying Eq. (5.1) in Eqs. (5.18) and (5.19), the resulting Poisson equation is

$$\nabla^2\Phi \;=\; \frac{3}{2}\mathcal{H}^2\Omega_m\Delta_m, \tag{5.24}$$

and the gravitational potential evolution is

$$\Phi' + \mathcal{H}\Phi \;=\; -\frac{3}{2}\mathcal{H}^2\Omega_m V_m. \tag{5.25}$$

The resulting matter overdensity evolution is

$$\Delta_m' - \frac{9}{2}\mathcal{H}^2\Omega_x(1+w_x)V_m \;=\; -\nabla^2 V_m, \tag{5.26}$$

where Eq. (5.20) remains unchanged, with Eqs. (5.22) and (5.23) being neglected (as required by Eq. (5.1)).

Then similarly, as done in Eq. (5.14), upon taking the time derivative of Eq. (5.24) and using Eqs. (5.25) and (5.26), given that $w = w_x\Omega_x$ and $\Omega_m' = 3\mathcal{H}w_x\Omega_x\Omega_m$, we get

$$\tilde{\Phi}' = -\mathcal{H}\Phi - \frac{3}{2}\mathcal{H}^2\Omega_m V_m + \mathcal{H}\hat{\Phi}, \tag{5.27}$$

$$\mathcal{H}\hat{\Phi} \equiv -\frac{27}{4}\mathcal{H}^5\Omega_m\Omega_x(1+w_x)k^{-2}V_m, \tag{5.28}$$

i.e. $\Phi' \to \tilde{\Phi}' = \Phi' + \mathcal{H}\hat{\Phi}$, where Φ' is given by Eq. (5.25), with k being the wavenumber. Indeed Eqs. (5.27) and (5.28) agree with Eqs. (5.16) and (5.17).

We notice a contradiction by Eq. (5.27) – which is that, Eq. (5.27) does not coincide with Eq. (5.25). The difference between the two equations is given by $\mathcal{H}\hat{\Phi}$. This way, the system of equations is no longer consistent: the equations can not be combined in any way to reproduce the associated gravitational potential evolution equation. Note that, $\hat{\Delta}_m$ and $\hat{\Delta}_x$ are only encountered via the Δ_m' and Δ_x' equations, respectively.

Moreover, note that by imposing the smooth DE condition (i.e. Eq. (5.1)) directly to Eqs. (5.22) and (5.23), one gets: $-(9/2)\mathcal{H}^2\Omega_m(1+w_x)V_m = 0$. However, by this it automatically implies that either (i) $w_x = -1$, or (ii) $V_m = 0$. But it is already taken that $w_x \neq -1$, and V_m cannot be zero. Hence that leads to a contradiction. Usually, in the literature the Δ_x' equation is merely disregarded (while keeping $w_x \neq -1$ and $V_m \neq 0$) – this is the source of inconsistency in the general relativistic equations, which has rightly been reported in the literature.

Thus since by Eq. (5.1), the Δ_x' equation (and hence, $\hat{\Delta}_x$) is discarded, we have (i.e. given Eq. (5.26)) that

$$\sum_{A=m,x}\Omega_A\hat{\Delta}_A = \frac{9}{2}\mathcal{H}^2\Omega_m\Omega_x(1+w_x)V_m = \mathcal{H}\Omega_m\hat{\Delta}_m, \tag{5.29}$$

which eventually lead to Eq. (5.28); thereby defying the consistency condition (5.15). Obviously by Eq. (5.29), unless $w_x = -1$, Eq. (5.1) leads to a contradiction – and hence a violation of the self-consistency of the equations of general relativity. Thus Eq. (5.1) is wrong, and the resulting 'smooth' DE from such assumption is 'unphysical'. However, Eq. (5.29) reveals why the ΛCDM satisfies general relativity, despite the fact that all the DE perturbations therein become zero (which is because $w_x = -1$ in ΛCDM).

However, if we consider a (generic) clustering DE, i.e. with $V_x \neq 0$ and $\Delta_x \neq 0 \neq \delta_x$. Then we will get that $\Omega_m\hat{\Delta}_m + \Omega_x\hat{\Delta}_x = 0$. It is a straightforward thing to show that, by taking the time derivative of Eq. (5.18) and applying the appropriate equations, we obtain Eq. (5.19). Hence, a clustering DE rightly upholds the consistency of the system of equations of general relativity. But as mentioned earlier, $\mathcal{H}\hat{\Delta}_m$ (for example) is physical and will contribute to the matter density perturbation Δ_m via Eq. (5.21). Generally, for the clustering DE, the growth of $\mathcal{H}\hat{\Delta}_m$ on super-Hubble scales will be restrained by the relative velocity potential $V_m - V_x$, while for the (unphysical) smooth DE this term grows almost linearly, driven by V_m (see Eq. (5.29)).

We illustrate these behaviours at the present epoch in Fig. 5.1, using QCDM: see Appendix B. These behaviours explain the matter power spectrum reported in chapter 4 (i.e. by [1]), where it is shown that a smooth DE defined by Eq. (5.1), leads to a false (unphysical) amplification of the linear matter power spectrum on super-Hubble scales. Henceforth, we reserve the name 'smooth' for the unphysical DE, defined by Eq. (5.1).

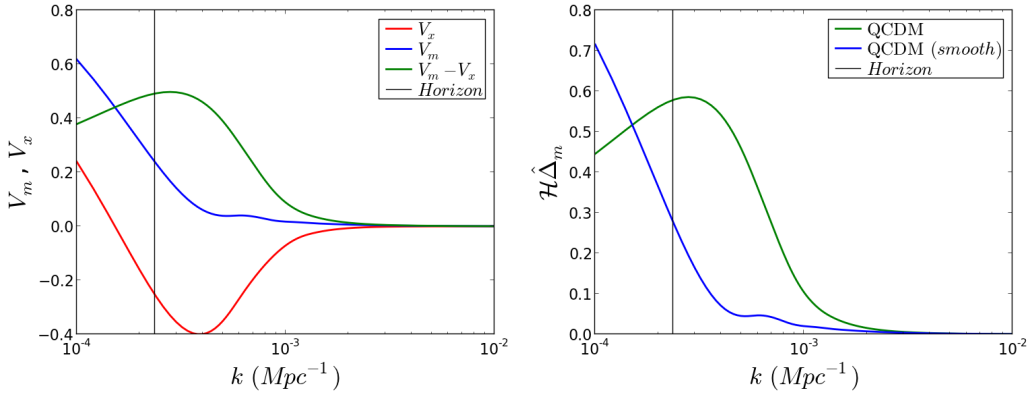

FIGURE 5.1: Plots at $z = 0$. *Left:* The DE and the matter velocity potentials, $V_x(k)$ (red) and $V_m(k)$ (blue), respectively; and their difference $V_m(k) - V_x(k)$ (green). *Right:* The parameter $\mathcal{H}\hat{\Delta}_m(k)$ – for clustering QCDM (green), and *smooth* QCDM (blue).

5.4.3 The large-scale galaxy power spectrum

In order to adequately account for the correct galaxy distribution on large scales, we use the observed galaxy density perturbation [1, 3, 5, 7, 9, 24] to compute that galaxy power spectrum $P_{\rm g}^{\rm obs}$, which is approximated in the flat-sky limit (in Fourier space) by [2, 5, 57]

$$\frac{P_{\rm g}^{\rm obs}}{P_m} = \left(b + f\mu^2\right)^2 + 2\left(b + f\mu^2\right)\mathcal{A}\frac{\mathcal{H}^2}{k^2} + \mathcal{A}^2\frac{\mathcal{H}^4}{k^4} - \mu^2\mathcal{B}^2\frac{\mathcal{H}^2}{k^2}. \tag{5.30}$$

where P_m is the matter power spectrum (2.25); μ is the cosine of the angle between the line-of-sight, with the wavenumber k here given in units of $\mathcal{H}$, and

$$\mathcal{A} = (3 - b_e)\, f + \left[4\mathcal{Q} - b_e - 1 + \frac{\mathcal{H}'}{\mathcal{H}^2} + 2\frac{(1-\mathcal{Q})}{r\mathcal{H}} + \frac{\Phi'}{\mathcal{H}\Phi}\right]\frac{k^2\Phi}{\mathcal{H}^2\Delta_m}, \tag{5.31}$$

$$\mathcal{B} = -\left[b_e - 2\mathcal{Q} - \frac{\mathcal{H}'}{\mathcal{H}^2} - 2\frac{(1-\mathcal{Q})}{r\mathcal{H}}\right] f, \tag{5.32}$$

where f is given by Eq. (2.45). Note that in ΛCDM, this f reduces to the standard growth rate of matter energy density (linear) perturbation. We have neglected all integral terms and set the galaxy evolution bias $b_e = 0$; r is the comoving distance (4.18) from the observer to the source at the observed z.

5.4.4 True homogeneous dark energy

A physical, consistent homogeneous DE should be one such that it maintains the consistency of the equations of general relativity, by upholding Eq. (5.15), irrespective of the nature of its equation of state parameter w_x.

Given that the entropy (perturbation) of any fluid measures the degree of disorderliness in the fluid, then homogeneity or inhomogeneity of the fluid may be defined with respect to its entropy. Particularly, that the (net) intrinsic entropy perturbation of the fluid vanishes. By the vanishing of the intrinsic entropy perturbation, it implies that the *net internal distortion* (i.e. the total change in the inherent distortions) of the fluid becomes zero. This way, the fluid may be thought to be constituted by an even distribution of equi-amplitude distortions – hence the fluid is homogeneous (or uniform).

Therefore in this context, 'homogeneity' refers to 'uniformity', so that a 'true' homogeneous DE is not one entirely devoid of perturbations, but one made up of uniformly distributed (equi-amplitude) thermodynamic perturbations. Thus when the DE intrinsic entropy perturbation vanishes, i.e. $\delta s_x = 0$, then Eq. (5.11) yields

$$(c_{sx}^2 - c_{ax}^2)\Delta_x \;=\; 0, \tag{5.33}$$

where either (*1*) $c_{ax}^2 = c_{sx}^2$, or (*2*) $\Delta_x = 0$. It is important to note that the definition (5.33) is independent of the choice of the spacetime gauge. It may also be pointed out that, if initially by a priori assumptions $c_{ax}^2 = c_{sx}^2$, then automatically $\delta s_x = 0$; however the converse is not necessarily true, i.e. if initially by a priori assumptions $\delta s_x = 0$ then it may or may not mean that $c_{ax}^2 = c_{sx}^2$, since it can also mean that $\Delta_x = 0$ instead.

In what that follows, we investigate the two cases (*1*) and (*2*), given above.

Case 1: $c_{ax}^2 = c_{sx}^2$

If the adiabatic sound speed is equal to the physical sound speed, i.e. $c_{ax}^2 = c_{sx}^2$, then Eq. (5.3) implies that

$$c_{ax}^2 \;=\; w_x - \frac{w_x'}{3\mathcal{H}(1+w_x)} \;=\; c_{sx}^2 \;\geq\; 0, \tag{5.34}$$

where this means $3\mathcal{H}w_x \geq w_x'/(1+w_x)$, and either:

$$\begin{aligned} &\text{(i)} \quad w_x > -1 \text{ and } w_x' < 0, \text{ or} \\ &\text{(ii)} \quad w_x < -1 \text{ and } w_x' > 0. \end{aligned}$$

Thus, unless $w_x \geq 0$, w_x cannot be an absolute constant. It may only be asymptotic to a fix value, such that $w_x' \neq 0$, otherwise c_{sx} becomes imaginary. Hence, the given homogeneous DE does not admit $w_x =$ constant < 0 (i.e. negative constants). Moreover, w_x can not oscillate: it may only be either monotonically decreasing ($w_x' < 0$) or monotonically increasing ($w_x' > 0$). Thus, *Case 1* (5.34) essentially 'fixes' the DE background evolutions.

To illustrate *Case 1* (5.34), we consider the well known Chevallier-Polarski-Linder (CPL) parametrization [114, 115]:

$$w_x \;=\; w_0 + w_a(1-a), \tag{5.35}$$

where the scale factor $a = (1+z)^{-1}$, with z being the redshift; w_0 and w_a are (free) constants. We consider two scenarios of w_x (5.35): a generic clustering DE (CPL) and a homogeneous DE (*hom*CPL), given by

$$\text{CPL}: \qquad w_x \geq -1,\; w_x' \geq 0,\; \Delta_x \neq 0, \tag{5.36}$$

$$\textit{hom}\text{CPL}: \qquad w_x > -1,\; w_x' < 0,\; \Delta_x \neq 0, \tag{5.37}$$

where we choose $w_0 = -0.8$ and $w_a = -0.2$ for CPL; $w_0 = -0.8$ and $w_a = 0.6$ for *hom*CPL, i.e. here we consider only the scenario (i) of *Case 1* (5.34). We show the behaviour of w_x (5.35) in Fig. 5.2 (left panel), for both the CPL (5.36) and the *hom*CPL (5.37), respectively.

Throughout this chapter, we initialize evolutions at the decoupling epoch, given by $1 + z_d = 10^3 = a_d^{-1}$. We have normalized all the power spectra on small scales, at $z = 0$:

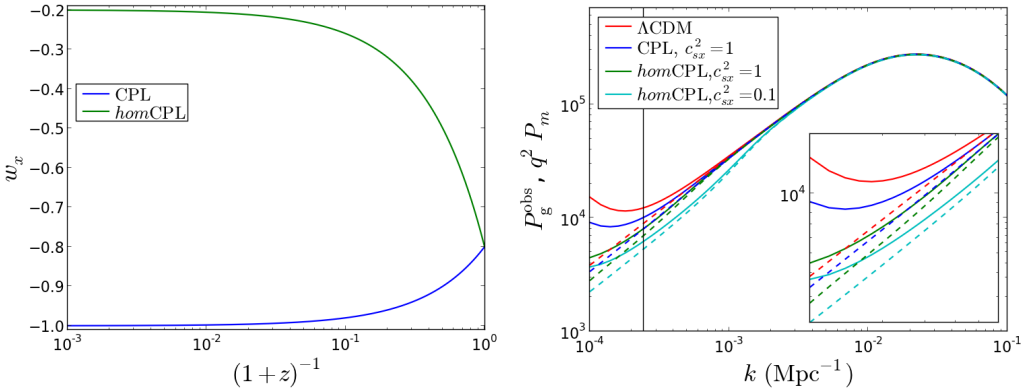

FIGURE 5.2: *Left panel:* The evolution of the equation of state parameter w_x, for the CPL (5.36) (blue) and the *hom*CPL (5.37) (green). *Right panel* (at $z = 0$): The radial (i.e. $\mu = 1$) galaxy power spectrum $P_{\rm g}^{\rm obs}$ (solid lines) with galaxy bias $b = 1$ and magnification bias $\mathcal{Q} = 1$; and the matter power spectrum, given by $q^2 P_m$ (dashed lines) with $q = \sqrt{2.1}$.

i.e. by choosing the same matter density parameter $\Omega_{m0} = 0.24$ and Hubble constant $H_0 = 73$ Kms^{-1}Mpc for all cases. (Thus the power spectra of *hom*CPL and ΛCDM match that of CPL at $z = 0$, on small scales.) We used adiabatic initial conditions (see Appendix C) for the perturbations.

We show in Fig. 5.2 (right panel), the radial galaxy power spectrum $P_{\rm g}^{\rm obs}$ (see Appendix 5.4.3) with galaxy bias [3–5] $b = 1$ and magnification bias [5] $\mathcal{Q} = 1$; and the matter power spectrum P_m: at the present epoch, i.e. $z = 0$. By our normalization, we see that $P_{\rm g}^{\rm obs}$ can be approximated on sub-Horizon scales by $q^2 P_m$, with $q = \sqrt{2.1}$. Moreover, although DE clusters in the CPL, we see that it rather leads to higher power on horizon scales in both $P_{\rm g}^{\rm obs}$ and P_m, i.e. relative to the *hom*CPL for equal values of c_{sx}^2 (see [84, 112, 116–125], for the effects of c_{sx}^2). This may be owing to the behaviour of w_x for *hom*CPL, which suggests that DE sets in relatively earlier for the *hom*CPL – hence causing the matter perturbations to have less room to cluster, thereby resulting in relatively lower power spectra. Obviously, *Case 1* (5.34) implies that for equal values of c_{sx}^2, the difference between a homogeneous DE and a clustering DE is mainly governed by the background, with little to do with the perturbations. However, one may expect that this difference strongly pertains perturbations, and that a homogeneous DE results in higher power spectra on large scales, relative to a clustering DE – given that the perturbative effect of the homogeneous DE should be negligible (or even absent).

We also observe the dependence of *hom*CPL on c_{sx}^2, i.e. in the power spectra, with smaller values of c_{sx}^2 resulting in more power suppression – since in which case the DE perturbations are able to cluster earlier and on smaller scales; thus suppressing most of the matter growth. However, we see the effect of the general relativistic (GR) corrections [1, 3, 5–9, 17, 19, 24] in $P_{\rm g}^{\rm obs}$: they lead to a sizeable power boost (relative to P_m) on horizon scales. Moreover, we observe that the GR corrections also result in significant differentiation of the given DE scenarios.

Nevertheless, for self-consistent models like the QCDM (see chapter 4) which evolve along a potential given (generically) by $U(\varphi) \neq$ constant, we have

$$c_{ax}^2 \;=\; 1 + \frac{2a^2 U_{|\varphi}}{3\mathcal{H}\bar{\varphi}'} \;\neq\; c_{sx}^2 \;=\; 1. \tag{5.38}$$

Thus by Eq. (5.38), $c_{ax}^2 \neq c_{sx}^2$, which then disallows *Case 1* (5.34). Therefore, w_x may oscillate (see, e.g. [105, 126, 127]) or take any behaviour. However, one may choose to fix $U(\varphi) =$ constant, thereby satisfying *Case 1* (5.34) (in principle). Practically though, this choice leads to w_x violating *Case 1* (5.34), i.e. by becoming $w_x = -1$ for $0 \leq z \lesssim 100$, in which case the perturbations equations become unsolvable numerically. Hence *Case 1* (5.34) is 'impractical' for the QCDM models.

In general, *Case 1* (5.34) is unsatisfactory, given that it still depends on the behaviour or choice of $c_{sx}^2 \geq 0$.

Case 2: $\Delta_x = 0$

On the other hand, if the DE comoving density perturbation vanishes – i.e. $\Delta_x = 0$, then Eq. (1.88) gives $\delta_x = 3\mathcal{H}(1 + w_x)V_x$. Therefore it implies that the correction to Eq. (5.1), is suitably given by

$$\Delta_x \; = \; 0, \qquad \delta_x \; = \; 3\mathcal{H}(1 + w_x)V_x, \qquad V_x \; \neq \; 0, \tag{5.39}$$

where consequently, $\Delta_x' = 0$. Thus Eq. (5.39) implies that the homogeneous DE should not have any density perturbations Δ_x in comoving gauge, but may posses the fractional density fluctuations δ_x which generate peculiar velocities with potentials V_x.

Note that given Eqs. (1.90), *Case 2* (5.39) implies that a homogeneous DE has zero density perturbation in its rest frame, i.e. $\delta\rho_x|_{\rm rf} = \bar{\rho}_x\Delta_x = 0$. This is the physical statement of *Case 2* (5.39). It is a crucial statement, since it suggests that DE homogeneity or inhomogeneity should be defined relative to the DE rest frame, i.e. whether or not its density perturbations vanish in its rest frame. Or particularly, that DE will be (physically) inhomogeneous if its intrinsic entropy perturbation is not zero.

In fact, *Case 2* (5.39) readily holds for the QCDM models (i.e. from Eq. (5.11)) when $\delta s_x = 0$; in which case we have

$$c_{ax}^2\delta\rho_\varphi \; = \; \delta p_\varphi \; = \; \delta\rho_\varphi + 3\mathcal{H}(1 + w_x)(c_{ax}^2 - 1)\bar{\rho}_\varphi V_x, \tag{5.40}$$

where $w_x = \bar{p}_\varphi/\bar{\rho}_\varphi$. By collecting terms with $\delta\rho_\varphi$ to one side and dividing through by $(c_{ax}^2 - 1)\bar{\rho}_\varphi$, we get $\delta_x = 3\mathcal{H}(1 + w_x)V_x$. We have used Eq. (5.38); $\bar{\varphi}'^2 = a^2(1 + w_x)\bar{\rho}_\varphi$, with the perturbations $V_x = -\delta\varphi/\bar{\varphi}'$, $\delta_x = \delta\rho_\varphi/\bar{\rho}_\varphi$: given that $\delta\rho_\varphi$ and δp_φ are given by Eqs. (1.113) and (1.114), respectively.

By considering the definition of the intrinsic entropy perturbation for QCDM, given by Γ [128], it will automatically follow that the DE comoving overdensity $\Delta_x \equiv \Delta_\varphi = 0$ when $\Gamma = 0$. Thus *Case 2* (5.39) suggests that DE may be homogeneous only when the observer is comoving with the source, irrespective of the DE background specifications. Hence a homogeneous DE may have perturbations, but only in such a way that these perturbations combine to cancel out in comoving gauge.

Moreover, the matter power spectrum physically makes sense only when computed in comoving gauge, since otherwise, it becomes gauge-dependent and varies with the observers on large scales (see e.g. [9, 129]). Thus *Case 2* (5.39), being defined in comoving gauge, can lead to (physical) observable implications in the power spectrum. Moreover, the effect of *Case 2* (5.39) on the matter perturbations will be imposed directly, rather than indirectly via the background evolutions – as in *Case 1* (5.34). This way, the imprint of the given homogeneous DE will bear directly on the growth of structure.

An important advantage of *Case 2* (5.39) over *Case 1* (5.34) is that, unlike *Case 1* (5.34), *Case 2* (5.39) permits an arbitrary background behaviour for the given DE:

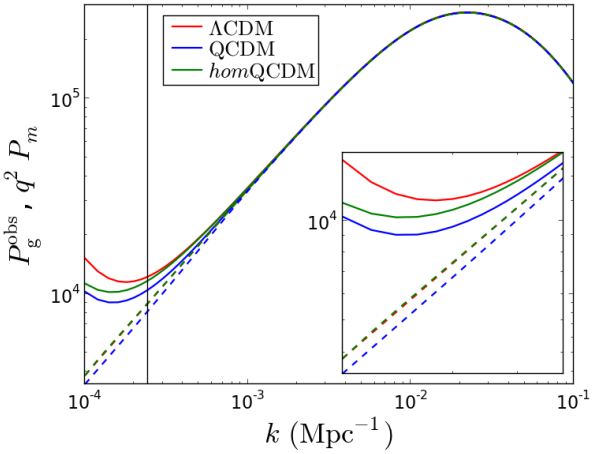

FIGURE 5.3: Plots at $z = 0$: The radial (i.e. $\mu = 1$) galaxy power spectrum $P_{\rm g}^{\rm obs}$ (solid lines) with galaxy bias $b = 1$ and magnification bias $\mathcal{Q} = 1$; and the matter power spectrum, given by $q^2 P_m$ (dashed lines) with $q = \sqrt{2.1}$. We used the RP potential (B.1) (with $w_{x0} \simeq -0.877$) for the QCDM models.

w_x may take any nature (constant or otherwise). This is important for models with either oscillatory or constant w_x. A further advantage of *Case 2* (5.39) is that it eliminates the dependence of the perturbations on c_{sx}^2 (via Eq. (5.22)), given that $\Delta_x = 0$ or $\delta_x = 3\mathcal{H}(1 + w_x)V_x$. Hence the given homogeneous DE is completely independent of the choice or nature of c_{sx}^2 (just like in ΛCDM). This further removes the risk that accompanies a bad choice or wrong modelling of c_{sx}^2. Moreover, it also reduces the parameter space that needs to be constrained.

To illustrate *Case 2* (5.39), we use the quintessence models (ignoring the CPL scenario, given that it leads to similar results, for $w_x > -1$; disregarding phantom crossing entirely). Henceforth, we denote clustering quintessence by QCDM and homogeneous quintessence by *hom*QCDM. We chose the same background parameters and conditions for both QCDM and *hom*QCDM. (The chosen parameters here leave the behaviour of w_x for the quintessence models as shown in Fig. 4.1.)

We show in Fig. 5.3 the galaxy power spectrum $P_{\rm g}^{\rm obs}$ with $b = 1$ and $\mathcal{Q} = 1$, and the associated matter power spectrum P_m: for QCDM and *hom*QCDM, at $z = 0$. We see that on sub-Hubble scales, $P_{\rm g}^{\rm obs}$ can be approximated by $q^2 P_m$, where $q = \sqrt{2.1}$. Moreover, unlike the results by *Case 1* (5.34) (see Fig. 5.2), where the clustering DE results in large-scale boost in the power spectra relative to the homogeneous DE, here we see that although $c_{sx}^2 = 1$ for the QCDM, we get large-scale power suppression in both $P_{\rm g}^{\rm obs}$ and P_m relative to those for *hom*QCDM (and ΛCDM) – i.e. the power spectra for QCDM are lower than those for *hom*QCDM, on horizon scales. This implies that on horizon scales, the effect of c_{sx}^2 in QCDM is less significant and hence the DE perturbations are able to cluster enough to suppress the growth of the matter perturbations. On the other hand, the DE density perturbations vanish on all scales for *hom*QCDM (in comoving gauge); thus the matter perturbations are able to grow more. Consequently, we get the relative boost in the power spectra in *hom*QCDM.

Moreover, we see that the ΛCDM gives a sizeable deviation in $P_{\rm g}^{\rm obs}$ relative to *hom*QCDM, on super-Hubble scales. This deviation illuminates the sensitivity of GR corrections to changes in w_x; this sensitivity will be crucial in discriminating the ΛCDM from a dynamical homogeneous DE model, with the future large scale surveys. We also

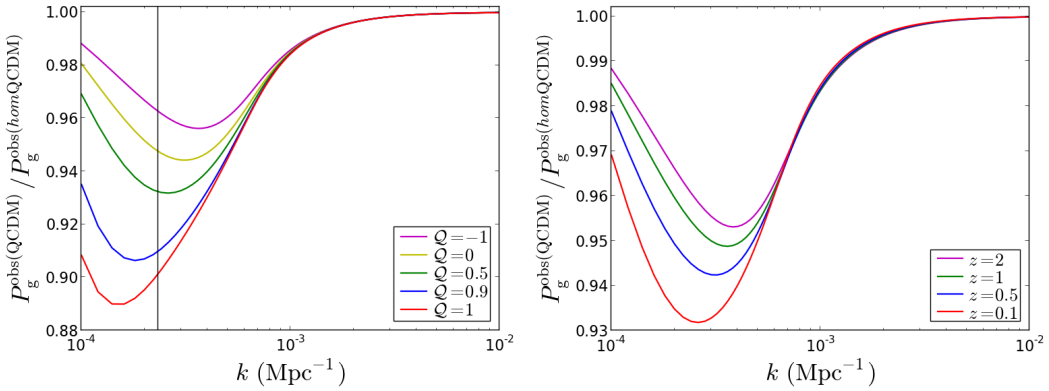

FIGURE 5.4: The ratios of P_g^{obs}, for QCDM relative to *hom*QCDM, using the RP potential (B.1). We used a galaxy bias $b = 1$. *Left panel:* Ratios at $z = 0.1$ with $\mathcal{Q} = 1,\ 0.9,\ 0.5,\ 0,\ -1$. *Right panel:* Ratios with $\mathcal{Q} = 0.5$ at $z = 0.1,\ 0.5,\ 1,\ 2$. The solid vertical line (left panel) denotes the Hubble horizon.

observe that, P_m of *hom*QCDM is identical to that of ΛCDM on all scales. This reveals that, the linear matter power spectrum is incapable of distinguishing a dynamical homogeneous DE (given by *Case 2* (5.39)) from ΛCDM, on large scales – when their power spectra are normalized on small scales (at the given epoch).

In Fig. 5.4 we illustrate the effect of the magnification bias $\mathcal{Q}$. In the left panel, we show the ratios of P_g^{obs} at the epoch $z = 0.1$ with $\mathcal{Q} = 1,\ 0.9,\ 0.5,\ 0,\ -1$; and galaxy bias $b = 1$. We see that as $\mathcal{Q}$ increases, QCDM is consistently suppressed relative to *hom*QCDM, i.e. the bigger the value of the magnification bias, the more the QCDM differentiates away from *hom*QCDM, and vice versa. This suggests that future surveys that depend on cosmic magnification, e.g. the radio surveys (see [1, 16, 17] for the 21 cm analysis, where $\mathcal{Q} = 1$), will be useful in distinguishing or identifying a dynamical homogeneous DE from other forms of DE in the large scale analysis, particularly at low z. Moreover, the ratios grow with decreasing $\mathcal{Q}$, suggesting that at a particular z, GR effects become enhanced as cosmic magnification (bias) decreases. However, these ratios tend to converge towards a certain value – which is mainly determined by our normalization (at $z = 0$).

We also show in Fig. 5.4 (right panel) the ratios of P_g^{obs} with $\mathcal{Q} = 0.5$ at $z = 0.1,\ 0.5,\ 1,\ 2$. The ratios grow as z increases. This implies that, for a given value of $\mathcal{Q}$, the effect of GR corrections grows with increasing z (and vice versa). Hence GR effects become magnified in the observed signal when we move backward in cosmic time. However, the QCDM tends to deviate more from the *hom*QCDM as z decreases. Thus for any fixed cosmic magnification, future surveys at low z hold more promise of disentangling a dynamical homogeneous DE from a clustering DE, on horizon scales.

We give in Fig. 5.5 the corresponding ratios of the matter power spectrum P_m at the epochs $z = 0.1,\ 0.5,\ 1,\ 2$. The ratios of P_m reveal that the large-scale clustering effect of DE on the growth of structure, diminishes with increasing z – i.e. as we go backward in time, the clustering DE gradually resembles a homogeneous DE. Moreover, just like the ratios of P_g^{obs}, the ratios of P_m show a convergence towards a given value (governed by our normalization). Similarly, the deviation of QCDM from *hom*QCDM, i.e. in P_m, is more pronounced at lower z. Again implying that distinguishing a homogeneous DE from a clustering DE may be suitable at the late epochs.

In general, unlike *Case 1* (5.34) which further depends on the perturbation modes

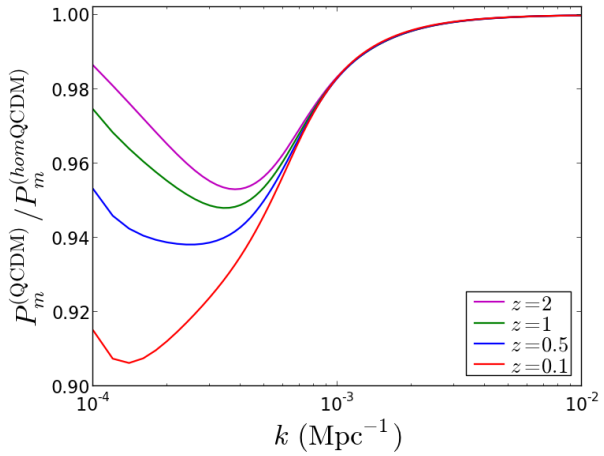

FIGURE 5.5: The ratios of P_m, for QCDM relative to *hom*QCDM, at the epochs $z = 0.1,\ 0.5,\ 1,\ 2$. We used the RP potential (B.1) for the illustration.

being well within the Hubble horizon and $c_{sx}^2 \simeq 1$, *Case 2* (5.39) is a definitive condition for DE homogeneity: once it is chosen, no other requirements are needed. Moreover, apart from solving the problem posed by Eq. (5.1) and the elimination of c_{sx}^2 from the equations, *Case 2* (5.39) can also conveniently admit particularly $w_x = -1$ while still allowing the DE perturbations. Thus *Case 2* (5.39) is more robust, and is hereby considered as the right DE homogeneity condition.

5.5 Conclusion

We have given an analytical analysis of the violation of the self-consistency of the equations of general relativity by the dark energy homogeneity assumption given by $\Delta_x = \delta_x = V_x = 0$ (i.e. with the evolution equations being discarded). We showed in Newtonian gauge that, unless the equation of state parameter of the given dark energy is strictly $w_x = -1$, this assumption causes the general relativistic system of equations to be inconsistent, i.e. by introducing contradictions in the equations.

We have proposed a correct homogeneity condition for dark energy, which is valid irrespective of the nature of the dark energy equation of state parameter or spacetime gauge – by supposing that the dark energy intrinsic entropy perturbation vanishes: consequently, the dark energy comoving density perturbation vanishes entirely in spacetime, i.e. $\Delta_x = 0$. This implies that the dark energy density perturbations vanish in its rest frame. Thus we correct the wrong homogeneity assumption (given above) by: $\delta_x = 3\mathcal{H}(1 + w_x)V_x$, with $V_x \neq 0$. Hence a homogeneous dark energy is essentially not one devoid of perturbations, but one with vanishing density perturbations in comoving gauge – i.e. one with zero density perturbations in its rest frame. Such kind of dark energy is not impractical.

We investigated the consequence of our approach in the galaxy and the matter power spectra, respectively – using phenomenological dark energy and quintessence models. By normalizing the models at the present epoch on small scales, we found that a dynamical homogeneous dark energy is distinguishable from a clustering dark energy in the power spectra, on horizon scales – suitably at low redshifts and high cosmic magnification bias.

At the normalization epoch, we found that the linear matter power spectrum is incapable of distinguishing a dynamical homogeneous dark energy from the (static) concordance model (ΛCDM), on all scales. However, GR corrections in the galaxy power spectrum (with substantial magnification bias) are able to disentangle a dynamical homogeneous dark energy from ΛCDM, on super-Hubble scales. Moreover we found that generally, at a particular epoch, GR effects become enhanced with decreasing magnification bias. Similarly, for a given magnification bias, GR effects grow with increasing redshift.

Chapter 6

Large Scale Imprint of Interacting Dark Energy

The dark sector, i.e. DE and (cold) dark matter (DM), does not interact with baryonic matter. Moreover, in the standard cosmologies, e.g. as described in chapters 4 and 5, DE and DM interact only indirectly by gravitation – i.e. via the Poisson equation. However, DE may interact with DM non-gravitationally: via a reciprocal exchange of energy and momentum – hence, is called interacting DE (IDE).

So far [2]: there is no concrete observational evidence for the existence of a non-gravitational interaction between DE and DM, nor is there guidance from fundamental theory as to the possible forms of such an interaction. However, there is also no consistent explanation for standard (i.e. non-interacting) DE from fundamental theory. And IDE is not ruled out by current observations. (For a range of work on IDE, see [130–212].) Various observations have been used to place constraints on IDE models. In nearly all cases, the IDE models are compatible with current observations, provided that the interaction is not too strong, i.e. the magnitude of the interaction parameter is small. A few of the models result in non-adiabatic large-scale instabilities (see, e.g. [170, 172]), and hence may be ruled out. However, several of these models can be 'fixed' by adjusting the DE equation of state (see, e.g. [149, 174, 194]).

Up to the time of writing this thesis, only [2] (to the best of knowledge) had done an analysis of the IDE imprints on structure formation that takes into account the GR effects on the galaxy power spectrum. These GR effects arise from observing galaxies on the past lightcone, and they become significant on very large scales [1, 3–22]. As previously mentioned, future galaxy surveys will cover wide sky areas and reach high redshifts, and thus begin to probe scales beyond the equality scale, and approaching the Hubble scale (at higher redshifts). In order to analyse observations on these scales, we need to use the correct theoretical model – i.e. including the GR effects which deviate from the Newtonian approximation that is only accurate on smaller scales.

Future large-volume galaxy surveys will allow us to: (i) extend tests of DE and modified gravity models – and general relativity itself – to horizon scales; (ii) measure the primordial non-Gaussian signal in the galaxy power spectrum at higher precision levels than the CMB. GR effects have been discussed in the case of (i) by [1, 17, 18] and in the case of (ii) by [4, 5, 16, 32, 34, 35]. Recently, [213] investigated the degeneracy between the large-scale imprint of primordial non-Gaussianity and the imprint of some IDE models, but without considering the GR corrections to the power spectrum.

Here we extend the work on DE models by investigating the GR effects on the galaxy

power spectrum in IDE, assuming primordial Gaussianity. Similarly as in chapter 5, we normalise each IDE model to give the same matter density parameter Ω_{m0} and Hubble constant H_0 as its corresponding standard non-interacting model. Then scale-dependent deviations from standard behaviour are clearly isolated on large scales at $z = 0$. For $z > 0$ however, the power spectra do not match on small scales. We show these behaviours in section 6.5.

The rest of this chapter is organised as follows. We describe the background IDE models in section 6.1 and the perturbed IDE models in section 6.2. Note that the equations given in chapter 1, correspond to the standard cosmologies. Thus for an IDE (non-standard cosmologies), as we shall see subsequently, these equations become modified. Here we assume that DE is described by a non-adiabatic (nonbarotropic) perfect fluid, with a dynamic energy density. In section 6.4, we investigate and discuss the very large scale behaviour of the galaxy power spectrum – including GR corrections.

6.1 Background Universe with Interacting Dark Energy

Immediately after the era of matter-radiation equality, matter perturbations are able to start growing. However, the growth of perturbations in the baryonic component is, by contrast, suppressed by radiation pressure because of the coupling to radiation [38]. Eventually, the baryonic component becomes negligible compared to DM, in the late epochs – with DM becoming the densest component, and hence controlling the growth of the matter perturbations. We shall therefore neglect baryons for simplicity.

Thus henceforth we shall assume a (late) Universe completely dominated by DM and DE. Then in the background Universe dominated by DM ($A = m$) and DE ($A = x$), the interaction is defined via energy density transfer rates $\bar{Q}_A$, given by

$$\bar{\rho}'_A + 3\mathcal{H}(1 + w_A)\bar{\rho}_A \;=\; a\bar{Q}_A. \tag{6.1}$$

The equation of state parameters are $w_m = 0$ and $w_x \neq 0$: Eq. (1.75). The conservation of the total energy-momentum tensor, $\nabla_\mu \sum_A \bar{T}^{\mu\nu}_A = 0$, then implies

$$\bar{Q}_m \;=\; -\bar{Q}_x. \tag{6.2}$$

The case $\bar{Q}_x > 0$ corresponds to energy density transfer from DM to DE, and vice versa for $\bar{Q}_x < 0$. We may define effective equation of state parameters

$$w_{A,\text{eff}} \;\equiv\; w_A - \frac{a\bar{Q}_A}{3\mathcal{H}\bar{\rho}_A}, \tag{6.3}$$

where

$$\bar{\rho}'_A + 3\mathcal{H}(1 + w_{A,\text{eff}})\bar{\rho}_A \;=\; 0, \tag{6.4}$$

so that $w_{A,\text{eff}}$ encode the deviations from the standard evolution of the dark sector energy densities.

The background field equations are determined by the total energy-momentum tensor $\sum_A \bar{T}^{\mu\nu}_A$, and thus do not explicitly contain the interaction – i.e. they retain the same form as Eq. (5.2) (or Eqs. (4.2) and (4.3)). We note that $\bar{\rho}_A$ implicitly contain the interaction. We discuss our various choices of $\bar{Q}_A$ in subsection 6.2.

6.2 Perturbed Universe with Interacting Dark Energy

We adopt the perturbed FRW metric (2.50). The perturbed field equations do not contain the interaction explicitly, when written in terms of Newtonian-gauge quantities, since they are determined by the total perturbed energy-momentum tensor $\sum_A \delta T^{\mu\nu}_A$ [2]. The gravitational evolution retains the same form as Eq. (5.5), and the relativistic Poisson equation (5.4) is given by

$$\nabla^2\Phi \;=\; \frac{3}{2}\mathcal{H}^2\sum_A \Omega_A\big[\delta_A - 3\mathcal{H}(1+w_A)V_A\big], \tag{6.5}$$

which follow from section 1.2.7. The velocity potentials V_A give the dark sector peculiar velocities, via the 4-velocities (4.7) – where the total velocity potential V (4.8), may also be given by

$$\Big(1+\sum_A \Omega_A w_A\Big)V \;=\; \sum_A \Omega_A(1+w_A)V_A. \tag{6.6}$$

It is convenient (e.g. to avoid any large-scale gauge artefacts) to use the comoving overdensities, as defined in Eq. (1.88). For IDE, these overdensities become

$$\Delta_A \;=\; \delta_A - 3\mathcal{H}(1+w_{A,\text{eff}})V_A, \tag{6.7}$$

where $w_{A,\text{eff}}$ are given by Eq. (6.3). Note that the right hand side of the Poisson equation (6.5) remains the same for both interacting and non-interacting DE, so that Φ is always determined by $\sum_A \Omega_A[\delta_A - 3\mathcal{H}(1+w_A)V_A]$. In the case of interacting DE, we have from (6.7) that $\delta_A - 3\mathcal{H}(1+w_A)V_A = \Delta_A - a\bar{Q}_A V_A/\bar{\rho}_A$, thus

$$\nabla^2\Phi \;=\; \frac{3}{2}\mathcal{H}^2\sum_A \Omega_A\Big[\Delta_A - \frac{a\bar{Q}_A}{\bar{\rho}_A}V_A\Big]. \tag{6.8}$$

Effectively, the Poisson equation is not affected by the interaction: the effect introduced by the explicit interaction term in the square bracket of Eq. (6.8), is completely offset by the implicit interaction in Δ_A. This implies that, the relativistic Poisson equation is independent of the (explicit) nature of interaction between DE and DM (or even between the dark and the luminous sectors). Thus it remains the same irrespective of the specifications of the DE. However, the gravitational potential itself is indirectly influenced by the interaction – via the total momentum density (6.6) of the system (see subsections 6.2.2 and 6.2.3).

6.2.1 Energy-momentum transfer 4-vectors

An interacting system is generally defined by the energy-momentum balance equations, given by [2, 170, 171, 179]

$$\nabla_\nu T^{\mu\nu}_A \;=\; Q^\mu_A, \qquad \sum_A Q^\mu_A \;=\; 0, \tag{6.9}$$

where Q^μ_A are the energy-momentum transfer 4-vectors

$$Q^\mu_A \;=\; Q_A u^\mu + F^\mu_A, \quad Q_A \;=\; \bar{Q}_A + \delta Q_A, \quad u_\mu F^\mu_A \;=\; 0. \tag{6.10}$$

The energy density transfer rate Q_A and the momentum density transfer rate F^μ_A are both relative to u^μ. In first-order perturbations, we have

$$F^\mu_A = a^{-1}\left(0,\ \partial^i f_A\right), \tag{6.11}$$

where f_A is the momentum density transfer potential. Then Eqs. (4.7), (6.6) and (6.10) imply that

$$Q^A_0 \ = \ -a\left[\bar{Q}_A(1+\Phi)+\delta Q_A\right], \qquad Q^A_i \ = \ a\partial_i\left[\bar{Q}_A V + f_A\right]. \tag{6.12}$$

6.2.2 General perturbed balance equations

By considering all species as perfect fluids, the perturbed energy-momentum tensor of species A is given by Eq. (5.6). The pressure perturbation (see subsection 1.2.7) for IDE is given by [149]

$$\delta p_A \ = \ c^2_{sA}\delta\rho_A + 3\mathcal{H}(c^2_{aA}-c^2_{sA})\left(1+w_{A,\text{eff}}\right)\bar{\rho}_A V_A. \tag{6.13}$$

Then given Eqs. (5.6), (6.9)–(6.11) and (6.13) we obtain the energy balance equation, given by [2]

$$\begin{aligned}\Delta'_A \ &- \ 3\mathcal{H}w_A\Delta_A - \frac{9}{2}\mathcal{H}^2(1+w_A)\sum_{B\neq A}\Omega_B(1+w_B)\left[V_A-V_B\right]+(1+w_A)\nabla^2 V_A \\ &= \ \frac{a}{\bar{\rho}_A}\left[\delta Q_A - 3\mathcal{H}f_A\right] + \frac{a^2\bar{Q}_A}{(1+w_A)\bar{\rho}^2_A}\left[f_A+\bar{Q}_A(V-V_A)\right] \\ &\quad + \frac{a\bar{Q}_A}{\bar{\rho}_A}\Big\{3\mathcal{H}(V_A-V)+\frac{\bar{Q}'_A}{\bar{Q}_A}V_A-\Big[1+\frac{c^2_{sA}}{1+w_A}\Big]\Delta_A\Big\},\end{aligned} \tag{6.14}$$

and the momentum balance equation is given by

$$V'_A+\mathcal{H}V_A \ = \ -\Phi - \frac{c^2_{sA}\Delta_A}{1+w_A} + \frac{a\bar{Q}_A\left(V-V_A\right)+af_A}{(1+w_A)\bar{\rho}_A}. \tag{6.15}$$

Here $c_{sm}=0$, and we take $c_{sx}=1$ (which is the value for quintessence).

6.2.3 The interacting dark energy models

We model DE as a fluid with constant equation of state w_x and consider two interactions. And henceforth we shall use wCDM to denote the non-interacting case, and iwCDM the interacting case. In these interaction models, we assume that the transfer 4-vectors Q^μ_A run parallel to the DE 4-velocity:

$$Q^\mu_x \ = \ Q_x u^\mu_x \ = \ -Q^\mu_m. \tag{6.16}$$

This means that there is zero momentum transfer in the DE rest frame, which is the case for example in the models of [72, 139, 143, 145, 155, 205, 209]. From Eq. (6.16), it follows that the momentum density transfer rates (relative to u^μ) become

$$f_x \ = \ \bar{Q}_x(V_x-V) \ = \ -f_m. \tag{6.17}$$

For transfer 4-vectors of the form (6.16), the balance equations (6.14) and (6.15) lead to

$$\begin{aligned}\Delta'_m &- \frac{9}{2}\mathcal{H}^2\Omega_x(1+w_x)\left[V_m - V_x\right] + \nabla^2 V_m - 3\mathcal{H}(V_m - V_x)\left[1 - \frac{a\bar{Q}_m}{3\mathcal{H}\bar{\rho}_m}\right]\frac{a\bar{Q}_m}{\bar{\rho}_m} \\ &= -\frac{a\bar{Q}_m}{\bar{\rho}_m}\left[\Delta_m - \frac{\delta Q_m}{\bar{Q}_m} - \frac{\bar{Q}'_m}{\bar{Q}_m}V_m\right], \end{aligned} \tag{6.18}$$

which defines the DM overdensity evolution, and the DM velocity potential evolves by

$$V'_m + \mathcal{H}V_m = -\Phi - \frac{a\bar{Q}_m}{\bar{\rho}_m}\left[V_m - V_x\right]. \tag{6.19}$$

As pointed out earlier, the interaction in the right hand side of Eq. (6.19) will implicitly influence the evolution of the gravitational potential in Eq. (5.19) – via V_m. The energy balance equation for IDE (with $w_x \neq -1$) is given by

$$\begin{aligned}\Delta'_x &- 3\mathcal{H}w_x\Delta_x - \frac{9}{2}\mathcal{H}^2\Omega_m(1+w_x)\left[V_x - V_m\right] + (1+w_x)\nabla^2 V_x \\ &= \frac{a}{\bar{\rho}_x}\left[\delta Q_x + \bar{Q}'_x V_x\right] - a\left[1 + \frac{c_{sx}^2}{1+w_x}\right]\frac{\bar{Q}_x}{\bar{\rho}_x}\Delta_x, \end{aligned} \tag{6.20}$$

while the corresponding momentum balance equation is

$$V'_x + \mathcal{H}V_x = -\Phi - \frac{c_{sx}^2}{1+w_x}\Delta_x, \tag{6.21}$$

where for generality we left c_{sx} unspecified – but we set it to 1 for numerical solutions. To fully specify an IDE model, we need to define the Q_A, which we choose as follows.

Model 1: $Q_x \propto \rho_x$

In this model, we use an energy density transfer rate given by [170, 179, 213]

$$Q_x = \Gamma\rho_x = \Gamma\bar{\rho}_x(1+\delta_x) = -Q_m, \tag{6.22}$$

where Γ is a universal constant (i.e. it is fixed under perturbations). In the case $\Gamma < 0$, this corresponds to decay of DE into DM. Then from Eqs. (4.7) and (6.22), we get

$$Q^x_\mu = a\Gamma\bar{\rho}_x\left[-(1+\delta_x+\Phi),\, \partial_i V_x\right] = -Q^m_\mu. \tag{6.23}$$

By Eq. (6.17), we obtain the momentum density transfer rates, given by

$$f_x = \Gamma\bar{\rho}_x(V_x - V) = -f_m. \tag{6.24}$$

Model 2: $Q_x \propto \Theta\rho_x$

It is common in the literature to use energy density transfer rates of the form $Q_x = \xi a^{-1}\mathcal{H}\rho_x$, where ξ is a constant – i.e. to use a transfer rate proportional to the Hubble rate, rather than a constant rate Γ, as *Model 1* (6.22). The motivation for this choice is that the background energy conservation equations are easily solved. However, the problem is that for the perturbed model, the Hubble rate $\mathcal{H}$ is typically not perturbed.

To resolve this problem, we use instead the self-consistent energy density transfer rate, as a second model, given by [2]

$$Q_x \;=\; \frac{1}{3}\xi\rho_x\Theta, \qquad \Theta \;=\; \nabla_\mu u^\mu. \tag{6.25}$$

In the background, this reduces to the usual form, but in the perturbed universe we pick up additional perturbations of the expansion rate:

$$\Theta \;=\; 3a^{-1}\left[\mathcal{H} - \left(\Phi' + \mathcal{H}\Phi\right) + \frac{1}{3}\nabla^2 V\right]. \tag{6.26}$$

This thus leads to

$$Q_x \;=\; a^{-1}\xi\mathcal{H}\bar{\rho}_x\Big[1 + \delta_x - \Phi - \frac{1}{3\mathcal{H}}\left(3\Phi' - \nabla^2 V\right)\Big] = -Q_m. \tag{6.27}$$

Then Eqs. (4.7), (6.16), (6.26) and (6.27) imply that

$$Q^x_\mu \;=\; \xi\mathcal{H}\bar{\rho}_x\left[-1 - \delta_x + \frac{1}{3\mathcal{H}}\left(3\Phi' - \nabla^2 V\right), \partial_i V_x\right]. \tag{6.28}$$

By Eq. (6.17), we obtain the momentum density transfer rates for this model, given by

$$f_x \;=\; a^{-1}\xi\mathcal{H}\bar{\rho}_x(V_x - V) \;=\; -f_m. \tag{6.29}$$

Thus for both models, the range of w_x is restricted by stability requirements, given by [160, 162, 179]

$$w_x > -1 \;\text{ for } \xi, \Gamma > 0; \qquad w_x < -1 \;\text{ for } \xi, \Gamma < 0. \tag{6.30}$$

These two cases correspond to different energy transfer directions, i.e. given *Model 1* (6.22) and *Model 2* (6.25), we have

$$\text{DM} \to \text{DE for } \xi, \Gamma > 0; \qquad \text{DE} \to \text{DM for } \xi, \Gamma < 0. \tag{6.31}$$

6.3 Background Evolution of the Models

We evolved the background equations from around decoupling, $a_d = 10^{-3}$, until today $a = 1$. The background initial conditions were chosen so that the matter density parameter Ω_{m0} and the Hubble constant H_0 are the same as in the non-interacting models. We used $\Omega_{m0} = 0.24$, $H_0 = 73$ Kms^{-1}Mpc.

It is easy to understand the behaviour of the effective equation of state parameter $w_{x,\text{eff}}$ in Fig. 6.1. For *Model 1* (6.22), $w_{x,\text{eff}} = w_x - a\Gamma/(3\mathcal{H})$, where $a\mathcal{H}^{-1}$ is a positive growing quantity. Hence $w_{x,\text{eff}}$ gradually decreases for $\Gamma > 0$ ($w_x = -0.8$) and increases for $\Gamma < 0$ ($w_x = -1.1$), with $|\Gamma|$ determining the strength of the interaction (solid lines). However, for *Model 2* (6.25) we have $w_{x,\text{eff}} = w_x - \xi/3$, which is a constant for constant w_x, shown in the dashed lines.

Figure 6.2 shows the evolution of the matter density parameters and Hubble rates, compared to the non-interacting case. When $|\bar{Q}_x|$ is small ($|\xi|, |\Gamma/H_0| \lesssim 0.1$), $w_{x,\text{eff}}$ is only slightly less (greater) than $w_x = -0.8$ ($w_x = -1.1$). This implies weaker (stronger) DE effects: the background matter density for iwCDM becomes enhanced (suppressed)

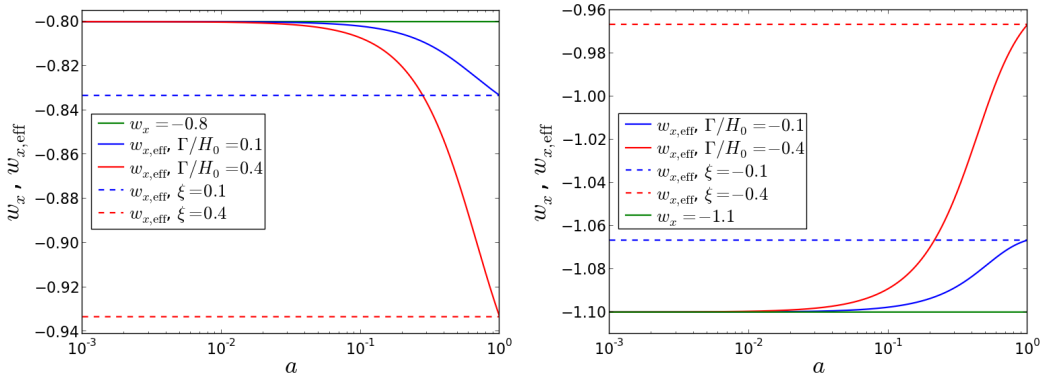

FIGURE 6.1: Evolution of the IDE effective equation of state parameters $w_{x,\mathrm{eff}}$, for the wCDM equation of state parameters $w_x = -0.8$ (*left panel*) and $w_x = -1.1$ (*right panel*). Solid lines correspond to *Model 1* (6.22) while dashed lines correspond to *Model 2* (6.25), and the w_x line denotes $\Gamma = 0 = \xi$.

relative to wCDM for $w_x = -0.8$ ($w_x = -1.1$). However, when the transfer rate is higher ($|\xi|, |\Gamma/H_0| \gtrsim 0.4$), $w_{x,\mathrm{eff}}$ is much smaller (bigger) than $w_x = -0.8$ ($w_x = -1.1$) and hence iwCDM has surplus (less) matter relative to wCDM for $w_x = -0.8$ ($w_x = -1.1$).

Notice the distinct separation between the ratios of the Hubble rates. To understand this, we know that during matter domination, when $\Omega_m \approx 1$ ($\Omega_x \ll 1$), the ratio is constant. In this work we fixed the background initial conditions in wCDM and let those in iwCDM vary with each value of Γ or ξ so as to recover the same values of Ω_{m0} and H_0 as in wCDM. As Γ or ξ vary, the initial conditions in iwCDM change, enough to amount to significantly differing initial amplitudes of the Hubble rates. The ratio does not evolve until DE domination, converging at $a = 1$ by our normalization.

6.4 The Linear Growth Functions

We are able to probe the large-scale structure of the late-time Universe by relating the linear perturbations at late epochs to the primordial potential – via growth functions (see subsection 2.1.4) and a transfer function (2.10), from which the matter power spectrum is computed. We adopt $\delta_H = 5.6\times10^{-5}$ (see [9]) for the scalar amplitude at horizon crossing and $n = 0.96$ for the scalar spectral index.

For IDE, the growth function D_m of the comoving matter overdensity (2.15) implicitly contains the interaction, i.e. the growth function transforms to

$$D_m(k,a) \;=\; D_m^0(k,a) + \frac{a\bar{Q}_m(a)}{k^2\bar{\rho}_m(a)} D_{V_m}(k,a), \tag{6.32}$$

where D_m^0 is now the growth function in the standard non-interacting scenario (i.e. of chapters 4 and 5). Equation (6.32) is obtained by using Eqs. (2.11), (2.15) and (2.17) in the Poisson equation (6.8) – and assumed matter domination ($\Omega_x \approx 0$). Moreover, the growth functions D_Φ and D_{V_m} in Eqs. (2.11) and (2.17) retain the same forms in both IDE and non-IDE scenarios – i.e. they do not explicitly contain the density transfer rate $\bar{Q}_m$. Similarly (see Eq. (4.15)), here we have $D_m = D_\Phi$ to hold true only on sub-Hubble scales $k \gg \mathcal{H}$ – i.e. generally for $w_x \neq -1$.

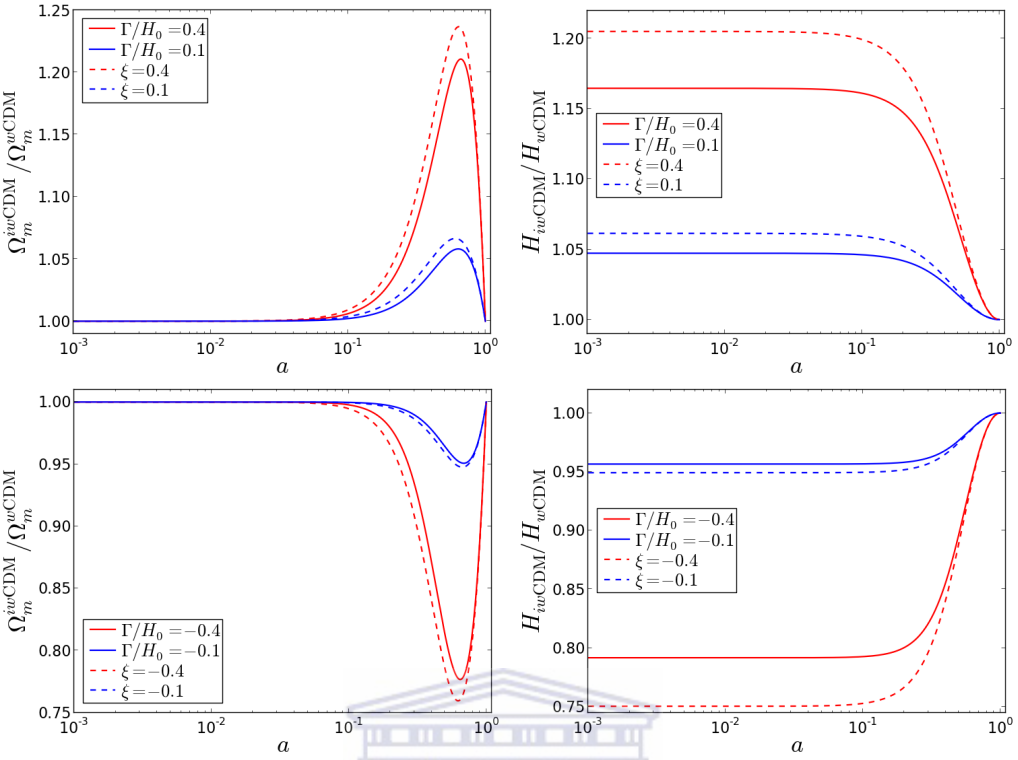

FIGURE 6.2: Ratios of the matter density parameters (*left*) and Hubble rates (*right*) for iwCDM relative to those of wCDM: with $w_x = -0.8$ (*top panels*) and $w_x = -1.1$ (*bottom panels*). Line styles are as in Fig. 6.1.

The DE velocity growth function is related to that of matter by

$$D_{V_x}(k,a) \;=\; \frac{\Omega_m(a)}{[1-\Omega_m(a)][1+w_x(a)]}\left[\frac{\partial}{\partial\eta}D_\Phi(k,a) - D_{V_m}(k,a)\right], \tag{6.33}$$

where we have used Eqs. (2.11) and (2.17) in Eq. (5.19) and assuming Einstein de Sitter regime – i.e. with $\Phi' = 0$. Thus the DE overdensity growth function is

$$D_x(k,a) = \frac{\Omega_m(a)}{1-\Omega_m(a)}\left[D_\Phi(k,a) - D_m(k,a) - \frac{a\bar{Q}_m(a)}{k^2\bar{\rho}_m(a)}\Big\{D_{V_x}(k,a) - D_{V_m}(k,a)\Big\}\right] \tag{6.34}$$

where we used Eqs. (2.11), (2.15) and (2.17) in the Poisson equation (6.8), and the fact that $\bar{Q}_x/\bar{\rho}_x = -\Omega_m\bar{Q}_m/(\Omega_x\bar{\rho}_m)$. Then in ΛCDM, given Eq. (2.59): $D_x = 0 = D_{V_x}$.

6.5 Relativistic Effects in the Observed Overdensity

Using cosmological perturbation theory, we can describe the evolution and distribution of matter density perturbation in the Universe. However, in reality the matter perturbation distribution is not directly observable – only objects such as galaxies, whose distribution traces that of the matter, are observable. The large-scale and scale-independent galaxy bias b is usually defined by Eq. (4.16). Nevertheless, different gauge choices for δ_m agree on sub-Hubble scales, but on near- and super-Hubble scales, they disagree. The scale-independent bias needs to be defined physically, in the rest-frame of DM and galaxies (which coincide on large scales). This leads to the galaxy contrast Δ_g, in Eq. (2.31).

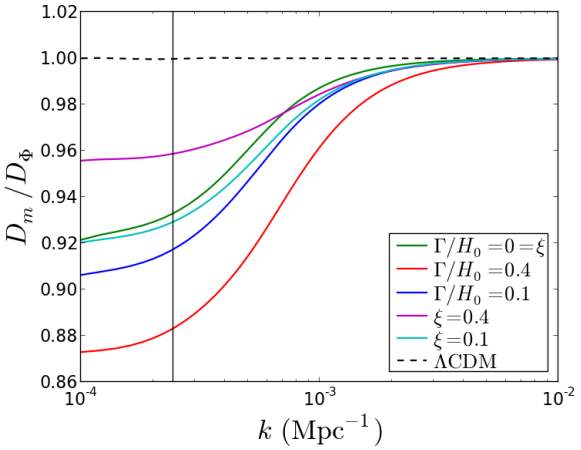

FIGURE 6.3: The ratio of the matter overdensity and gravitational potential growth functions, at $a = 1$ (or $z = 0$), with $w_x = -0.8$. Solid lines correspond to *Model 1* (6.22) and dashed lines to *Model 2* (6.25). The ΛCDM case (dashed black line) and the Hubble horizon (solid black line) are also shown.

The observed galaxy overdensity acquires relativistic corrections from lightcone effects, and these corrections grow on very large scales. It is known that upcoming galaxy surveys in the optical, infrared and radio bands will probe increasingly large wavelength modes and reach higher redshifts. In order to exploit the new data on large scales, an accurate analysis requires inclusion of the relativistic effects. This is especially the case for primordial non-Gaussianity and for extending tests of DE models to horizon scales. Here we investigate the latter, in a Universe with IDE: noting that interaction in the dark sector can also lead to large-scale deviations in the power spectrum.

Furthermore, we do not observe in real space, but in redshift space, leading to the Kaiser redshift-space distortion term (2.47) – here taken as the standard term [2]:

$$\Delta_{\rm g}^{\rm std}(k,\mu,a) \;=\; \big[b(a) + f(k,a)\mu^2\big]\Delta_m(k,a), \tag{6.35}$$

where given Eqs. (2.15) and (2.17), the redshift-distortion parameter (2.45) becomes

$$f \;=\; \frac{D_{V_m}}{\mathcal{H}D_m}, \tag{6.36}$$

which is general for dynamical DE (i.e. with $w_x \neq -1$): IDE and non-IDE (e.g. like in chapters 4 and 5). This illustrates that it is the peculiar velocities that source the redshift-space distortions in the overdensity. Moreover as shown in section 2.5, for ΛCDM: f reduces to the standard linear growth rate (2.60) of matter overdensity. However for non-IDE, f reduces to the matter linear growth rate only during matter domination, where the evolution equation for matter overdensity reduces to exactly Eq. (2.57), of ΛCDM. Note that f in Eq. (6.36) is different from f_m and f_x in Eq. (6.17): the latter are the DM and DE momentum density transfer rates, respectively.

The Kaiser term is a flat-sky and sub-Hubble approximation to the full redshift-space distortion, which includes further velocity and Sachs-Wolfe type terms. In addition to the redshift distortion, there are other relativistic effects from observing galaxies on the past lightcone. These include a contribution from weak lensing convergence, which can be significant on sub-Hubble scales at higher redshifts. In addition there are additional Sachs-Wolfe and Doppler terms, and ISW and time-delay terms [3, 5–7, 9, 15, 214].

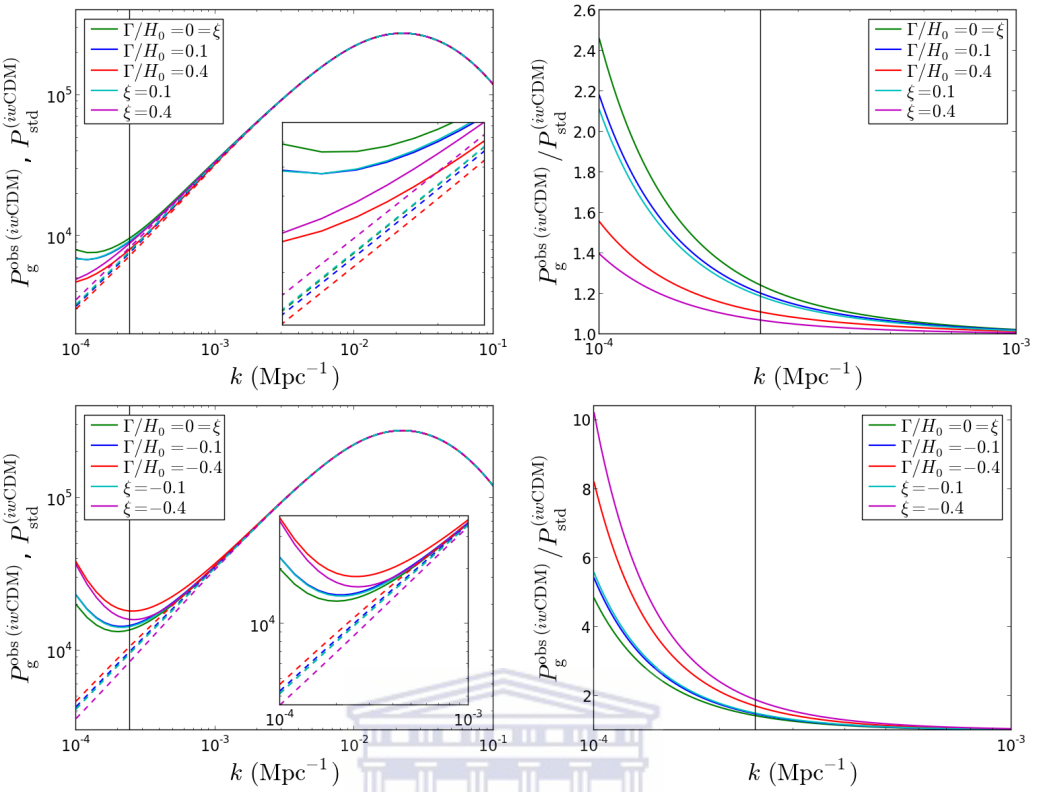

FIGURE 6.4: Observed galaxy power spectrum $P_{\rm g}^{\rm obs}$ (solid lines) and the standard power spectrum $P_{\rm g}^{\rm std}$ (dashed lines) along the line of sight ($\mu = 1$), at $z = 0$: for $w_x = -0.8$ (*top*); and for $w_x = -1.1$ (*bottom*). The corresponding ratios of the power spectra are given on the right panels.

If we want an accurate analysis that includes near- and super-Hubble scales, we should use the galaxy overdensity that is observed on the lightcone, including all GR effects. This observed overdensity is automatically gauge-invariant. Here we will neglect the integrated terms and use a flat-sky approximation, generalizing the ΛCDM form given in [5]:

$$\Delta_{\rm g}^{\rm obs}(k,\mu,a) \;=\; \Delta_{\rm g}^{\rm std}(k,\mu,a) + \Delta_{\rm g}^{\rm GR}(k,\mu,a), \tag{6.37}$$

where $\Delta_{\rm g}^{\rm std}$ is given by Eq. (6.35). Note that in Eq. (6.37) we do not have a priori the time-delay, ISW and weak lensing integrated terms, and

$$\Delta_{\rm g}^{\rm GR} \;=\; \left[\mathcal{A}\frac{\mathcal{H}^2}{k^2} + i\mu\mathcal{B}\frac{\mathcal{H}}{k}\right]\Delta_m. \tag{6.38}$$

This form arises by using the field and conservation equations to relate velocity and potential to overdensity. (See e.g. [1, 15, 19] for the full GR expression including integrated terms.) The coefficients in (6.38) are given in the ΛCDM case by Eq. [5]. We generalize

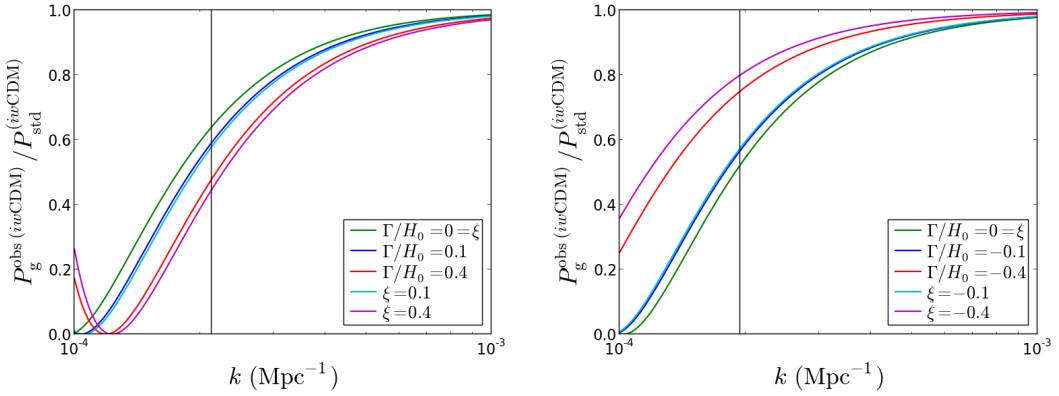

FIGURE 6.5: Ratios of the observed galaxy power spectrum $P_{\rm g}^{\rm obs}$ to the standard power spectrum $P_{\rm g}^{\rm std}$ along the line of sight ($\mu = 1$), at $z = 1$: for $w_x = -0.8$ (*left*) and $w_x = -1.1$ (*right*).

their expressions for the case of IDE (see chapter 5 for the non-IDE case):

$$\mathcal{A} = -\frac{3\Omega_{m0}H_0^2}{2\,\mathcal{H}^2 D_m}\Big[4\mathcal{Q} - b_e - 1 + \frac{\mathcal{H}'}{\mathcal{H}^2} + 2\frac{(1-\mathcal{Q})}{r\mathcal{H}} + \frac{a^2}{D_\Phi}\frac{\partial}{\partial a}\Big(\frac{D_\Phi}{a}\Big)\Big]\frac{D_\Phi}{a}, + (3 - b_e)\, f, \tag{6.39}$$

$$\mathcal{B} = -\Big[b_e - 2\mathcal{Q} - \frac{\mathcal{H}'}{\mathcal{H}^2} - 2\frac{(1-\mathcal{Q})}{r\mathcal{H}} + \frac{a\bar{Q}_m}{\mathcal{H}\bar{\rho}_m}\Big(1 - \frac{D_{V_x}}{D_{V_m}}\Big)\Big] f, \tag{6.40}$$

where we have used Eqs. (2.11), (2.15) and (2.17). Here r, $\mathcal{Q}$ and b_e retain the same definitions as in chapter 5. The interaction enters $\mathcal{B}$ through the last term in Eq. (5.32). This term arises from the perturbed Euler equation (6.19), which comes in via the total derivative $dV_m^{\parallel}/d\lambda$ in Eq. (3.58): where the derivative is taken along the photon geodesic, in the direction from source to observer – i.e. with λ being the affine parameter along the photon geodesic. The Q_m term is absent in ΛCDM [3, 5–7, 9] and in non-interacting DE models [1] (see chapter 5). It would also be absent in IDE models with Q_A^μ parallel to the matter 4-velocity u_m^μ, since in these models the DM follows geodesics and the perturbed Euler equation is the same as for non-interacting DE.

6.6 The Large-scale Galaxy Power Spectrum

From Eqs. (6.37)–(6.40), we obtain the power spectrum $P_{\rm g}^{\rm obs}$ of the observed galaxy overdensity in the conformal Newtonian gauge (we give only the real part), given by Eq. (5.30). The standard power spectrum, i.e. the Kaiser approximation (2.48), is

$$P_{\rm g}^{\rm std}(k,\mu,a) = \big[b(a) + f(k,a)\mu^2\big]^2\, P_m(k,a), \tag{6.41}$$

where the matter power spectrum is given by Eq. (2.25). We note that the third and fourth terms in Eq. (5.30) correspond to the auto-correlations of $\Delta_{\rm g}^{\rm GR}$, and the second term corresponds to the cross-correlation between $\Delta_{\rm g}^{\rm std}$ and $\Delta_{\rm g}^{\rm GR}$.

To compute the growth functions, we employ adiabatic initial conditions: see Appendix C (section C.3). For the goal of this work, it is reasonable to assume a constant comoving galaxy number density so that $b_e = 0$. We also set (henceforth) the galaxy

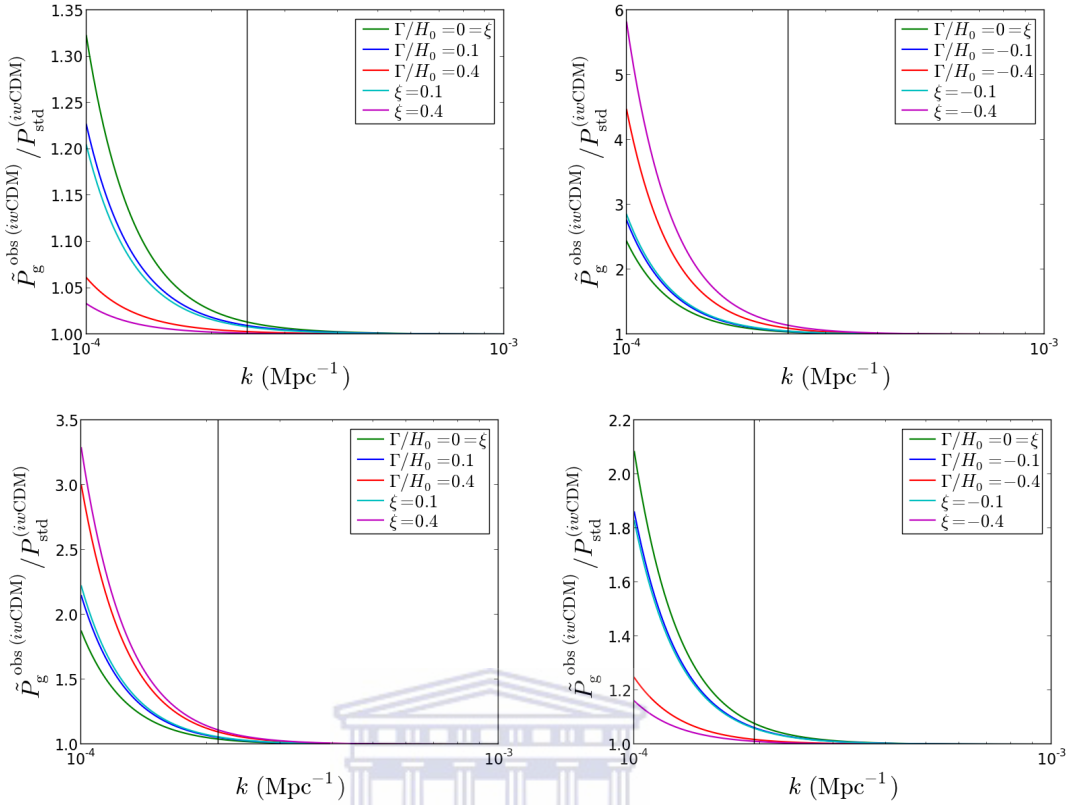

FIGURE 6.6: Ratios of $\tilde{P}_{\rm g}^{\rm obs}$, which is $P_{\rm g}^{\rm obs}$ with the correlation between $\Delta_{\rm g}^{\rm std}$ and $\Delta_{\rm g}^{\rm GR}$ subtracted, to the standard power spectrum $P_{\rm g}^{\rm std}$, along the line of sight ($\mu = 1$). Top panels have $z = 0$, for $w_x = -0.8$ (top left) and $w_x = -1.1$ (top right). Similarly for $z = 1$ in the bottom panels.

bias to $b = 1$ for simplicity. We considered the case with the magnification bias

$$\mathcal{Q} \;=\; 1, \tag{6.42}$$

which corresponds to intensity mapping of the neutral hydrogen (HI) 21cm emission line [1, 17, 215]. In this case, the lensing convergence and time delay terms drop out of $\Delta_{\rm g}^{\rm obs}$, and the remaining integrated term, the ISW term, typically makes a negligible contribution. This gives a strong justification for our neglect of the integrated terms in Eqs. (6.38)–(5.32).

Equation (2.25) shows that the induced changes in P_m arising from the interaction will be imprinted via the ratio $D_m/D_{\Phi 0}$. This ratio is exactly unity on all scales in ΛCDM while for dynamical DE it tends to 1 (by normalization) only on small scales $k \gg \mathcal{H}$, where the DE perturbations are negligible. This is illustrated in Fig. 6.3 using iwCDM with $w_x = -0.8$ as an example. In this case, DM loses energy to DE, causing suppression of the matter growth function, which shows up in the matter power spectrum. Note that in the absence of interaction (as in the standard cosmologies), the clustering of DE causes large-scale *suppression* in the matter power [1]. Moreover, the growth functions show that *Model 1* (6.22) is relatively more sensitive to the values of the interaction parameter, compared to *Model 2* (6.25).

For $w_x = -1.1$ in iwCDM, the corresponding plots for $D_m/D_{\Phi 0}$ simply have all the curves reflected across that of ΛCDM.

In Fig. 6.4 we present the line-of-sight GR corrected galaxy power spectrum $P_{\rm g}^{\rm obs}$ and the standard power spectrum $P_{\rm g}^{\rm std}$ in the Kaiser approximation, for the iwCDM models at $z = 0$. On sub-Hubble scales, Eq. (5.30) shows that

$$\frac{P_{\rm g}^{\rm obs}}{P_m} \;\to\; (1+f)^2 \quad \text{for } k \gg \mathcal{H}, \tag{6.43}$$

i.e. $P_{\rm g}^{\rm obs} \to P_{\rm g}^{\rm std}$. We also see that iwCDM gives a large-scale boost in galaxy power for both $\Gamma,\ \xi > 0$ ($w_x > -1$) and $\Gamma,\ \xi < 0$ ($w_x < -1$). As remarked above, there is less sensitivity to the values of $|\xi|$, so that *Model 2* (6.25) predicts relatively larger amplitudes on super-horizon scales than does *Model 1* (6.22).

The large-scale boost in galaxy power in Fig. 6.4 for wCDM arises purely from GR effects. The smaller boost (relative suppression) in power for iwCDM with $\Gamma,\ \xi > 0$ (top left) comes from the fact that DM loses energy to DE, so that the higher the DM rate of loss of energy (i.e. larger $|\Gamma|,\ |\xi|$), the more the power suppression. For $\Gamma,\ \xi < 0$ (bottom left), where DE loses energy to DM, larger values of $|\Gamma|$ and $|\xi|$ give more boost relative to wCDM. Here, GR corrections in the galaxy power spectrum result in large-scale galaxy power enhancement. This implies that if we ignore the GR effects, i.e. if we do not subtract them in order to isolate the IDE effects, then we arrive at an incorrect estimate of the imprint of IDE on very large scales.

In Fig. 6.4 (right panels), we also show the corresponding ratios of the total galaxy power spectrum relative to the Kaiser approximation, at $z = 0$. The ratios show that, for $\Gamma,\ \xi > 0$ (top right), GR effects are suppressed relative to wCDM by the interaction. This is consistent with previous explanations above. Conversely, for $\Gamma,\ \xi < 0$ (bottom right), GR effects are enhanced relative to wCDM. However, note that the total galaxy power spectrum contains not only the individual contributions of the standard Kaiser redshift-space distortion and GR terms, but also their cross-correlation. This cross-correlation makes a positive contribution at low z, and a negative contribution at high z: for the given magnification bias Eq. (6.42). Hence, the ratios shown (at $z = 0$) contain positive contributions of this cross correlation term, as well as the auto-correlation of the GR corrections. The ratios at $z = 0$ are thus enhanced on horizon scales.

The GR effects in our IDE models, where we use Gaussian primordial perturbations, show a similar behaviour to the effects of primordial non-Gaussianity in non-interacting DE models (with $f_{\rm NL} > 0$). The degeneracy between GR effects and primordial non-Gaussianity in the ΛCDM model has been investigated by [4, 5, 16, 32, 34, 35]. It was recently shown by [213] that IDE effects (in the case where GR effects are neglected) can be degenerate with primordial non-Gaussianity.

In Fig. 6.5, we show the ratios of the observed galaxy power spectrum to the Kaiser approximation at higher redshift, $z = 1$. For higher values of the interaction parameters, the case with $\Gamma,\ \xi > 0$ (left) shows lower large-scale GR effects in comparison to the case with $\Gamma,\ \xi < 0$ (right). For the magnification bias (6.42) (corresponding to HI intensity mapping), the observed line-of-sight power spectrum falls to zero for both non-interacting and interacting DE. At higher z the IDE effects are weaker, since the effects of DE in general are weaker at earlier times. By contrast, the GR effects are typically stronger at higher z – but with $\Delta_{\rm g}^{\rm GR}$ having negative amplitude. Hence its correlation with the Kaiser term gives negative contribution in the power spectrum, thereby gradually reducing galaxy power on horizon scales.

For completeness, we illustrate this phenomenon in Fig. 6.6, which shows the ratio of $\tilde{P}_{\rm g}^{\rm obs}$, which is $P_{\rm g}^{\rm obs}$ with the correlation between $\Delta_{\rm g}^{\rm std}$ and $\Delta_{\rm g}^{\rm GR}$ subtracted, to $P_{\rm g}^{\rm std}$.

In the top panels, $z = 0$, and $z = 1$ in the bottom panels. On the left, $w_x > -1$ and $\Gamma,\ \xi > 0$, and on the right, $w_x < -1$ and $\Gamma,\ \xi < 0$. By comparing the top left and top right panels, with the top right and the bottom right panels of Fig. 6.4, respectively, we see that the correlation between the GR and the Kaiser terms is positive at low z. Similarly, by comparing the bottom left and the bottom right panels, with the left and right panels of Fig. 6.5, respectively, we see that the cross correlation is negative and of larger amplitude at $z = 1$.

Generally, we see (Figs. 6.3–6.6) that in order that the imprint of IDE is correctly identified, we need to subtract the large-scale contribution of relativistic effects in the power spectrum. The relativistic effects dominate in the large-scale ratios: Figs. 6.4–6.6. Incorrect interpretations of the IDE effects could lead to a bias in constraints on IDE on very large scales. Moreover, we see (Fig. 6.6) that at low z, the correlation between the GR term and the (standard) Kaiser term has a positive contribution in the galaxy power spectrum, while at high z, this term gives a negative contribution that grows with increasing z. Upcoming wide surveys that have deep-field reach will, in principle, provide an avenue for disentangling any IDE effects from GR effects: by comparing the observed power spectrum at low and high z. The challenge though will be on measuring super-Hubble effects, because of cosmic variance (which can be reduced enough for detection of the GR effects [34], by the use of multi-tracer techniques [216]).

6.7 Conclusion

We have investigated the relativistic effects in the observed galaxy power spectrum in two interacting dark energy models, in comparison with the corresponding standard non-interacting dark energy scenarios. We focused on the case of magnification bias $\mathcal{Q} = 1$, which corresponds to HI intensity mapping. We normalized the power spectra of the interacting dark energy scenarios to those of their non-interacting dark energy counterparts – on small scales at $z = 0$, i.e. by requiring that they have the same Ω_{m0} and H_0 (as done in the quintessence case above). Doing so would isolate the deviations arising from the relativistic effects and the interacting dark energy – on very large scales.

We found that if the relativistic effects are disregarded, i.e. if they are not subtracted in order to isolate the effects of the interacting dark energy, then we arrive at an incorrect estimate of the imprint of interacting dark energy on horizon scales. This could lead to a bias in constraints on models of interacting dark energy – on the given scales. We also found that at low z, the correlation between the general relativistic term and the (standard) Kaiser redshift-space distortion term had a positive contribution in the galaxy power spectrum, while at high z, this term gave a negative contribution that grew with increasing z.

Future wide and deep-field surveys may be able to disentangle any possible interacting dark energy effects from general relativistic effects, by comparing the observed power at low and high z. However, detecting super-Hubble effects will be challenging because of cosmic variance. But if the multi-tracer method [216] can be applied, cosmic variance can be reduced enough for detection of these effects [34].

Chapter 7

Conclusion

As we enter the era of precision cosmology, where surveys extending to high redshifts z and covering large sky areas are expected to reveal more of the observable Universe with an unprecedented accuracy, we need to use a relativistic analysis which corrects for general relativistic effects in the observed density perturbation – in order to realise the full potential of these surveys. In this thesis, we have fully discussed the theory of this (relativistic) framework, in linear perturbation theory: within a flat homogeneous and isotropic FRW Universe.

In chapter 1, after a general overview, we gave a basic description of linear cosmological perturbations in a FRW Universe. We reviewed the metric tensor that describes the spacetime of the gravitational field; deriving the gravitational field and the energy-momentum conservation equations – in general and in specific gauges. Moreover, we gave an overview of hydrodynamical and scalar field perturbations, respectively – also in general and in specific gauges: throughout using conformal coordinates.

In chapter 2, we discussed the large-scale structure in the Universe. By adopting gauge-invariant perturbation variables in flat space with vanishing anisotropic stress, we discussed linear clustering of cosmological fluctuations: from their origin and generation, to their evolution to the late cosmic epochs where they collapse into structures. We also discussed the large-scale fluctuation spectrum, outlining the basics of the correlation function and the power spectrum. We gave a concise discussion of biasing in the large-scale structure. Furthermore, we gave a comprehensive description of the Kaiser approximation of the galaxy number density perturbation. We ended with a brief, straight-to-the-point description of the standard model of cosmology – i.e. ΛCDM, where dark energy is taken as the vacuum energy with static density Λ. We outlined the basic background and perturbations equations, and described the associated growth parameters – which are special cases of the general scenarios.

In chapter 3, we gave a complete derivation of the relativistic density perturbation, which corrects for general relativistic effects, that is observed in galaxy redshift surveys. We started by deriving the general relativistic geodesic equations; whence we derived the (physical) observed galaxy overdensity in the relativistic context, i.e. the relativistic density perturbation: where we correctly computed the redshift-space density distortion, the volume distortion and the magnification distortion. All of which quantities contained the appropriate terms that correct for the general relativistic effects.

In chapter 4, we discussed the clustering effects of standard (non-interacting) quintessence on very large (horizon) scales. After a short introduction to known properties of

quintessence, we illustrated how the assumption of smooth quintessence is incompatible with the Einstein field equations at first order in perturbations (on large scales). We then described the clustering effect of inhomogeneous quintessence on the linear matter power spectrum by comparing it to the same power spectrum in ΛCDM, and found that power is slightly suppressed on large scales at $z = 0$. Finally, we provided a fully relativistic investigation (using the framework previously established in chapter 3) of quintessence and matter perturbations in the post-recombination large-scale angular power spectrum. We applied the relativistic formalism to the specific case of HI intensity mapping for which the weak lensing magnification can be neglected. In that case, quintessence model lead to an increase (∼15%) in the power spectrum on large scales – but this is due to the background evolution only.

In chapter 5, we elaborated on the detailed reasons why smooth dark energy is a bad approximation to the dynamics on large scales. We explicitly showed, in the Newtonian gauge, that for a generic dark energy different from the cosmological constant, the relativistic equations at first order exhibits some formal inconsistencies. The consequences of these inconsistencies were further demonstrated. A correct homogeneity condition for dark energy, which is valid irrespective of the nature of the dark energy equation of state parameter or spacetime gauge, was then presented. The consequence of such definition was investigated in the galaxy and the matter power spectra, respectively. It was found that on super-Hubble scales, relativistic corrections in the observed galaxy power spectrum are capable of distinguishing a homogeneous dark energy from ΛCDM and from an inhomogeneous dark energy, at low z and for high magnification bias. However, the matter power spectrum: is incapable of distinguishing a homogeneous dark energy from ΛCDM (on all scales), at $z = 0$; but is capable of differentiating it from an inhomogeneous dark energy, particularly at low z. It was also found that relativistic effects become enhanced with decreasing magnification bias, and with increasing z.

Furthermore, in chapter 6 we investigated the relativistic effects in the observed galaxy power spectrum in interacting dark energy, i.e. dark energy that has some interaction with dark matter, by which they exchange energy and momentum. Such couplings are currently not ruled out and their study could tell us a lot about the physics of the dark sector. In the first part of the chapter, we outlined the background and perturbation equations in a suitable way to incorporate them in the relativistic formalism developed previously for non-interacting dark energy (chapters 4 and 5). Once again, by probing the linear power spectra of the given models of interacting dark energy, it was found that the none incorporation of the relativistic effects could lead to incorrect predictions for the effects of interaction in the dark sector – on the very large scales, and thus, to an impossibility to use future data for accurate constraints on dark energy (and/or gravity).

In general, the main lesson of this thesis is that: when analysing future survey data in order to determine the nature of dark energy, relativistic effects will have to be taken into account – if one wants an accurate interpretation of the dark energy effects.

Appendix A

Derivation of the Relativistic Density Perturbation

A.1 The Geodesic Equation

A geodesic x^μ may be defined as a path between two points on surface for which $\int_i^f \delta(ds) = 0$, where ds measures the infinitesimal distance between any two adjacent positions along the path [68] – given by the metric (1.3) as

$$ds^2 \;=\; g_{\mu\nu} dx^\mu dx^\nu. \tag{A.1}$$

To determine the geodesic equation, given that the end points (i.e. initial i; final f) are fixed, we give the path a deformation by perturbing every intermediate point so that the line element ds between the end points yields

$$2\,\delta(ds) \;=\; \delta x^\alpha \frac{dx^\mu}{ds} dx^\nu\, \partial_\alpha g_{\mu\nu} + g_{\mu\nu} \frac{d(\delta x^\mu)}{ds} dx^\nu + g_{\mu\nu} \frac{dx^\mu}{ds} d(\delta x^\nu), \tag{A.2}$$

where we used $\delta g_{\mu\nu} = \delta x^\alpha \partial_\alpha g_{\mu\nu}$. Thus by applying the stationary condition $\int_i^f \delta(ds) = 0$ between the terminal points, we have

$$0 \;=\; \frac{1}{2}\int_i^f ds \left[\delta x^\alpha \frac{dx^\mu}{ds}\frac{dx^\nu}{ds} \partial_\alpha g_{\mu\nu} + \left(g_{\alpha\nu}\frac{dx^\nu}{ds} + g_{\mu\alpha}\frac{dx^\mu}{ds} \right) \frac{d(\delta x^\alpha)}{ds} \right] \tag{A.3}$$

$$\;=\; \frac{1}{2}\int_i^f ds \left[\frac{dx^\mu}{ds}\frac{dx^\nu}{ds} \partial_\alpha g_{\mu\nu} - \frac{d}{ds}\left(g_{\alpha\nu}\frac{dx^\nu}{ds} + g_{\mu\alpha}\frac{dx^\mu}{ds} \right) \right] \delta x^\alpha, \tag{A.4}$$

where we set the dummies $\mu = \alpha = \nu$ in Eq. (A.3), and we obtain Eq. (A.4) by integrated by parts (once) the second term in the square bracket of Eq. (A.3) – and applying the condition $\delta x^\alpha|_i = 0 = \delta x^\alpha|_f$. Then since Eq. (A.4) holds for all values of $\delta x^\alpha(s)$ at every point between the end points of the path, it implies that the square bracket of the integrand must vanish. (Note that s becomes a parameter along x^α.)

Thus we expand the second term in the square bracket of Eq. (A.4) and collect like terms. Furthermore, we use that $dg_{\alpha\nu} = \partial_\mu g_{\alpha\nu} dx^\mu$, and set the dummy indices μ and ν on second derivatives as $\nu = \beta = \mu$. Then by multiplying through by $-g^{\sigma\alpha}$ we obtain the required geodesic equations, given by [68]

$$\frac{d^2 x^\sigma}{d\lambda^2} + \Gamma^\sigma{}_{\mu\nu} \frac{dx^\mu}{d\lambda}\frac{dx^\nu}{d\lambda} \;=\; 0, \tag{A.5}$$

where the Christoffel symbols (1.18) are given by

$$\Gamma^{\sigma}{}_{\mu\nu} \;=\; \frac{1}{2}g^{\sigma\alpha}\left(\partial_\nu g_{\mu\alpha} + \partial_\mu g_{\alpha\nu} - \partial_\alpha g_{\mu\nu}\right). \tag{A.6}$$

For convenience we adopted a re-parametrization by $x^\mu(s) \to x^\mu(\lambda)$ such that $dx^\mu/ds = dx^\mu/d\lambda$, with λ thus called the *affine parameter*. Moreover, we can rewrite the geodesic equation (A.5) in the simple form

$$n^\mu \nabla_\mu n^\sigma \;=\; 0, \tag{A.7}$$

where $n^\mu = dx^\mu/d\lambda$ is the tangent 4-vector to the geodesic $x^\mu(\lambda)$, and

$$\nabla_\mu n^\sigma \;=\; \partial_\mu n^\sigma + \Gamma^{\sigma}{}_{\mu\nu} n^\nu, \tag{A.8}$$

with the total derivative with respect to λ being $d/d\lambda = n^\mu \partial_\mu$, i.e. along the geodesic.

Then Eq. (A.7) implies that

$$\frac{dn^\mu}{d\lambda} \;=\; -\Gamma^{\mu}{}_{\alpha\beta}\, n^\alpha n^\beta. \tag{A.9}$$

In a perturbed Universe, we have the (background and perturbation) decompositions

$$n^\mu \;=\; \bar{n}^\mu + \delta n^\mu, \qquad \Gamma^{\mu}{}_{\alpha\beta} \;=\; \bar{\Gamma}^{\mu}{}_{\alpha\beta} + \delta\Gamma^{\mu}{}_{\alpha\beta}, \tag{A.10}$$

where $\bar{\Gamma}^{\mu}{}_{\alpha\beta}$ is given purely by the background metric tensor, via Eq. (A.6), and

$$\delta\Gamma^{\mu}{}_{\alpha\beta} \;=\; \frac{1}{2}\bar{g}^{\mu\nu}\left(\partial_\beta \delta g_{\alpha\nu} + \partial_\alpha \delta g_{\nu\beta} - \partial_\nu \delta g_{\alpha\beta}\right) + \frac{1}{2}\delta g^{\mu\nu}\left(\partial_\beta \bar{g}_{\alpha\nu} + \partial_\alpha \bar{g}_{\nu\beta} - \partial_\nu \bar{g}_{\alpha\beta}\right). \tag{A.11}$$

Hence, after some calculations, we obtain that

$$\frac{d\delta n^\mu}{d\lambda} \;=\; -\bar{g}^{\mu\nu}\frac{d}{d\lambda}\left(\bar{n}^\beta \delta g_{\nu\beta}\right) + \frac{1}{2}\bar{g}^{\mu\nu}\bar{n}^\alpha \bar{n}^\beta \partial_\nu \delta g_{\alpha\beta}, \tag{A.12}$$

where we used $d\bar{g}_{\mu\nu}/d\lambda = 0$, by which $\bar{\Gamma}^{\mu}{}_{\alpha\beta}\bar{n}^\alpha \delta n^\beta = 0$, and that

$$\delta\Gamma^{\mu}{}_{\alpha\beta}\bar{n}^\alpha \bar{n}^\beta \;=\; \frac{1}{2}\bar{g}^{\mu\nu}\bar{n}^\alpha \bar{n}^\beta \left(2\partial_\alpha \delta g_{\nu\beta} - \partial_\nu \delta g_{\alpha\beta}\right). \tag{A.13}$$

By integrating the perturbed geodesic equation (A.12), from i up to f, we obtain the perturbed tangent 4-vector given by [41]

$$\delta n^\mu|_i^f \;=\; -\left[\bar{g}^{\mu\nu}\delta g_{\nu\beta}\,\bar{n}^\beta\right]_i^f + \frac{1}{2}\bar{g}^{\mu\nu}\int_i^f d\lambda\, \bar{n}^\alpha \bar{n}^\beta \partial_\nu \delta g_{\alpha\beta}, \tag{A.14}$$

which gives the general perturbation in an arbitrary tangent 4-vector along any geodesic.

For a photon geodesic in particular, we have that

$$\tilde{n}^\mu \;=\; a^{-2} n^\mu \;=\; a^{-2}(1 + \delta n^0,\, \bar{n}^i + \delta n^i), \tag{A.15}$$

where $\bar{\tilde{n}}^\mu \bar{\tilde{n}}_\mu = \bar{n}^\mu \bar{n}_\mu = 0$. The temporal component is normalized by $\bar{n}^0 \bar{n}_0 = -1$, with $\bar{n}^0 = 1$; and the spatial component is normalized by $\bar{n}^i \bar{n}_i = 1$.

A.2 The Deviation Vector

We derive the components of the perturbed vector δn^μ tangent to the perturbed geodesic $\delta x^\mu(\lambda)$, as discussed in section A.1. By initializing integrations at the source S, then integrating until the observer O, gives the perturbed tangent 4-vector (3.13), as

$$\delta n^\mu\Big|_S^O = -\left[\bar{g}^{\mu\nu}\delta g_{\nu\beta}\,\bar{n}^\beta\right]_S^O - \frac{1}{2}\bar{g}^{\mu\nu}\int_{\bar{r}_S}^0 d\bar{r}\,\bar{n}^\alpha\bar{n}^\beta\partial_\nu\delta g_{\alpha\beta}, \tag{A.16}$$

where we used Eq. (3.17) in the integral, and that $\bar{r}(\bar{\eta}_S) = \bar{r}_S$ and $\bar{r}(\bar{\eta}_O) = 0$. Then given that $\delta n^\mu \equiv \delta n^\mu|_O^S = -\delta n^\mu|_S^O$, we obtain

$$\delta n^0 = \delta g_{0\beta}\,\bar{n}^\beta - \frac{1}{2}\int_{\bar{r}_S}^0 d\bar{r}\,\delta g'_{\alpha\beta}\bar{n}^\alpha\bar{n}^\beta, \tag{A.17}$$

$$\delta n^i = -\bar{g}^{ij}\delta g_{j\beta}\,\bar{n}^\beta + \frac{1}{2}\bar{g}^{ij}\int_{\bar{r}_S}^0 d\bar{r}\,\partial_j(\delta g_{\alpha\beta})\bar{n}^\alpha\bar{n}^\beta, \tag{A.18}$$

which give the temporal and spatial components of the perturbed tangent 4-vector. The terms outside the integrals are evaluated at S.

To compute the deviation 4-vector (see subsection 3.1.3), i.e. the 4-displacement which describes infinitesimal deviations in motion of objects away from their background world lines, we use Eqs. (3.15), (A.17) and (A.18) as follows

$$\begin{aligned}
\delta x^i &= -\int_0^{\bar{r}_S} d\lambda\,\left(\delta n^i - \bar{n}^i\delta n^0\right)\\
&= \int_0^{\bar{r}_S} d\bar{r}\,\left(\bar{g}^{ij}\delta g_{j\beta} + \delta g_{0\beta}\bar{n}^i\right)\bar{n}^\beta - \frac{1}{2}\int_0^{\bar{r}_S} d\bar{r}\left\{\int_{\bar{r}_S}^{\bar{r}} d\tilde{r}\,\left[\bar{g}^{ij}\partial_j(\delta g_{\alpha\beta}) + \delta g'_{\alpha\beta}\bar{n}^i\right]\bar{n}^\alpha\bar{n}^\beta\right\}\\
&= \int_0^{\bar{r}_S} d\bar{r}\,\left(\bar{g}^{ij}\delta g_{j\beta} + \delta g_{0\beta}\bar{n}^i\right)\bar{n}^\beta - \frac{1}{2}\int_0^{\bar{r}_S} d\bar{r}\,(\bar{r}-\bar{r}_S)\left[\bar{g}^{ij}\partial_j(\delta g_{\alpha\beta}) + \delta g'_{\alpha\beta}\bar{n}^i\right]\bar{n}^\alpha\bar{n}^\beta,
\end{aligned} \tag{A.19}$$

where we obtain the last line by integrating the inner integral in the second line by parts once – and neglecting surface terms. Equation (A.19) thus gives the deviation 4-vector, incurred on a geodesic, in an inhomogeneous Universe.

A.3 The Redshift Perturbation

The perturbation δz (3.31) in the observed redshift z (3.30), evaluates as follows

$$\begin{aligned}
\frac{\delta z}{1+\bar{z}} &= \left[\mathbf{n}\cdot\mathbf{v} + \phi - \sigma'\right]_S^O - \int_{\bar{r}_S}^0 d\bar{r}\,(\Phi' + \Psi'),\\
&= -\left[V_\parallel + \Phi + \Psi - \psi\right]_O^S - \int_{\bar{r}_S}^0 d\bar{r}\,(\Phi' + \Psi'),
\end{aligned} \tag{A.20}$$

where in the second line we have (hereafter) neglected the unmeasurable term $\partial_r E'$ in $\mathbf{n}\cdot\mathbf{v}$, and $V_\parallel = \bar{n}^i\partial_i V$ with V given by Eq. (3.29) – i.e. we have also used Eqs. (3.27) and (3.28). The intrinsic peculiar velocity potential is given by

$$\mathbf{n}\cdot\mathbf{v} = V_\parallel - \bar{n}^i\partial_i E'. \tag{A.21}$$

Moreover, in Eq. (A.20) we have used Eqs. (3.17), (3.27), (3.28) and (A.17), and

$$\delta(n^\mu u_\mu) \;=\; \delta(g_{\mu\nu}n^\mu u^\nu) \;=\; \bar{g}_{\mu\nu}\bar{n}^\mu\delta u^\nu + \bar{g}_{\mu\nu}\delta n^\mu \bar{u}^\nu + \delta g_{\mu\nu}\bar{n}^\mu\bar{u}^\nu. \tag{A.22}$$

We have also used that $\bar{n}^\alpha\bar{n}^\beta\delta g'_{\alpha\beta} = (\delta g_{\alpha\beta}\,\bar{n}^\alpha\bar{n}^\beta)'$, and

$$\delta g_{\alpha\beta}\,\bar{n}^\alpha\bar{n}^\beta \;=\; -2\left[\Phi + \Psi - \frac{dB}{d\lambda} - \left(\frac{d^2E}{d\lambda^2} - 2\frac{dE'}{d\lambda} + E''\right)\right], \tag{A.23}$$

where the metric tensor $g_{\mu\nu}$ is given by Eq. (3.7). We used that for any scalar X:

$$\frac{dX}{d\lambda} \;=\; X' + \bar{n}^i\partial_i X, \tag{A.24}$$

which therefore yields that

$$\bar{n}^i B_{|i} \;=\; \frac{dB}{d\lambda} - B', \tag{A.25}$$

and (given that $E_{ij} = E_{|ij} - \frac{1}{3}\delta_{ij}\nabla^2 E$) we have

$$\begin{aligned}\bar{n}^i\bar{n}^j E_{ij} \;&=\; \bar{n}^i\bar{n}^j E_{|ij} - \frac{1}{3}\nabla^2 E,\\ &=\; \left[\frac{d^2E}{d\lambda^2} - 2\frac{dE'}{d\lambda} + E''\right] - \frac{1}{3}\nabla^2 E,\end{aligned} \tag{A.26}$$

where $\delta_{ij}\bar{n}^i\bar{n}^j = \bar{n}^i\bar{n}_i = 1$. In Fourier space the total Laplacian will transform as $\nabla^2 \to -k^2$. Moreover, we note that partial derivatives are commutative.

A.4 The Radial and Angular Perturbations

Here we compute the perturbations in the comoving radial distance r and the polar zenith and azimuthal angles, θ and ϑ, respectively. Then if we consider Eqs. (3.49)–(3.51) and (A.19), we get that

$$\begin{aligned}\delta r \;=\; -\bar{n}_i\delta x^i \;&=\; -\int_0^{\bar{r}_S} d\bar{r}\,\delta g_{\alpha\beta}\bar{n}^\alpha\bar{n}^\beta + \frac{1}{2}\int_0^{\bar{r}_S} d\bar{r}\,(\bar{r}-\bar{r}_{\,S})\,\bar{n}^\nu\partial_\nu(\delta g_{\alpha\beta})\bar{n}^\alpha\bar{n}^\beta\\ &=\; -\frac{1}{2}\int_0^{\bar{r}_S} d\bar{r}\,\delta g_{\alpha\beta}\bar{n}^\alpha\bar{n}^\beta,\end{aligned} \tag{A.27}$$

where given Eq. (3.17) we use that $d/d\lambda = \bar{n}^\nu\partial_\nu = -d/d\bar{r}$ (i.e. to lowest order). We have integrated the second integral in the first line, by parts once – and applied the stationary condition to get vanishing surface terms.

Similarly, given Eqs. (3.49)–(3.51), it straightly follows that

$$\bar{r}_{\,S}\,\delta\theta \;=\; e_{\theta i}\,\delta x^i \;=\; \int_0^{\bar{r}_S} d\bar{r}\left[\delta g_{j\beta}\,e^j_\theta\,\bar{n}^\beta - \frac{1}{2}\,(\bar{r}-\bar{r}_{\,S})e^j_\theta\,\partial_j\,(\delta g_{\alpha\beta})\,\bar{n}^\alpha\bar{n}^\beta\right], \tag{A.28}$$

where $e^i_\theta\,\bar{n}_i = 0$, by orthogonality. Moreover, Eqs. (3.49)–(3.51), yield

$$\bar{r}_{\,S}\,\sin\theta\,\delta\vartheta \;=\; e_{\vartheta i}\,\delta x^i \;=\; \int_0^{\bar{r}_S} d\bar{r}\left[\delta g_{j\beta}\,e^j_\vartheta\,\bar{n}^\beta - \frac{1}{2}\,(\bar{r}-\bar{r}_{\,S})e^j_\vartheta\,\partial_j\,(\delta g_{\alpha\beta})\,\bar{n}^\alpha\bar{n}^\beta\right], \tag{A.29}$$

where also, $e^i_\vartheta\,\bar{n}_i = 0$. Thus Eq. (A.27)–(A.29) give the explicit expressions for the perturbations δr, $\delta\theta$ and $\delta\vartheta$.

A.5 The Volume Perturbation

Similarly, in the polar coordinates the various components of the 3-gradient $\check{\boldsymbol{\nabla}}$, are

$$\partial_r \;=\; -\bar{n}^i\partial_i, \qquad \frac{1}{r}\,\partial_\theta \;=\; e^i_\theta\partial_i, \qquad \frac{1}{r\,\sin\theta}\,\partial_\vartheta \;=\; e^i_\vartheta\partial_i, \tag{A.30}$$

where we set $e^i_r = -\bar{n}^i$. Hence we have that [9]

$$\begin{aligned} e^j_\theta\partial_j\left(\delta g_{\alpha\beta}\right)\,\bar{n}^\alpha\bar{n}^\beta \;&=\; \frac{1}{\bar{r}}\left[\partial_\theta(\delta g_{\alpha\beta}\,\bar{n}^\alpha\bar{n}^\beta) - \delta g_{\alpha\beta}\,\partial_\theta(\bar{n}^\alpha\bar{n}^\beta)\right] \\ &=\; \frac{1}{\bar{r}}\left[\partial_\theta(\delta g_{\alpha\beta}\,\bar{n}^\alpha\bar{n}^\beta) + 2\,\delta g_{\alpha j}\,\bar{n}^\alpha e^j_\theta\right], \end{aligned} \tag{A.31}$$

where we used that $\partial_\theta\bar{n}^\alpha = \delta^\alpha{}_i\partial_\theta\bar{n}^i = -\delta^\alpha{}_i e^i_\theta$. Similarly, given Eq. (A.30), we have

$$e^j_\vartheta\partial_j\left(\delta g_{\alpha\beta}\right)\,\bar{n}^\alpha\bar{n}^\beta \;=\; \frac{1}{\bar{r}\,\sin\theta}\left[\partial_\vartheta(\delta g_{\alpha\beta}\,\bar{n}^\alpha\bar{n}^\beta) + 2\,\delta g_{\alpha j}\,\bar{n}^\alpha e^j_\vartheta\sin\theta\right], \tag{A.32}$$

where $\partial_\vartheta\bar{n}^\alpha = -\delta^\alpha{}_i e^i_\vartheta\,\sin\theta$. Then given Eqs. (A.28), (A.29), (A.31) and (A.32), we get the perturbation in the volume due to the angular perturbations, given by [9]

$$\delta_\Omega \;\equiv\; (\cot\theta + \partial_\theta)\,\delta\theta + \partial_\vartheta\delta\vartheta, \tag{A.33}$$

$$\begin{aligned} &=\; -\frac{1}{2}\int_0^{\bar{r}_S} d\bar{r}\frac{(\bar{r}_S - \bar{r})}{\bar{r}_S\,\bar{r}}\nabla^2_\Omega(\delta g_{\alpha\beta}\bar{n}^\alpha\bar{n}^\beta) \\ &\quad + \frac{1}{2}\int_0^{\bar{r}_S} d\bar{r}\frac{1}{\bar{r}}\left[(\cot\theta + \partial_\theta)\,(\delta g_{i\beta}e^i_\theta\bar{n}^\beta) + \frac{\partial_\theta}{\sin\theta}\left(\delta g_{i\beta}e^i_\vartheta\bar{n}^\beta\right)\right], \end{aligned} \tag{A.34}$$

where the angular part of the Laplacian is given by

$$\nabla^2_\Omega \;\equiv\; (\cot\theta + \partial_\theta)\,\partial_\theta + \frac{1}{\sin\theta}\partial^2_\vartheta. \tag{A.35}$$

Furthermore, we compute the following terms – i.e. given Eqs. (A.24) and (A.30),

$$\begin{aligned} \delta g_{\alpha j}\,\bar{n}^\alpha e^j_\theta \;&=\; \frac{\partial_\theta B}{\bar{r}} + 2\bar{n}^i e^j_\theta E_{|ij} \\ &=\; \frac{\partial_\theta B}{\bar{r}} + \frac{2}{\bar{r}}\partial_\theta\left[\frac{dE}{d\lambda} - E'\right]. \end{aligned} \tag{A.36}$$

Then in a similar manner, we obtain that

$$\delta g_{\alpha j}\,\bar{n}^\alpha e^j_\vartheta \;=\; \frac{\partial_\vartheta B}{\bar{r}\sin\theta} + \frac{2}{\bar{r}\sin\theta}\partial_\vartheta\left[\frac{dE}{d\lambda} - E'\right]. \tag{A.37}$$

By using Eqs. (A.34), (A.36) and (A.37), the angular volume perturbation – i.e. the angular part of the volume density perturbation – thus becomes

$$\begin{aligned}\delta_\Omega &= -\int_0^{\bar{r}_S} d\bar{r}\frac{(\bar{r}_S-\bar{r})}{\bar{r}_S\bar{r}}\nabla^2_\Omega\left(\Phi+\Psi\right)+\int_0^{\bar{r}_S} d\bar{r}\frac{1}{\bar{r}}\nabla^2_\Omega\left[\frac{B}{\bar{r}}+\frac{2}{\bar{r}}\left(\frac{dE}{d\lambda}-E'\right)\right]\\ &\quad -\int_0^{\bar{r}_S} d\bar{r}\frac{(\bar{r}_S-\bar{r})}{\bar{r}_S\bar{r}}\nabla^2_\Omega\left[\frac{dB}{d\lambda}+\left(\frac{d^2E}{d\lambda^2}-2\frac{dE'}{d\lambda}\right)\right]\\ &= -\int_0^{\bar{r}_S} d\bar{r}\left(\bar{r}_S-\bar{r}\right)\frac{\bar{r}}{\bar{r}_S}\nabla^2_\perp\left(\Phi+\Psi\right)-\left[\nabla^2_\perp E\right]^S_O, \end{aligned} \tag{A.38}$$

where in the second line we have done integration by parts once, and set surface terms to vanish. We have also used Eq. (3.17), and

$$\nabla^2_\perp \equiv \frac{1}{\bar{r}^2}\nabla^2_\Omega = \nabla^2-\partial_r^2-\frac{2}{\bar{r}}\partial_r, \tag{A.39}$$

which is the 'screen space' Laplacian, i.e. in the plane of the source, perpendicular to the line of sight. Thus the quantity $\nabla^2_\perp E$, is transverse to the photon geodesic, with

$$\nabla^2_\perp E = \nabla^2 E-\left(\frac{d^2E}{d\lambda^2}-2\frac{dE'}{d\lambda}+E''\right)+\frac{2}{\bar{r}}\left(\frac{dE}{d\lambda}-E'\right), \tag{A.40}$$

i.e. in Fourier space. Here we have used Eqs. (A.24), (A.30) and (A.39).

Then the volume density fractional perturbation (3.47), is

$$\tilde{\delta}_{\mathcal{V}} = -3D-V_\parallel-\frac{d\delta r}{d\lambda}+\frac{a}{\mathcal{H}}\frac{d\delta z}{d\lambda}+2\frac{\delta r}{\bar{r}_S}+\delta_\Omega+a\left(4-\frac{2}{\bar{r}_S\mathcal{H}}-\frac{\mathcal{H}'}{\mathcal{H}^2}\right)\delta z, \tag{A.41}$$

$$\begin{aligned}&= -\int_0^{\bar{r}_S} d\bar{r}\left(\bar{r}_S-\bar{r}\right)\frac{\bar{r}}{\bar{r}_S}\nabla^2_\perp\left(\Phi+\Psi\right)-4V_\parallel-2\left(\Phi+\Psi\right)\\ &\quad +3\int_0^{\bar{r}_S} d\bar{r}\left(\Phi'+\Psi'\right)+\frac{2}{\bar{r}_S}\int_0^{\bar{r}_S} d\bar{r}\left(\Phi+\Psi\right)\\ &\quad -\frac{1}{\mathcal{H}}\left[\frac{d}{d\lambda}\left(-\psi+V_\parallel\right)+\frac{d\Psi}{d\lambda}-\Psi'-\partial_r\Phi\right]\\ &\quad +\left(\frac{2}{\bar{r}_S\mathcal{H}}+\frac{\mathcal{H}'}{\mathcal{H}^2}\right)\left[\mathcal{H}E-\mathcal{H}B+\Phi+V_\parallel-\int_0^{\bar{r}_S} d\bar{r}\left(\Phi'+\Psi'\right)\right]\\ &\quad +\left(E''+\frac{2}{\bar{r}_S}E'\right)+\frac{2}{\bar{r}_S}\left(B-2E'\right)-\frac{dB}{d\lambda}, \end{aligned} \tag{A.42}$$

where given Eqs. (3.17), (A.20), (A.23) and (A.27), we used

$$\begin{aligned}\frac{a}{\mathcal{H}}\frac{d\delta z}{d\lambda} &= \Phi+\Psi-\psi+V_\parallel-\int_0^{\bar{r}_S} d\bar{r}\left(\Phi'+\Psi'\right)\\ &\quad -\frac{1}{\mathcal{H}}\left[\frac{d}{d\lambda}\left(-\psi+V_\parallel\right)-\partial_r\left(\Phi+\Psi\right)\right], \end{aligned} \tag{A.43}$$

and the perturbation in the comoving radial distance as

$$2\frac{\delta r}{\bar{r}_S} = \frac{2}{\bar{r}_S}\int_0^{\bar{r}_S} d\bar{r}\left(\Phi+\Psi\right)+\frac{2}{\bar{r}_S}\left[B+\left(\frac{dE}{d\lambda}-2E'\right)\right], \tag{A.44}$$

with the total derivative given by

$$\frac{d\delta r}{d\lambda} \;=\; -\left[\Phi+\Psi-B-\left(\frac{dE}{d\lambda}-2E'\right)\right]. \tag{A.45}$$

Then from Eq. (A.42), we make the following simplification

$$\left(E''+\frac{2}{\bar{r}_{_S}}E'\right)+\frac{2}{\bar{r}_{_S}}\left(B-2E'\right)-\frac{dB}{d\lambda}+\mathcal{H}\left(\frac{2}{\bar{r}_{_S}\mathcal{H}}+\frac{\mathcal{H}'}{\mathcal{H}^2}\right)[E-B]= \\ -\left(\frac{dB}{d\lambda}+\frac{\mathcal{H}'}{\mathcal{H}}B\right)+\left(\frac{dE'}{d\lambda}+\frac{\mathcal{H}'}{\mathcal{H}}E'\right),$$

and given Eq. (3.28), we have that

$$\frac{1}{\mathcal{H}}\frac{d\Psi}{d\lambda} \;=\; \frac{1}{\mathcal{H}}\frac{d}{d\lambda}\left(D+\frac{1}{3}\nabla^2E\right)+\left(\frac{dE'}{d\lambda}+\frac{\mathcal{H}'}{\mathcal{H}}E'\right)-\left(\frac{dB}{d\lambda}+\frac{\mathcal{H}'}{\mathcal{H}}B\right). \tag{A.46}$$

Finally we have, the total volume density perturbation given by

$$\begin{aligned}\tilde{\delta}_{_\mathcal{V}} \;=\;& -\int_0^{\bar{r}_S}d\bar{r}\frac{(\bar{r}_{_S}-\bar{r})}{\bar{r}_{_S}\bar{r}}\nabla_\Omega\left(\Phi+\Psi\right)-4V_{\parallel}-2\left(\Phi+\Psi\right)\\ &+3\int_0^{\bar{r}_S}d\bar{r}\left(\Phi'+\Psi'\right)+\frac{2}{\bar{r}_{_S}}\int_0^{\bar{r}_S}d\bar{r}\left(\Phi+\Psi\right)+\frac{1}{\mathcal{H}}\left[\Phi'+\partial_r\Psi-\frac{dV_{\parallel}}{d\lambda}\right]\\ &+\left(\frac{2}{\bar{r}_{_S}\mathcal{H}}+\frac{\mathcal{H}'}{\mathcal{H}^2}\right)\left[\Phi+V_{\parallel}-\int_0^{\bar{r}_S}d\bar{r}\left(\Phi'+\Psi'\right)\right].\end{aligned} \tag{A.47}$$

A.6 The Magnification Perturbation

Consider the area density (3.67) – which is transverse to the photon geodesic. Then the only non-vanishing terms to yield

$$\mathcal{A} \;=\; a^{-2}\sqrt{-\tilde{g}}\left[1+\frac{\delta u^0}{\bar{u}^0}+\frac{\delta\ell^l}{\bar{\ell}^l}\right]\epsilon_{ijk}\,\bar{\ell}^i\,\frac{\partial\tilde{x}^j}{\partial\tilde{\theta}_{_S}}\frac{\partial\tilde{x}^k}{\partial\tilde{\vartheta}_{_S}}\left|\frac{\partial(\tilde{\theta}_{_S},\tilde{\vartheta}_{_S})}{\partial(\theta_{_O},\vartheta_{_O})}\right|, \tag{A.48}$$

$$\;=\; a^2\bar{r}^2\sin\tilde{\theta}_{_S}\left[1-3D-\phi+\bar{n}^iB_{|i}-\frac{1}{2}\delta g_{\mu\nu}\bar{n}^\alpha\bar{n}^\beta\right]\left|\frac{\partial(\tilde{\theta}_{_S},\tilde{\vartheta}_{_S})}{\partial(\theta_{_O},\vartheta_{_O})}\right|, \tag{A.49}$$

$$\;=\; a^2\bar{r}^2\sin\theta_{_O}\left[1-3D-\phi+\bar{n}^iB_{|i}-\frac{1}{2}\delta g_{\mu\nu}\bar{n}^\alpha\bar{n}^\beta+2\frac{\delta r}{\bar{r}}+\left(\cot\theta_{_O}+\partial_\theta\right)\delta\theta+\partial_\vartheta\delta\vartheta\right], \tag{A.50}$$

where $\sqrt{-\tilde{g}}$ is given by Eq. (3.43), with $\bar{\tilde{u}}^\mu=a^{-1}\delta^\mu{}_0$ and $\bar{\tilde{u}}_\mu=-a\delta^0{}_\mu$ as given by Eq. (3.8). The determinant of the transformation matrix is given by $|J|=1+\partial_\theta\delta\theta+\partial_\vartheta\delta\vartheta$ (3.42), and for small $\delta\theta$ we have $\sin\tilde{\theta}_{_S}=(1+\delta\theta\cot\theta_{_O})\sin\theta_{_O}$. Also, Eq. (3.68) becomes

$$\tilde{\ell}^\nu \;=\; a^{-1}\left(u^\nu+\frac{n^\nu}{n^\alpha u_\alpha}\right) \;=\; a^{-1}\ell^\nu. \tag{A.51}$$

Given Eqs. (3.8) and (A.15)we have $\bar{\ell}^0 = 0$ and $\bar{\tilde{\ell}}^i = a^{-1}\bar{\ell}^i = -a^{-1}\bar{n}^i/\bar{n}^0$. Then,

$$\frac{\delta\ell^i}{\bar{\ell}^i} = -\bar{n}_i v^{|i} + \bar{n}_i \delta n^i - \delta n^0 + \delta u^0 - \bar{\ell}^i \delta u_i, \tag{A.52}$$

$$= \bar{n}^i B_{|i} - \phi - \frac{1}{2}\delta g_{\alpha\beta}\bar{n}^\alpha \bar{n}^\beta, \tag{A.53}$$

where in the first line we used the identity $\bar{n}_i = 1/\bar{n}^i$, and the second line comes by combining Eqs. (A.17) and (A.18) and integrating once: with the integrals as indefinite integrals (i.e. with the limits dropped). By using Eqs. (3.28) and (A.24), we get

$$\delta_\psi \equiv -3D - \phi + \bar{n}^i B_{|i} - \frac{1}{2}\delta g_{\mu\nu}\bar{n}^\alpha \bar{n}^\beta, \tag{A.54}$$

$$= -2\Psi - E + 2\mathcal{H}\sigma - \sigma' - B' - \left(\frac{d^2E}{d\lambda^2} - 2\frac{dE'}{d\lambda}\right). \tag{A.55}$$

Then given Eqs. (A.38), (A.40), (A.44), (A.50) and (A.55), we obtain

$$\mathcal{A} = a^2\bar{r}^2 \sin\theta_O \left[1 - 2\Psi + \frac{2}{\bar{r}_S}\int_0^{\bar{r}_S} d\bar{r}\,(\Phi + \Psi) + \int_0^{\bar{r}_S} d\bar{r}\,(\bar{r} - \bar{r}_S)\frac{\bar{r}}{\bar{r}_S}\nabla_\perp^2(\Phi + \Psi) + 2\mathcal{H}\left(1 - \frac{1}{\bar{r}_S\mathcal{H}}\right)\sigma\right]. \tag{A.56}$$

By taking a gauge transformation (1.42), we get the redshift-space perturbation

$$\tilde{\delta}_\mathcal{A} = \frac{\mathcal{A} - \bar{\mathcal{A}}}{\bar{\mathcal{A}}} - \frac{d\ln\bar{\mathcal{A}}}{d\bar{z}}\delta z, \tag{A.57}$$

$$= -2\Psi + \frac{2}{\bar{r}_S}\int_0^{\bar{r}_S} d\bar{r}\,(\Phi + \Psi) + \int_0^{\bar{r}_S} d\bar{r}\,(\bar{r} - \bar{r}_S)\frac{\bar{r}}{\bar{r}_S}\nabla_\perp^2(\Phi + \Psi) + 2\left(1 - \frac{1}{\bar{r}_S\mathcal{H}}\right)[\mathcal{H}\sigma + a\,\delta z], \tag{A.58}$$

where $\delta_\mathcal{A} \equiv \delta\mathcal{A}/\bar{\mathcal{A}} = (\mathcal{A} - \bar{\mathcal{A}})/\bar{\mathcal{A}}$, with $\bar{\mathcal{A}} \equiv a^2\bar{r}^2\sin\theta_O$, and

$$\frac{d\ln\bar{\mathcal{A}}}{d\bar{z}} = 2a\left(\frac{1}{\bar{r}_S\mathcal{H}} - 1\right)\delta z. \tag{A.59}$$

Thus given Eq. (A.20), and that $\tilde{\mathcal{M}}^{-1} = 1 + \tilde{\delta}_\mathcal{A}$ (3.63), we get

$$\tilde{\mathcal{M}}^{-1} = 1 - \tilde{\delta}_\mathcal{M}, \tag{A.60}$$

$$= 1 - 2\Psi + \frac{2}{\bar{r}_S}\int_0^{\bar{r}_S} d\bar{r}\,(\Phi + \Psi) + \int_0^{\bar{r}_S} d\bar{r}\,(\bar{r} - \bar{r}_S)\frac{\bar{r}}{\bar{r}_S}\nabla_\perp^2(\Phi + \Psi) - 2\left(1 - \frac{1}{\bar{r}_S\mathcal{H}}\right)\left[\Phi + V_\parallel - \int_0^{\bar{r}_S} d\bar{r}\,(\Phi' + \Psi')\right]. \tag{A.61}$$

The magnification contrast $\tilde{\delta}_\mathcal{M}$ is hence given by Eq. (A.60) – which measures the magnification distortion (up to the magnification bias (2.36)) in the observed overdensity.

To get the 'relativistic density perturbation', we sum Eqs. (3.33) and (A.47) and $\tilde{\delta}_{\mathcal{M}}$ (A.61), and using Eqs. (3.60) and (3.62), we obtain

$$\begin{aligned}\Delta_{\rm g}^{\rm obs}(\mathbf{n},z) &= \Delta_{\rm g}(\mathbf{n},z)+\frac{1}{\mathcal{H}}\partial_r V_{\parallel}(\mathbf{n},z)\\ &+(1-\mathcal{Q})\int_0^{\bar{r}_S}d\bar{r}\,(\bar{r}-\bar{r}_S)\,\frac{\bar{r}}{\bar{r}_S}\nabla_\perp^2\,(\Phi+\Psi)\,(\mathbf{n},z)\\ &+\ (3-b_e)\,\mathcal{H}V(\mathbf{n},z)-\left(b_e-1-2\mathcal{Q}-\frac{\mathcal{H}'}{\mathcal{H}^2}-\frac{2(1-\mathcal{Q})}{\bar{r}_S\mathcal{H}}\right)\Phi(\mathbf{n},z)\\ &+\frac{1}{\mathcal{H}}\Psi'(\mathbf{n},z)-2(1-\mathcal{Q})\Psi(\mathbf{n},z)+\frac{2(1-\mathcal{Q})}{\bar{r}_S}\int_0^{\bar{r}_S}d\bar{r}\,(\Phi+\Psi)\,(\mathbf{n},z)\\ &-\left(b_e-2\mathcal{Q}-\frac{\mathcal{H}'}{\mathcal{H}^2}-\frac{2(1-\mathcal{Q})}{\bar{r}_S\mathcal{H}}\right)\left[V_{\parallel}-\int_0^{\bar{r}_S}d\bar{r}\,\left(\Phi'+\Psi'\right)\right](\mathbf{n},z).\end{aligned} \tag{A.62}$$

This gives the correct (physical) observed density perturbation of galaxy redshift surveys. This generalizes the Kaiser approximation (2.44). We also see the effect of cosmic magnification in the observed number density of galaxies. Hence this also covers the case of magnification-dependent surveys, as well as magnification-independent surveys.

Appendix B

Quintessence Models

Here we outline the features of the quintessence models we used in chapters 4 and 5. Note that in chapter 4 we denote all quintessence parameters by subscript "q", and in chapter 5 we used a generic subscript "x".

B.1 Ratra-Peebles Potential

The Ratra-Peebles (RP) potential [1, 25, 57, 79, 103] is given by

$$U(\varphi) \;=\; \frac{M^{4+\alpha}}{\varphi^{\alpha}}, \quad \alpha > 0. \tag{B.1}$$

The mass scale M is chosen [1]: so that $(\sqrt{8\pi G})^{2+\alpha} M^{4+\alpha}/(3H_0^2) = 0.58$ (see [103]) and (in chapter 4) we used the constant $\alpha \simeq 0.501898922$. We obtain $w_{q0} \simeq -0.85927$, i.e. value at today. (In chapter 5 we varied the values of the potential parameters, while maintaining the same behaviour for w_x. We used $\alpha = 0.468339983$; thus $w_{x0} \simeq -0.877$.)

B.2 Super Gravity Potential

The SUGRA potential [1, 25, 57, 79, 217, 218] is a super-gravity correction to the RP potential, given by

$$U(\varphi) \;=\; \frac{M^{4+\alpha}}{\varphi^{\alpha}} \exp\left(4\pi G\varphi^2\right), \tag{B.2}$$

where we choose [1] (in chapter 4): $(\sqrt{8\pi G})^{2+\alpha} M^{4+\alpha}/(3H_0^2) = 0.45$ (see [103]) and $\alpha \simeq 0.65705469$. This leads to the value of the equation of state parameter at today, as $w_{q0} \simeq -0.9395$ (at today).

In chapter 5, we varied the values of the potential parameters while maintaining the evolution behaviour of the equation of state parameter. We chose $(\sqrt{8\pi G})^{2+\alpha} M^{4+\alpha}/(3H_0^2) = 0.594521$ and $\alpha = 0.650176$, hence $w_{x0} \simeq -0.964$ – i.e. as given in [57].

B.3 Double Exponential Potential

The double exponential (DExp) potential [1, 57, 103, 105, 218, 219] is given by

$$U(\varphi) \;=\; M_1^4 \exp\left(\alpha\varphi\sqrt{8\pi G}\right) + M_2^4 \exp\left(\beta\varphi\sqrt{8\pi G}\right), \tag{B.3}$$

where we note that the behaviour of Ω_q and w_q is very sensitive to the choice of the parameters α and β. We choose M_1 [1] (in chapter 4): via $8\pi G M_1^4/(3H_0^2) = 0.88926578$ (see [103]), set $M_2^4 = 0.4101 M_1^4$ and take $\beta = 1$. Then we calculate $\alpha \simeq -6.25166029$ and find the value $w_{q0} \simeq -0.99993$ (i.e. at today).

Similarly, in chapter 5, we varied the values of the potential parameters – with the equations of state parameter behaviour remaining the same. We chose M_1 via $8\pi G M_1^4/(3H_0^2) = 0.8345477$, and set $M_2^4 = 0.1 M_1^4$ with $\beta = 5$. We take $\alpha = -1.5$; and we obtain $w_{x0} \simeq -0.998$.

Appendix C

Adiabatic Initial Conditions

In this Appendix, we give the initial conditions, i.e. initial values, of the relevant perturbations at decoupling $a = a_d$ – at which epoch we initialize all evolutions.

C.1 Quintessence

In chapter 4, the adiabatic initial conditions (4.14), together with the Einstein-de Sitter condition $\Phi'(a_d) = 0$, lead to the perturbation initial values given by [1]

$$\Delta_m = \frac{-2k^2\left[k^2 + 9\mathcal{H}^2(c_{sq}^2 - c_{aq}^2)\right]}{3\mathcal{H}^2\left[k^2(1+w_q-w_q\Omega_m) + 9\mathcal{H}^2\Omega_m(c_{sq}^2-c_{aq}^2)\right]}\Phi_d(k), \tag{C.1}$$

$$\Delta_q = \frac{-2k^4(1+w_q)}{3\mathcal{H}^2\left[k^2(1+w_q-w_q\Omega_m) + 9\mathcal{H}^2\Omega_m(c_{sq}^2-c_{aq}^2)\right]}\Phi_d(k), \tag{C.2}$$

which specify the matter and dark energy (comoving) density perturbations, respectively. The associated velocity potentials at decoupling a_d are given by

$$V_m = \frac{-2}{3\mathcal{H}}\left[\frac{k^2(1+w_q-w_q\Omega_m)(1-3c_{sq}^2+3c_{aq}^2) + 3\Omega_m(k^2+3\mathcal{H}^2)(c_{sq}^2-c_{aq}^2)}{(1+w_q-w_q\Omega_m)\left[k^2(1+w_q-w_q\Omega_m) + 9\mathcal{H}^2\Omega_m(c_{sq}^2-c_{aq}^2)\right]}\right]\Phi_d(k), \tag{C.3}$$

$$V_q = \frac{-2}{3\mathcal{H}(1+w_q-w_q\Omega_m)}\left[\frac{k^2(1+w_q-w_q\Omega_m) + 3\Omega_m(k^2+3\mathcal{H}^2)(c_{sq}^2-c_{aq}^2)}{k^2(1+w_q-w_q\Omega_m) + 9\mathcal{H}^2\Omega_m(c_{sq}^2-c_{aq}^2)}\right]\Phi_d(k), \tag{C.4}$$

where $\Phi_d = \Phi(a_d)$, and $\Phi_d(k)$ is given by Eq. (2.12), and

$$c_{aq}^2 \equiv \frac{p_q'}{\rho_q'} = w_q - \frac{w_q'}{3\mathcal{H}(1+w_q)}. \tag{C.5}$$

All scale-factor-dependent (i.e. background) quantities above are evaluated at a_d, and we assumed $1 + w_q(a_d) \neq 0$. In the ΛCDM case, we have

$$\Delta_m = -\frac{2k^2}{3\Omega_m\mathcal{H}^2}\Phi_d(k), \qquad V_m = -\frac{2}{3\Omega_m\mathcal{H}}\Phi_d(k), \tag{C.6}$$

which are the only the initial perturbations. We note that here, $\Delta_q = 0 = V_q$.

C.2 Homogeneoeus Dark Energy

In chapter 5 we used adiabatic initial conditions which follow from the vanishing of the relative entropy perturbation [1, 108–111, 128] (see Eq. (4.14)), given at a_d by

$$\delta_x(a_d) \;=\; (1 + w_x(a_d))\,\delta_m(a_d). \tag{C.7}$$

By using that at a_d, we have

$$V_x(a_d) \;=\; V_m(a_d), \tag{C.8}$$

whence we obtain the following

$$\Delta_x(a_d) \;=\; (1 + w_x(a_d))\Delta_m(a_d). \tag{C.9}$$

These equations together with the Einstein de Sitter initial condition $\Phi'(a_d) = 0$, lead to the initial perturbations

$$\Delta_m(k) \;=\; \frac{-2k^2}{3\,(1 + \Omega_x w_x)\,\mathcal{H}^2}\Phi_d(k), \tag{C.10}$$

$$V_m(k) \;=\; \frac{-2}{3\,(1 + \Omega_x w_x)\,\mathcal{H}}\Phi_d(k). \tag{C.11}$$

C.3 Interacting Dark Energy

Similarly, in chapter 6 we used the Einstein-de Sitter initial condition $\Phi'(a_d) = 0$, given that $\Omega_x(a_d) \ll 1$. Adiabatic initial conditions are imposed by the vanishing of the relative entropy perturbation S_{xm}, given by [2]

$$S_{xm}(a_d) \;=\; 0, \qquad S_{xm} \;\equiv\; \frac{\delta_x}{1 + w_{x,\mathrm{eff}}} - \frac{\delta_m}{1 + w_{m,\mathrm{eff}}}. \tag{C.12}$$

We assume the equality of the DE and DM velocities, given by

$$V_x(a_d) \;=\; V_m(a_d), \tag{C.13}$$

which then leads to the initial density perturbations, given by

$$\frac{\Delta_x(a_d)}{1 + w_{x,\mathrm{eff}}(a_d)} \;=\; \frac{\Delta_m(a_d)}{1 + w_{m,\mathrm{eff}}(a_d)}. \tag{C.14}$$

Together with Eqs. (5.5) and (6.8), this leads to the initial DM and DE perturbations:

$$\Delta_m(k) \;=\; \frac{-2k^2\,(1 + w_{m,\mathrm{eff}})}{3\mathcal{H}^2\,(1 + \Omega_m w_{m,\mathrm{eff}} + \Omega_x w_{x,\mathrm{eff}})}\Phi_d(k), \tag{C.15}$$

$$\Delta_x(k) \;=\; \frac{-2k^2\,(1 + w_{x,\mathrm{eff}})}{3\mathcal{H}^2\,(1 + \Omega_m w_{m,\mathrm{eff}} + \Omega_x w_{x,\mathrm{eff}})}\Phi_d(k), \tag{C.16}$$

where given Eq. (C.13), we have

$$V_x(k) \;=\; \frac{-2}{3\mathcal{H}\,(1 + \Omega_x w_x)}\Phi_d(k) \;=\; V_m(k), \tag{C.17}$$

where $w_{m,\text{eff}}$ and $w_{x,\text{eff}}$ are given by Eq. (6.3), and $\Phi_d(k)$ is given by Eq. (2.12). Thus Eqs. (C.12)–(C.17) specify the initial conditions for the evolutions in chapter 6.

Bibliography

[1] Didam Duniya, Daniele Bertacca, and Roy Maartens. Clustering of quintessence on horizon scales and its imprint on HI intensity mapping. *JCAP*, 1310:015, 2013. doi: 10.1088/1475-7516/2013/10/015.

[2] Didam Duniya, Daniele Bertacca, and Roy Maartens. Probing the imprint of interacting dark energy on very large scales. *Phys.Rev.*, D91:063530, 2015. doi: 10.1103/PhysRevD.91.063530.

[3] Anthony Challinor and Antony Lewis. The linear power spectrum of observed source number counts. *Phys.Rev.*, D84:043516, 2011. doi: 10.1103/PhysRevD.84.043516.

[4] Marco Bruni, Robert Crittenden, Kazuya Koyama, Roy Maartens, Cyril Pitrou, et al. Disentangling non-Gaussianity, bias and GR effects in the galaxy distribution. *Phys.Rev.*, D85:041301, 2012. doi: 10.1103/PhysRevD.85.041301.

[5] Donghui Jeong, Fabian Schmidt, and Christopher M. Hirata. Large-scale clustering of galaxies in general relativity. *Phys.Rev.*, D85:023504, 2012. doi: 10.1103/PhysRevD.85.023504.

[6] Jaiyul Yoo, A. Liam Fitzpatrick, and Matias Zaldarriaga. A New Perspective on Galaxy Clustering as a Cosmological Probe: General Relativistic Effects. *Phys.Rev.*, D80:083514, 2009. doi: 10.1103/PhysRevD.80.083514.

[7] Jaiyul Yoo. General Relativistic Description of the Observed Galaxy Power Spectrum: Do We Understand What We Measure? *Phys.Rev.*, D82:083508, 2010. doi: 10.1103/PhysRevD.82.083508.

[8] N. Bartolo, S. Matarrese, and A. Riotto. Relativistic Effects and Primordial Non-Gaussianity in the Galaxy bias. *JCAP*, 1104:011, 2011. doi: 10.1088/1475-7516/2011/04/011.

[9] Camille Bonvin and Ruth Durrer. What galaxy surveys really measure. *Phys.Rev.*, D84:063505, 2011. doi: 10.1103/PhysRevD.84.063505.

[10] Tobias Baldauf, Uros Seljak, Leonardo Senatore, and Matias Zaldarriaga. Galaxy Bias and non-Linear Structure Formation in General Relativity. *JCAP*, 1110:031, 2011. doi: 10.1088/1475-7516/2011/10/031.

[11] Jaiyul Yoo, Nico Hamaus, Uros Seljak, and Matias Zaldarriaga. Testing General Relativity on Horizon Scales and the Primordial non-Gaussianity. *arXiv:1109.0998*, 2011.

[12] Fabian Schmidt and Donghui Jeong. Cosmic Rulers. *Phys.Rev.*, D86:083527, 2012. doi: 10.1103/PhysRevD.86.083527.

[13] Donghui Jeong and Fabian Schmidt. Large-Scale Structure with Gravitational Waves I: Galaxy Clustering. *Phys.Rev.*, D86:083512, 2012. doi: 10.1103/PhysRevD.86.083512.

[14] Fabian Schmidt and Donghui Jeong. Large-Scale Structure with Gravitational Waves II: Shear. *Phys.Rev.*, D86:083513, 2012. doi: 10.1103/PhysRevD.86.083513.

[15] Daniele Bertacca, Roy Maartens, Alvise Raccanelli, and Chris Clarkson. Beyond the plane-parallel and Newtonian approach: Wide-angle redshift distortions and convergence in general relativity. *JCAP*, 1210:025, 2012. doi: 10.1088/1475-7516/2012/10/025.

[16] Roy Maartens, Gong-Bo Zhao, David Bacon, Kazuya Koyama, and Alvise Raccanelli. Relativistic corrections and non-Gaussianity in radio continuum surveys. *JCAP*, 1302:044, 2013. doi: 10.1088/1475-7516/2013/02/044.

[17] Alex Hall, Camille Bonvin, and Anthony Challinor. Testing General Relativity with 21-cm intensity mapping. *Phys.Rev.*, D87(6):064026, 2013. doi: 10.1103/PhysRevD.87.064026.

[18] Lucas Lombriser, Jaiyul Yoo, and Kazuya Koyama. Relativistic effects in galaxy clustering in a parametrized post-Friedmann universe. *Phys.Rev.*, D87:104019, 2013. doi: 10.1103/PhysRevD.87.104019.

[19] Jaiyul Yoo and Vincent Desjacques. All-Sky Analysis of the General Relativistic Galaxy Power Spectrum. *Phys.Rev.*, D88(2):023502, 2013. doi: 10.1103/PhysRevD.88.023502.

[20] Alvise Raccanelli, Daniele Bertacca, Olivier Dore, and Roy Maartens. Large-scale 3D galaxy correlation function and non-Gaussianity. *JCAP*, 1408:022, 2014. doi: 10.1088/1475-7516/2014/08/022.

[21] Camille Bonvin, Lam Hui, and Enrique Gaztanaga. Asymmetric galaxy correlation functions. *Phys.Rev.*, D89(8):083535, 2014. doi: 10.1103/PhysRevD.89.083535.

[22] Alvise Raccanelli, Daniele Bertacca, Roy Maartens, Chris Clarkson, and Olivier Dore. Lensing and time-delay contributions to galaxy correlations. *arXiv:1311.6813*, 2013.

[23] Camille Bonvin. Isolating relativistic effects in large-scale structure. *Class.Quant.Grav.*, 31(23):234002, 2014. doi: 10.1088/0264-9381/31/23/234002.

[24] Jaiyul Yoo. Relativistic Effect in Galaxy Clustering. *Class.Quant.Grav.*, 31: 234001, 2014. doi: 10.1088/0264-9381/31/23/234001.

[25] Edmund J. Copeland, M. Sami, and Shinji Tsujikawa. Dynamics of dark energy. *Int.J.Mod.Phys.*, D15:1753–1936, 2006. doi: 10.1142/S021827180600942X.

[26] Shinji Tsujikawa. Quintessence: A Review. *Class.Quant.Grav.*, 30:214003, 2013. doi: 10.1088/0264-9381/30/21/214003.

[27] L. Amendola and S. Tsujikawa. *Dark Energy: Theory and Observations*. Cambridge University Press, The Edinburgh Building, Cambridge CB2 8RU, UK, 2010.

[28] Timothy Clifton, Pedro G. Ferreira, Antonio Padilla, and Constantinos Skordis. Modified Gravity and Cosmology. *Phys.Rept.*, 513:1–189, 2012. doi: 10.1016/j.physrep.2012.01.001.

[29] H.T. Diehl et al. The Dark Energy Survey and Operations: Year 1. *Proc.SPIE Int.Soc.Opt.Eng.*, 9149:91490V, 2014. doi: 10.1117/12.2056982.

[30] R. Scaramella et al. Euclid space mission: a cosmological challenge for the next 15 years. *arXiv:1501.04908*, 2015.

[31] Daniel J. Eisenstein et al. SDSS-III: Massive Spectroscopic Surveys of the Distant Universe, the Milky Way Galaxy, and Extra-Solar Planetary Systems. *Astron.J.*, 142:72, 2011. doi: 10.1088/0004-6256/142/3/72.

[32] Stefano Camera, Mario G. Santos, and Roy Maartens. Probing primordial non-Gaussianity with SKA galaxy redshift surveys: a fully relativistic analysis. *Mon.Not.Roy.Astron.Soc.*, 448:1035, 2015. doi: 10.1093/mnras/stv040.

[33] Roy Maartens, Filipe B. Abdalla, Matt Jarvis, and Mario G. Santos. Cosmology with the SKA – overview. *arXiv:1501.04076*, 2015.

[34] Jaiyul Yoo, Nico Hamaus, Uros Seljak, and Matias Zaldarriaga. Going beyond the Kaiser redshift-space distortion formula: a full general relativistic account of the effects and their detectability in galaxy clustering. *Phys.Rev.*, D86:063514, 2012. doi: 10.1103/PhysRevD.86.063514.

[35] Stefano Camera, Roy Maartens, and Mario G. Santos. Einstein's legacy in galaxy surveys. *MNRAS Letters*, 451(L80), 2014. doi: 10.1093/mnrasl/slv069.

[36] M. Geller. The universe nearby. In L. Martinet and M. Mayor, editors, *Large scale structures in the universe*, volume 17 of *Saas-Fee Series*, pages 71–172, Geneva Observatory, CH-1290 Sauverny-Versoix, Switzerland, 1987. Swiss Soceity of Astronomy and Astrophysics, Geneva Observatory.

[37] A. Szalay. The fluctuation spectrum of the universe. In L. Martinet and M. Mayor, editors, *Large scale structures in the universe*, volume 17 of *Saas-Fee Series*, pages 175–260, Geneva Observatory, CH-1290 Sauverny-Versoix, Switzerland, 1987. Swiss Soceity of Astronomy and Astrophysics, Geneva Observatory.

[38] Nature Publishing Group. *Encyclopedia of Astronomy and Astrophysics*. Ataraxiainc, 111 River Street, Hoboken, NJ 07030-5774, 2005.

[39] H. Kodama and M. Sasaki. Cosmological Perturbation Theory. *Prog.Theor.Phys.Suppl.*, 78:1–166, 1984. doi: 10.1143/PTPS.78.1.

[40] V. F. Mukhanov, H.A. Feldman, and R. H. Brandenberger. Theory of cosmological perturbations. Part 1. Classical perturbations. Part 2. Quantum theory of perturbations. Part 3. Extensions. *Phys.Rept.*, 215:203–333, 1992. doi: 10.1016/0370-1573(92)90044-Z.

[41] Ruth Durrer. Gauge invariant cosmological perturbation theory: A General study and its application to the texture scenario of structure formation. *Fund.Cosmic Phys.*, 15:209, 1994.

[42] K. A. Malik. *Cosmological Perturbations in an Inflationary Universe*. Phd. thesis, University of Portsmouth, Portsmouth, UK, Jan 2001. [arXiv:astro-ph/0101563].

[43] S. Dodelson. *Modern Cosmology*. Academic Press, San Diego, California 92101-4495, USA, 2003.

[44] Hannu Kurki-Suonio. Cosmological perturbation theory. *unpublished lecture notes available online (referenced 23 Oct. 2005)*, 2005. URL `http://theory.physics.helsinki.fi/~cpt/CosPer_26Apr2011.pdf`.

[45] M. Giovannini. *A Primer on the Physics of the Microwave Background*. World Scientific, Singapore 596224, 2008.

[46] R. Durrer. *The Cosmic Microwave Background*. Cambridge University Press, Cambridge, 2008.

[47] S. Carroll. *Spacetime and Geometry: An Introduction to general Relativity*. Addison Wesley, San Francisco, 2003.

[48] M. P. Hobson, G. Efstathiou, and A. N. Lasenby. *General Relativity: An Introduction for Physicists*. Cambridge University Press, Cambridge, CB2 2RU, 2006.

[49] J. N. Islam. *An Introduction to Mathematical Cosmology*. Cambridge University Press, Cambridge, UK, 2004.

[50] L. P. Hughston and K. P. Tod. *An Introduction to General Relativity*. Number 05 in London Mathematical Soceity Student Texts. Cambridge University Press, Cambridge, CB2 1RP, 1994.

[51] M. Carmeli. *Classical Fields: General Relativity and Gauge Theory*. John Wiley & Sons, Inc., New York, USA, 1982.

[52] R. M. Wald. *General Relativity*. The University of Chicago Press, Chicago 60637, USA, 1984.

[53] S. Weinberg. *Cosmology*. Oxford University Press, Great Clarendon Street, Oxford OX2 6DP, 2008.

[54] James M. Bardeen. Gauge Invariant Cosmological Perturbations. *Phys.Rev.*, D22: 1882–1905, 1980. doi: 10.1103/PhysRevD.22.1882.

[55] Sergei M. Kopeikin, Juan Ramirez, Bahram Mashhoon, and Mikhail V. Sazhin. Cosmological perturbations: A New gauge invariant approach. *Phys.Lett.*, A292: 173–180, 2001. doi: 10.1016/S0375-9601(01)00777-0.

[56] Chung-Pei Ma and Edmund Bertschinger. Cosmological perturbation theory in the synchronous and conformal Newtonian gauges. *Astrophys.J.*, 455:7–25, 1995. doi: 10.1086/176550.

[57] Didam Duniya. Dark energy homogeneity in general relativity: are we applying it correctly? *arXiv:1505.03436*, 2015.

[58] Alan H. Guth. Inflation. *arXiv:astro-ph/0404546*, pages 31–52, 2004.

[59] Latham A. Boyle, Paul J. Steinhardt, and Neil Turok. Inflationary predictions reconsidered. *Phys.Rev.Lett.*, 96:111301, 2006. doi: 10.1103/PhysRevLett.96.111301.

[60] Bruce A. Bassett, Shinji Tsujikawa, and David Wands. Inflation dynamics and reheating. *Rev.Mod.Phys.*, 78:537–589, 2006. doi: 10.1103/RevModPhys.78.537.

[61] Camille Bonvin. Galaxy clustering. Saas-Fee Advanced Course, 2014. URL `http://saasfee2014.epfl.ch/files/content/sites/saasfee2014/files/Bonvin_Notes.pdf`.

[62] P. Schneider, C. Kochanek, and J. Wambsganss. *Gravitational Lensing: Strong, Weak and Micro*, volume 33 of *Saas-Fee Advanced Course*. Springer-Verlag, Berlin Heidelberg, 2006.

[63] John A. Peacock. *Cosmological Physics*. Cambridge University Press, Cambridge, UK, 1998.

[64] Nick Kaiser. Clustering in real space and in redshift space. *Mon.Not.Roy.Astron.Soc.*, 227:1–27, 1987.

[65] Michael A. Strauss and Jeffrey A. Willick. The Density and peculiar velocity fields of nearby galaxies. *Phys.Rept.*, 261:271–431, 1995. doi: 10.1016/0370-1573(95)00013-7.

[66] Michael A. Strauss. Recent advances in redshift surveys of the local universe. *astro-ph/9610033*, 1996.

[67] A. J. S. Hamilton. Linear redshift distortions: A Review. *astro-ph/9708102*, 1997.

[68] B. D. Gupta. *Mathematical Physics*. Vikas Publishing House PVT Ltd, Jangpura, New Delhi-110 014, 2008.

[69] Ivaylo Zlatev, Li-Min Wang, and Paul J. Steinhardt. Quintessence, cosmic coincidence, and the cosmological constant. *Phys.Rev.Lett.*, 82:896–899, 1999. doi: 10.1103/PhysRevLett.82.896.

[70] Philippe Brax and Jerome Martin. The Robustness of quintessence. *Phys.Rev.*, D61:103502, 2000. doi: 10.1103/PhysRevD.61.103502.

[71] Paul J. Steinhardt, Li-Min Wang, and Ivaylo Zlatev. Cosmological tracking solutions. *Phys.Rev.*, D59:123504, 1999. doi: 10.1103/PhysRevD.59.123504.

[72] William J. Potter and Sirichai Chongchitnan. A Gauge-invariant approach to interactions in the dark sector. *JCAP*, 1109:005, 2011. 24 pages, 9 figures. Accepted for publication in JCAP.

[73] Sean M. Carroll. Quintessence and the rest of the world. *Phys.Rev.Lett.*, 81:3067–3070, 1998. doi: 10.1103/PhysRevLett.81.3067.

[74] Christopher F. Kolda and David H. Lyth. Quintessential difficulties. *Phys.Lett.*, B458:197–201, 1999. doi: 10.1016/S0370-2693(99)00657-7.

[75] P.A.R. Ade et al. Planck 2013 Results. XXIV. Constraints on primordial non-Gaussianity. *Astron.Astrophys.*, 571:A24, 2014. doi: 10.1051/0004-6361/201321554.

[76] L. Raul Abramo and Katie E. Leonard. Why multi-tracer surveys beat cosmic variance. *Mon.Not.Roy.Astron.Soc.*, 432:318, 2013. doi: 10.1093/mnras/stt465.

[77] Sanil Unnikrishnan, H.K. Jassal, and T.R. Seshadri. Scalar Field Dark Energy Perturbations and their Scale Dependence. *Phys.Rev.*, D78:123504, 2008. doi: 10.1103/PhysRevD.78.123504.

[78] H.K. Jassal. A comparison of perturbations in fluid and scalar field models of dark energy. *Phys.Rev.*, D79:127301, 2009. doi: 10.1103/PhysRevD.79.127301.

[79] J.-M. Alimi, A. Fuzfa, V. Boucher, Y. Rasera, J. Courtin, et al. Imprints of Dark Energy on Cosmic Structure Formation. I. Realistic Quintessence Models. *Mon.Not.Roy.Astron.Soc.*, 401:775, 2010. doi: 10.1111/j.1365-2966.2009.15712.x.

[80] Chan-Gyung Park, Jai-chan Hwang, Jae-heon Lee, and Hyerim Noh. Roles of dark energy perturbations in the dynamical dark energy models: Can we ignore them? *Phys.Rev.Lett.*, 103:151303, 2009. doi: 10.1103/PhysRevLett.103.151303.

[81] Sirichai Chongchitnan and Lindsay King. Imprints of dynamical dark energy on weak-lensing measurements. *Mon.Not.Roy.Astron.Soc.*, 407:1989–1997, 2010. doi: 10.1111/j.1365-2966.2010.17054.x.

[82] H.K. Jassal. Evolution of perturbations in distinct classes of canonical scalar field models of dark energy. *Phys.Rev.*, D81:083513, 2010. doi: 10.1103/PhysRevD.81.083513.

[83] H.K. Jassal. Scalar field dark energy perturbations and the Integrated Sachs Wolfe effect. *Phys.Rev.*, D86:043528, 2012. doi: 10.1103/PhysRevD.86.043528.

[84] Masahiro Takada. Can A Galaxy Redshift Survey Measure Dark Energy Clustering? *Phys.Rev.*, D74:043505, 2006. doi: 10.1103/PhysRevD.74.043505.

[85] Will J. Percival. Cosmological structure formation in a homogeneous dark energy background. *Astron.Astrophys.*, 443:819, 2005. doi: 10.1051/0004-6361:20053637.

[86] Eric V. Linder and Robert N. Cahn. Parameterized Beyond-Einstein Growth. *Astropart. Phys.*, 28:481–488, 2007. doi: 10.1016/j.astropartphys.2007.09.003.

[87] S. Nesseris and Leandros Perivolaropoulos. Testing Lambda CDM with the Growth Function delta(a): Current Constraints. *Phys. Rev.*, D77:023504, 2008. doi: 10.1103/PhysRevD.77.023504.

[88] Spyros Basilakos, S. Nesseris, and L. Perivolaropoulos. Is the CMB shift parameter connected with the growth of cosmological perturbations? *Mon. Not. Roy. Astron. Soc.*, 387:1126–1130, 2008. doi: 10.1111/j.1365-2966.2008.13303.x.

[89] James B. Dent, Sourish Dutta, and Thomas J. Weiler. A new perspective on the relation between dark energy perturbations and the late-time ISW effect. *Phys.Rev.*, D79:023502, 2009. doi: 10.1103/PhysRevD.79.023502.

[90] David Polarski and Radouane Gannouji. On the growth of linear perturbations. *Phys. Lett.*, B660:439–443, 2008. doi: 10.1016/j.physletb.2008.01.032.

[91] Shinji Tsujikawa, Radouane Gannouji, Bruno Moraes, and David Polarski. The dispersion of growth of matter perturbations in f(R) gravity. *Phys. Rev.*, D80: 084044, 2009. doi: 10.1103/PhysRevD.80.084044.

[92] Spyros Basilakos, J. C. Bueno Sanchez, and Leandros Perivolaropoulos. The spherical collapse model and cluster formation beyond the Λ cosmology: Indications for a clustered dark energy? *Phys. Rev.*, D80:043530, 2009. doi: 10.1103/PhysRevD.80.043530.

[93] Yungui Gong, Mustapha Ishak, and Anzhong Wang. Growth factor parametrization in curved space. *Phys. Rev.*, D80:023002, 2009. doi: 10.1103/PhysRevD.80.023002.

[94] Emiliano Sefusatti and Filippo Vernizzi. Cosmological structure formation with clustering quintessence. *JCAP*, 1103:047, 2011. doi: 10.1088/1475-7516/2011/03/047.

[95] L. Campanelli, G. L. Fogli, T. Kahniashvili, A. Marrone, and Bharat Ratra. Galaxy cluster number count data constraints on cosmological parameters. *Eur. Phys. J.*, C72:2218, 2012. doi: 10.1140/epjc/s10052-012-2218-4.

[96] Shinji Tsujikawa, Antonio De Felice, and Jailson Alcaniz. Testing for dynamical dark energy models with redshift-space distortions. *JCAP*, 1301:030, 2013. doi: 10.1088/1475-7516/2013/01/030.

[97] R.C. Batista and F. Pace. Structure formation in inhomogeneous Early Dark Energy models. *JCAP*, 1306:044, 2013. doi: 10.1088/1475-7516/2013/06/044.

[98] Olga Avsajanishvili, Natalia A. Arkhipova, Lado Samushia, and Tina Kahniashvili. Growth Rate in the Dynamical Dark Energy Models. *Eur. Phys. J.*, C74(11):3127, 2014. doi: 10.1140/epjc/s10052-014-3127-5.

[99] Ahmad Mehrabi, Mohammad Malekjani, and Francesco Pace. Can observational growth rate data favor the clustering dark energy models? *Astrophys. Space Sci.*, 356(1):129–135, 2015. doi: 10.1007/s10509-014-2185-3.

[100] Spyros Basilakos. The growth index of matter perturbations using the clustering of dark energy. *Mon. Not. Roy. Astron. Soc.*, 449(2):2151–2155, 2015. doi: 10.1093/mnras/stv411.

[101] Ronaldo C. Batista. Impact of dark energy perturbations on the growth index. *Phys. Rev.*, D89(12):123508, 2014. doi: 10.1103/PhysRevD.89.123508.

[102] O. F. Piattella, D. L. A. Martins, and L. Casarini. Sub-horizon evolution of cold dark matter perturbations through dark matter-dark energy equivalence epoch. *JCAP*, 1410(10):031, 2014. doi: 10.1088/1475-7516/2014/10/031.

[103] G. Barro Calvo and Antonio Lopez Maroto. Confronting quintessence models with recent high-redshift supernovae data. *Phys.Rev.*, D74:083519, 2006. doi: 10.1103/PhysRevD.74.083519.

[104] Michael J. Mortonson, Wayne Hu, and Dragan Huterer. Falsifying Paradigms for Cosmic Acceleration. *Phys.Rev.*, D79:023004, 2009. doi: 10.1103/PhysRevD.79.023004.

[105] Bruce A. Bassett, Mike Brownstone, Antonio Cardoso, Marina Cortes, Yabebal Fantaye, et al. Is the Dynamics of Tracking Dark Energy Detectable? *JCAP*, 0807:007, 2008. doi: 10.1088/1475-7516/2008/07/007.

[106] R. R. Caldwell, Rahul Dave, and Paul J. Steinhardt. Cosmological imprint of an energy component with general equation of state. *Phys. Rev. Lett.*, 80:1582–1585, 1998. doi: 10.1103/PhysRevLett.80.1582.

[107] Savvas Nesseris and Domenico Sapone. On the accuracy of the growth index in the presence of dark energy perturbations. *arXiv:1505.06601*, 2015.

[108] Hideo Kodama and Misao Sasaki. Cosmological Perturbation Theory. *Prog.Theor.Phys.Suppl.*, 78:1–166, 1984. doi: 10.1143/PTPS.78.1.

[109] David Wands, Karim A. Malik, David H. Lyth, and Andrew R. Liddle. A New approach to the evolution of cosmological perturbations on large scales. *Phys.Rev.*, D62:043527, 2000. doi: 10.1103/PhysRevD.62.043527.

[110] Karim A. Malik, David Wands, and Carlo Ungarelli. Large scale curvature and entropy perturbations for multiple interacting fluids. *Phys.Rev.*, D67:063516, 2003. doi: 10.1103/PhysRevD.67.063516.

[111] Karim A. Malik and David Wands. Adiabatic and entropy perturbations with interacting fluids and fields. *JCAP*, 0502:007, 2005. doi: 10.1088/1475-7516/2005/02/007.

[112] Rachel Bean and Olivier Dore. Probing dark energy perturbations: The Dark energy equation of state and speed of sound as measured by WMAP. *Phys.Rev.*, D69:083503, 2004. doi: 10.1103/PhysRevD.69.083503.

[113] James B. Dent and Sourish Dutta. On the dangers of using the growth equation on large scales. *Phys.Rev.*, D79:063516, 2009. doi: 10.1103/PhysRevD.79.063516.

[114] Michel Chevallier and David Polarski. Accelerating universes with scaling dark matter. *Int.J.Mod.Phys.*, D10:213–224, 2001. doi: 10.1142/S0218271801000822.

[115] Eric V. Linder. Exploring the expansion history of the universe. *Phys.Rev.Lett.*, 90:091301, 2003. doi: 10.1103/PhysRevLett.90.091301.

[116] Paolo Creminelli, Guido D'Amico, Jorge Norena, and Filippo Vernizzi. The Effective Theory of Quintessence: the w¡-1 Side Unveiled. *JCAP*, 0902:018, 2009. doi: 10.1088/1475-7516/2009/02/018.

[117] Paolo Creminelli, Guido D'Amico, Jorge Norena, Leonardo Senatore, and Filippo Vernizzi. Spherical collapse in quintessence models with zero speed of sound. *JCAP*, 1003:027, 2010. doi: 10.1088/1475-7516/2010/03/027.

[118] Roland de Putter, Dragan Huterer, and Eric V. Linder. Measuring the Speed of Dark: Detecting Dark Energy Perturbations. *Phys.Rev.*, D81:103513, 2010. doi: 10.1103/PhysRevD.81.103513.

[119] Guillermo Ballesteros and Julien Lesgourgues. Dark energy with non-adiabatic sound speed: initial conditions and detectability. *JCAP*, 1010:014, 2010. doi: 10.1088/1475-7516/2010/10/014.

[120] Domenico Sapone, Martin Kunz, and Luca Amendola. Fingerprinting Dark Energy II: weak lensing and galaxy clustering tests. *Phys.Rev.*, D82:103535, 2010. doi: 10.1103/PhysRevD.82.103535.

[121] Youness Ayaita, Bjorn Malte Schaefer, and Maik Weber. Investigating clustering dark energy with 3d weak cosmic shear. *Mon.Not.Roy.Astron.Soc.*, 422:3056–3066, 2012.

[122] H.A. Rizwan ul and S. Unnikrishnan. Effect of dark energy sound speed and equation of state on CDM power spectrum. *J.Phys.Conf.Ser.*, 484:012048, 2014. doi: 10.1088/1742-6596/484/1/012048.

[123] Rizwan Ul Haq Ansari and Sanil Unnikrishnan. Perturbations in dark energy models with evolving speed of sound. *arXiv:1104.4609*, 2011.

[124] Tobias Basse, Ole Eggers Bjaelde, Steen Hannestad, and Yvonne Y.Y. Wong. Confronting the sound speed of dark energy with future cluster surveys. *arXiv:1205.0548*, 2012.

[125] Olga Sergijenko and Bohdan Novosyadlyj. Sound speed of scalar field dark energy: weak effects and large uncertainties. *Phys.Rev.*, D91(8):083007, 2015. doi: 10.1103/PhysRevD.91.083007.

[126] P. M. Okouma, Y. Fantaye, and B. A. Bassett. How Flat is Our Universe Really? *Phys. Lett.*, B719:1–4, 2013. doi: 10.1016/j.physletb.2012.12.070.

[127] Arman Shafieloo. Falsifying Cosmological Constant. *Nucl. Phys. Proc. Suppl.*, 246-247:171–177, 2014. doi: 10.1016/j.nuclphysbps.2013.10.081.

[128] Nicola Bartolo, Pier Stefano Corasaniti, Andrew R. Liddle, and Michael Malquarti. Perturbations in cosmologies with a scalar field and a perfect fluid. *Phys.Rev.*, D70:043532, 2004. doi: 10.1103/PhysRevD.70.043532.

[129] Samuel F. Flender and Dominik J. Schwarz. Newtonian versus relativistic cosmology. *Phys.Rev.*, D86:063527, 2012. doi: 10.1103/PhysRevD.86.063527.

[130] Luis P. Chimento, Alejandro S. Jakubi, Diego Pavon, and Winfried Zimdahl. Interacting quintessence solution to the coincidence problem. *Phys.Rev.*, D67:083513, 2003. doi: 10.1103/PhysRevD.67.083513.

[131] Manasse R. Mbonye. Cosmology with interacting dark energy. *Mod.Phys.Lett.*, A19:117–134, 2004. doi: 10.1142/S021773230401285X.

[132] Chas A. Egan and Charles H. Lineweaver. Dark-Energy Dynamics Required to Solve the Cosmic Coincidence. *Phys.Rev.*, D78:083528, 2008. doi: 10.1103/PhysRevD.78.083528.

[133] Khamphee Karwan. The Coincidence Problem and Interacting Holographic Dark Energy. *JCAP*, 0805:011, 2008. doi: 10.1088/1475-7516/2008/05/011.

[134] Sergio del Campo, Ramon Herrera, and Diego Pavon. Interacting models may be key to solve the cosmic coincidence problem. *JCAP*, 0901:020, 2009. doi: 10.1088/1475-7516/2009/01/020.

[135] F.E.M. Costa, Jr. Barboza, E.M., and J.S. Alcaniz. Cosmology with interaction in the dark sector. *Phys.Rev.*, D79:127302, 2009. doi: 10.1103/PhysRevD.79.127302.

[136] Sean Z.W. Lip. Interacting Cosmological Fluids and the Coincidence Problem. *Phys.Rev.*, D83:023528, 2011. doi: 10.1103/PhysRevD.83.109902,10.1103/PhysRevD.83.023528.

[137] Yi Zhang, Hui Li, Yungui Gong, Zong-Hong Zhu, Yungui Gong, et al. Interactions in Dark Energy Models. *arXiv:1103.0718*, 2011.

[138] Pedro C. Ferreira, Diego Pavn, and Joel C. Carvalho. On detecting interactions in the dark sector with H(z) data. *Phys.Rev.*, D88:083503, 2013. doi: 10.1103/PhysRevD.88.083503.

[139] Luca Amendola. Linear and non-linear perturbations in dark energy models. *Phys.Rev.*, D69:103524, 2004. doi: 10.1103/PhysRevD.69.103524.

[140] Xin-min Zhang. Dark energy and its interactions with neutrinos. *AIP Conf.Proc.*, 805:3–9, 2006. doi: 10.1063/1.2149667.

[141] Kiyotomo Ichiki and Yong-Yeon Keum. Cosmological Signatures of the Interaction between Dark-Energy and Massive Neutrinos. *arXiv:0803.3142*, 2008.

[142] Luis P. Chimento and Martn G. Richarte. Interacting dark sector with transversal interaction. *AIP Conf.Proc.*, 1647:44–49, 2015. doi: 10.1063/1.4913335.

[143] Luca Amendola and Claudia Quercellini. Tracking and coupled dark energy as seen by WMAP. *Phys.Rev.*, D68:023514, 2003. doi: 10.1103/PhysRevD.68.023514.

[144] Rachel Bean, Eanna E. Flanagan, Istvan Laszlo, and Mark Trodden. Constraining Interactions in Cosmology's Dark Sector. *Phys.Rev.*, D78:123514, 2008. doi: 10.1103/PhysRevD.78.123514.

[145] Jun-Qing Xia. Constraint on coupled dark energy models from observations. *Phys.Rev.*, D80:103514, 2009. doi: 10.1103/PhysRevD.80.103514.

[146] Rong-Gen Cai and Qiping Su. On the Dark Sector Interactions. *Phys.Rev.*, D81:103514, 2010. doi: 10.1103/PhysRevD.81.103514.

[147] Elcio Abdalla, L. Raul Abramo, and Jose C.C. de Souza. Signature of the interaction between dark energy and dark matter in observations. *Phys.Rev.*, D82:023508, 2010. doi: 10.1103/PhysRevD.82.023508.

[148] E. Abdalla, Elisa G. M. Ferreira, Jerome Quintin, and Bin Wang. New Evidence for Interacting Dark Energy from BOSS. *arXiv:1412.2777*, 2014.

[149] Jussi Valiviita, Roy Maartens, and Elisabetta Majerotto. Observational constraints on an interacting dark energy model. *Mon.Not.Roy.Astron.Soc.*, 402:2355–2368, 2010. doi: 10.1111/j.1365-2966.2009.16115.x.

[150] Hao Wei. Revisiting the Cosmological Constraints on the Interacting Dark Energy Models. *Phys.Lett.*, B691:173–182, 2010. doi: 10.1016/j.physletb.2010.06.038.

[151] Ximing Chen, Bin Wang, Nana Pan, and Yungui Gong. Constraining the interacting dark energy models from weak gravity conjecture and recent observations. *Phys.Lett.*, B695:30–36, 2011. doi: 10.1016/j.physletb.2010.11.032.

[152] Shuo Cao and Nan Liang. Testing the phenomenological interacting dark energy with observational $H(z)$ data. *Mon.Not.Roy.Astron.Soc.*, 416:1099, 2011. doi: 10.1111/j.1365-2966.2011.19105.x.

[153] Xiao-Dong Xu, Jian-Hua He, and Bin Wang. Breaking parameter degeneracy in interacting dark energy models from observations. *Phys.Lett.*, B701:513–519, 2011. doi: 10.1016/j.physletb.2011.06.043.

[154] Alejandro Aviles and Jorge L. Cervantes-Cota. Dark degeneracy and interacting cosmic components. *Phys.Rev.*, D84:083515, 2011. doi: 10.1103/PhysRevD.84.083515,10.1103/PhysRevD.84.089905.

[155] Marco Baldi and Paolo Salucci. Constraints on interacting dark energy models from galaxy Rotation Curves. *JCAP*, 1202:014, 2012. doi: 10.1088/1475-7516/2012/02/014.

[156] Marco Baldi. Structure formation in Multiple Dark Matter cosmologies with long-range scalar interactions. *Mon.Not.Roy.Astron.Soc.*, 428:2074, 2013. doi: 10.1093/mnras/sts169.

[157] Valeria Pettorino, Luca Amendola, Carlo Baccigalupi, and Claudia Quercellini. Constraints on coupled dark energy using CMB data from WMAP and SPT. *Phys.Rev.*, D86:103507, 2012. doi: 10.1103/PhysRevD.86.103507.

[158] Freddy Cueva Solano and Ulises Nucamendi. Reconstruction of the interaction term between dark matter and dark energy using SNe Ia, BAO, CMB, H(z) and X-ray gas mass fraction. *arXiv:1207.0250*, 2012.

[159] Shuo Cao and Nan Liang. Interaction between dark energy and dark matter: observational constraints from OHD, BAO, CMB and SNe Ia. *Int.J.Mod.Phys.*, D22:1350082, 2013. doi: 10.1142/S021827181350082X.

[160] Valentina Salvatelli, Andrea Marchini, Laura Lopez-Honorez, and Olga Mena. New constraints on Coupled Dark Energy from the Planck satellite experiment. *Phys.Rev.*, D88(2):023531, 2013. doi: 10.1103/PhysRevD.88.023531.

[161] Luis P. Chimento, Martn G. Richarte, and Ivn E. Snchez Garca. Interacting dark sector with variable vacuum energy. *Phys.Rev.*, D88:087301, 2013. doi: 10.1103/PhysRevD.88.087301.

[162] Andr A. Costa, Xiao-Dong Xu, Bin Wang, Elisa G. M. Ferreira, and E. Abdalla. Testing the Interaction between Dark Energy and Dark Matter with Planck Data. *Phys.Rev.*, D89(10):103531, 2014. doi: 10.1103/PhysRevD.89.103531.

[163] Weiqiang Yang, Lixin Xu, Yuting Wang, and Yabo Wu. Constraints on a decomposed dark fluid with constant adiabatic sound speed by jointing the geometry test and growth rate after Planck data. *Phys.Rev.*, D89(4):043511, 2014. doi: 10.1103/PhysRevD.89.043511.

[164] Yun-He Li and Xin Zhang. Large-scale stable interacting dark energy model: Cosmological perturbations and observational constraints. *Phys.Rev.*, D89(8):083009, 2014. doi: 10.1103/PhysRevD.89.083009.

[165] Weiqiang Yang and Lixin Xu. Cosmological constraints on interacting dark energy with redshift-space distortion after Planck data. *Phys.Rev.*, D89(8):083517, 2014. doi: 10.1103/PhysRevD.89.083517.

[166] Arpine Piloyan, Valerio Marra, Marco Baldi, and Luca Amendola. Linear Perturbation constraints on Multi-coupled Dark Energy. *JCAP*, 1402:045, 2014. doi: 10.1088/1475-7516/2014/02/045.

[167] Weiqiang Yang and Lixin Xu. Testing coupled dark energy with large scale structure observation. *JCAP*, 1408:034, 2014. doi: 10.1088/1475-7516/2014/08/034.

[168] J.S. Wang and F.Y. Wang. Cosmological model of the interaction between dark matter and dark energy. *Astron.Astrophys.*, 564:A137, 2014. doi: 10.1051/0004-6361/201322606.

[169] Rafael C. Nunes and Edesio M. Barboza. Dark matter-dark energy interaction for a time-dependent EoS parameter. *Gen.Rel.Grav.*, 46:1820, 2014. doi: 10.1007/s10714-014-1820-1.

[170] Jussi Valiviita, Elisabetta Majerotto, and Roy Maartens. Instability in interacting dark energy and dark matter fluids. *JCAP*, 0807:020, 2008. doi: 10.1088/1475-7516/2008/07/020.

[171] Kazuya Koyama, Roy Maartens, and Yong-Seon Song. Velocities as a probe of dark sector interactions. *JCAP*, 0910:017, 2009. doi: 10.1088/1475-7516/2009/10/017.

[172] L. Lopez Honorez and 0. Mena. Instabilities in dark coupled models and constraints from cosmological data. *AIP Conf.Proc.*, 1241:1016–1024, 2010. doi: 10.1063/1.3462595.

[173] Yu.L. Bolotin, V.A. Cherkaskiy, G.I. Ivashkevych, O.A. Lemets, and D.A. Yerokhin. Dynamics of the Universe in Problems. *arXiv:0904.0382*, 2009.

[174] Elisabetta Majerotto, Jussi Valiviita, and Roy Maartens. Adiabatic initial conditions for perturbations in interacting dark energy models. *Mon.Not.Roy.Astron.Soc.*, 402:2344–2354, 2010. doi: 10.1111/j.1365-2966.2009.16140.x.

[175] Luis P. Chimento. Linear and nonlinear interactions in the dark sector. *Phys.Rev.*, D81:043525, 2010. doi: 10.1103/PhysRevD.81.043525.

[176] Hao Wei. Cosmological Evolution of Quintessence and Phantom with a New Type of Interaction in Dark Sector. *Nucl.Phys.*, B845:381–392, 2011. doi: 10.1016/j.nuclphysb.2010.12.010.

[177] Sergio del Campo, Ramon Herrera, and Diego Pavon. $H(z)$ diagnostics on the nature of dark energy. *Int.J.Mod.Phys.*, D20:561–579, 2011. doi: 10.1142/S0218271811018871.

[178] Cheng-Yi Sun and Rui-Hong Yue. New Interaction between Dark Energy and Dark Matter Changes Sign during Cosmological Evolution. *Phys.Rev.*, D85:043010, 2012. doi: 10.1103/PhysRevD.85.043010.

[179] Timothy Clemson, Kazuya Koyama, Gong-Bo Zhao, Roy Maartens, and Jussi Valiviita. Interacting Dark Energy – constraints and degeneracies. *Phys.Rev.*, D85:043007, 2012. doi: 10.1103/PhysRevD.85.043007.

[180] Xi-ming Chen, Yungui Gong, Emmanuel N. Saridakis, Yungui Gong, and Emmanuel N. Saridakis. Time-dependent interacting dark energy and transient acceleration. *Int.J.Theor.Phys.*, 53:469–481, 2014. doi: 10.1007/s10773-013-1831-9.

[181] Fabiola Arevalo, Anna Paula Ramos Bacalhau, and Winfried Zimdahl. Cosmological dynamics with non-linear interactions. *Class.Quant.Grav.*, 29:235001, 2012. doi: 10.1088/0264-9381/29/23/235001.

[182] Luis P. Chimento. Exactly solved models of interacting dark matter and dark energy. *AIP Conf.Proc.*, 1471:30–38, 2012. doi: 10.1063/1.4756808.

[183] Luis P. Chimento and Martn G. Richarte. Dark matter, dark energy, and dark radiation coupled with a transversal interaction. *Phys.Rev.*, D86:103501, 2012. doi: 10.1103/PhysRevD.86.103501.

[184] Cheng-Yi Sun, Yu Song, and Rui-Hong Yue. Stability of curvature perturbation with new covariant form for energy-momentum transfer in dark sector. *Eur.Phys.J.*, C73(2):2331, 2013. doi: 10.1140/epjc/s10052-013-2331-z,10.1140/epjc/s10052-013-2372-3.

[185] Cheng-Yi Sun and Rui-Hong Yue. Stable large-scale perturbations in interacting dark-energy model. *JCAP*, 1308:018, 2013. doi: 10.1088/1475-7516/2013/08/018.

[186] A. Pourtsidou, C. Skordis, and E.J. Copeland. Models of dark matter coupled to dark energy. *Phys.Rev.*, D88(8):083505, 2013. doi: 10.1103/PhysRevD.88.083505.

[187] Yu. L. Bolotin, A. Kostenko, O.A. Lemets, and D.A. Yerokhin. Cosmological Evolution With Interaction Between Dark Energy And Dark Matter. *Int.J.Mod.Phys.*, D24(03):1530007, 2014. doi: 10.1142/S0218271815300074.

[188] S. Carneiro and H.A. Borges. On dark degeneracy and interacting models. *JCAP*, 1406:010, 2014. doi: 10.1088/1475-7516/2014/06/010.

[189] Jannis Bielefeld, Robert R. Caldwell, and Eric V. Linder. Dark Energy Scaling from Dark Matter to Acceleration. *Phys.Rev.*, D90(4):043015, 2014. doi: 10.1103/PhysRevD.90.043015.

[190] Yun-He Li, Jing-Fei Zhang, and Xin Zhang. Parametrized Post-Friedmann Framework for Interacting Dark Energy. *Phys.Rev.*, D90(6):063005, 2014. doi: 10.1103/PhysRevD.90.063005.

[191] Valentina Salvatelli, Najla Said, Marco Bruni, Alessandro Melchiorri, and David Wands. Indications of a late-time interaction in the dark sector. *Phys.Rev.Lett.*, 113(18):181301, 2014. doi: 10.1103/PhysRevLett.113.181301.

[192] Joschka Beyer. Adiabatic perturbations in coupled scalar field cosmologies. *arXiv:1407.0186*, 2014.

[193] Luca Amendola, Tiago Barreiro, and Nelson J. Nunes. Multifield coupled quintessence. *Phys.Rev.*, D90(8):083508, 2014. doi: 10.1103/PhysRevD.90.083508.

[194] Gabriela Caldera-Cabral, Roy Maartens, and Bjoern Malte Schaefer. The Growth of Structure in Interacting Dark Energy Models. *JCAP*, 0907:027, 2009. doi: 10.1088/1475-7516/2009/07/027.

[195] Jian-Hua He, Bin Wang, and Y.P. Jing. Effects of dark sectors' mutual interaction on the growth of structures. *JCAP*, 0907:030, 2009. doi: 10.1088/1475-7516/2009/07/030.

[196] Jian-Hua He, Bin Wang, Elcio Abdalla, and Diego Pavon. The Imprint of the interaction between dark sectors in galaxy clusters. *JCAP*, 1012:022, 2010. doi: 10.1088/1475-7516/2010/12/022.

[197] N.A. Koshelev. On the growth of perturbations in interacting dark energy and dark matter fluids. *Gen.Rel.Grav.*, 43:1309–1321, 2011. doi: 10.1007/s10714-010-1113-2.

[198] Baojiu Li and John D. Barrow. On the Effects of Coupled Scalar Fields on Structure Formation. *Mon.Not.Roy.Astron.Soc.*, 413:262–270, 2011. doi: 10.1111/j.1365-2966.2010.18130.x.

[199] Jian-Hua He, Bin Wang, and Pengjie Zhang. The Imprint of the interaction between dark sectors in large scale cosmic microwave background anisotropies. *Phys.Rev.*, D80:063530, 2009. doi: 10.1103/PhysRevD.80.063530.

[200] Matteo Martinelli, Laura Lopez Honorez, Alessandro Melchiorri, and Olga Mena. Future CMB cosmological constraints in a dark coupled universe. *Phys.Rev.*, D81:103534, 2010. doi: 10.1103/PhysRevD.81.103534.

[201] Xiao-Dong Xu, Bin Wang, and Elcio Abdalla. The signature of the scattering between dark sectors in large scale cosmic microwave background anisotropies. *Phys.Rev.*, D85:083513, 2012. doi: 10.1103/PhysRevD.85.083513.

[202] Carmelita Carbone, Marco Baldi, Valeria Pettorino, and Carlo Baccigalupi. Maps of CMB lensing deflection from N-body simulations in Coupled Dark Energy Cosmologies. *JCAP*, 1309:004, 2013. doi: 10.1088/1475-7516/2013/09/004.

[203] Francesco De Bernardis, Matteo Martinelli, Alessandro Melchiorri, Olga Mena, and Asantha Cooray. Future weak lensing constraints in a dark coupled universe. *Phys.Rev.*, D84:023504, 2011. doi: 10.1103/PhysRevD.84.023504.

[204] Emma Beynon, Marco Baldi, David J. Bacon, Kazuya Koyama, and Cristiano Sabiu. Weak lensing predictions for coupled dark energy cosmologies at non-linear scales. *Mon.Not.Roy.Astron.Soc.*, 422:3546–3553, 2012. doi: 10.1111/j.1365-2966.2012.20864.x.

[205] Andrea V. Maccio, Claudia Quercellini, Roberto Mainini, Luca Amendola, and Silvio A. Bonometto. N-body simulations for coupled dark energy: Halo mass function and density profiles. *Phys.Rev.*, D69:123516, 2004. doi: 10.1103/PhysRevD.69.123516.

[206] Baojiu Li and John D. Barrow. N-Body Simulations for Coupled Scalar Field Cosmology. *Phys.Rev.*, D83:024007, 2011. doi: 10.1103/PhysRevD.83.024007.

[207] Ewan R.M. Tarrant, Carsten van de Bruck, Edmund J. Copeland, and Anne M. Green. Coupled Quintessence and the Halo Mass Function. *Phys.Rev.*, D85:023503, 2012. doi: 10.1103/PhysRevD.85.023503.

[208] Weiguang Cui, Marco Baldi, and Stefano Borgani. The halo mass function in interacting Dark Energy models. *Mon.Not.Roy.Astron.Soc.*, 424:993, 2012. doi: 10.1111/j.1365-2966.2012.21267.x.

[209] Francesco Pace, Marco Baldi, Lauro Moscardini, David Bacon, and Robert Crittenden. Ray-tracing simulations of coupled dark energy models. *Mon.Not.Roy.Astron.Soc.*, 447(1):858–874, 2015. doi: 10.1093/mnras/stu2513.

[210] Jussi Valiviita and Elina Palmgren. Distinguishing interacting dark energy from wCDM with CMB, lensing, and baryon acoustic oscillation data. *arXiv:1504.02464*, 2015.

[211] C. Skordis, A. Pourtsidou, and E.J. Copeland. The Parameterized Post-Friedmannian Framework for Interacting Dark Energy Theories. *arXiv:1502.07297*, 2015.

[212] Yuting Wang, Gong-Bo Zhao, David Wands, Levon Pogosian, and Robert G. Crittenden. Reconstruction of the dark matter-vacuum energy interaction. *arXiv:1505.01373*, 2015.

[213] Mahmoud Hashim, Daniele Bertacca, and Roy Maartens. Degeneracy between primordial non-Gaussianity and interaction in the dark sector. *Phys.Rev.*, D90 (10):103518, 2014. doi: 10.1103/PhysRevD.90.103518.

[214] Wayne Hu and Asantha Cooray. Gravitational time delay effects on cosmic microwave background anisotropies. *Phys.Rev.*, D63:023504, 2001. doi: 10.1103/PhysRevD.63.023504.

[215] Jeffrey B. Peterson, Roy Aleksan, Reza Ansari, Kevin Bandura, Dick Bond, et al. 21 cm Intensity Mapping. *arXiv:0902.3091*, 2009.

[216] Uros Seljak. Extracting primordial non-gaussianity without cosmic variance. *Phys.Rev.Lett.*, 102:021302, 2009. doi: 10.1103/PhysRevLett.102.021302.

[217] Philippe Brax and Jerome Martin. Quintessence and supergravity. *Phys.Lett.*, B468:40–45, 1999. doi: 10.1016/S0370-2693(99)01209-5.

[218] Philippe Brax, Jerome Martin, and Alain Riazuelo. Exhaustive study of cosmic microwave background anisotropies in quintessential scenarios. *Phys.Rev.*, D62: 103505, 2000. doi: 10.1103/PhysRevD.62.103505.

[219] T. Barreiro, Edmund J. Copeland, and N.J. Nunes. Quintessence arising from exponential potentials. *Phys.Rev.*, D61:127301, 2000. doi: 10.1103/PhysRevD.61.127301.